A REVISED LATEST CRETACEOUS AND EARLY CENOZOIC APPARENT POLAR WANDER PATH FOR THE PACIFIC PLATE

A Thesis

by

MELISSA A. BEAMAN

Submitted to the Office of Graduate Studies of
Texas A&M University
in partial fulfillment of the requirements for the degree of

MASTER OF SCIENCE

May 2006

Major Subject: Oceanography

A REVISED LATEST CRETACEOUS AND EARLY CENOZOIC APPARENT POLAR WANDER PATH FOR THE PACIFIC PLATE

A Thesis

by

MELISSA A. BEAMAN

Submitted to the Office of Graduate Studies of
Texas A&M University
in partial fulfillment of the requirements for the degree of

MASTER OF SCIENCE

Approved by:

Chair of Committee, William W. Sager
Committee Members, Thomas W.C. Hilde
Paul. J. Fox
Head of Department, John Morse

May 2006

Major Subject: Oceanography

ABSTRACT

A Revised Latest Cretaceous and Early Cenozoic Apparent Polar Wander Path for the Pacific Plate. (May 2006)

Melissa A. Beaman, B.S., Arizona State University

Chair of Advisory Committee: Dr. Wiliam W. Sager

The apparent polar wander path (APWP) for the Pacific plate during the Late Cretaceous and Early Cenozoic has been constrained primarily by seamount magnetic anomaly inversions and seafloor magnetic anomaly skewness. The reliability of these data types is uncertain and data are too sparse to provide a consistent or detailed APWP. In an effort to refine the Pacific APWP, we collected a larger, more diverse data set that allowed for the calculation of new mean paleomagnetic poles for the latest Cretaceous and Paleogene. We combined four types of data including sediment core paleocolatitudes, basalt core paleocolatitudes, seamount magnetic anomaly inversion declinations, and effective inclinations from magnetic anomaly skewness calculations. This diverse data set yields paleomagnetic poles that are less affected by bias from any particular data type. We found reasonably good agreement between data types and calculated five mean paleomagnetic poles representing the Oligocene (30 Ma), Late (39 Ma) and Early (49 Ma) Eocene, and Paleocene (61 Ma) epochs and the Maastrichtian (68 Ma) stage. Though a significant percentage of the data are from azimuthally-unoriented cores, which do not provide constraint on paleodeclination, a wide distribution of sites and the use of declination data from seamount anomaly inversions

gave relatively good control on pole paleolongitude. The large numbers of data in our calculations allow for reasonably compact uncertainty bounds and the overall agreement among most data implies insignificant systematic errors in the data set. The greatest disagreement among data occurs due to a divergence between poles from anomaly skewness and other data types prior to 55 Ma. As a whole, the new APWP implies northward Pacific plate drift. However, this motion is punctuated with a stillstand from the Late Cretaceous (~80 Ma) until the middle Eocene, (~49 Ma). This stillstand suggests a lack of northward Pacific plate motion during this time, counter to most accepted models. This APWP is consistent with paleomagnetic results from the Emperor Chain that indicate the Hawaiian hotspot moved south during formation of the Emperor Chain, but it implies an amount of motion slightly greater than that previously proposed for hotspot drift.

DEDICATION

To my grandparents for encouraging me to dig in the backyard and collect rocks, and who told me I could do anything.

ACKNOWLEDGMENTS

I would like to thank my committee chair, Dr. Sager and my committee members, Dr. Hilde and Dr. Fox for their encouragement and guidance throughout this research.

Thanks also to the faculty, staff and students of the Oceanography Department at Texas A&M University for their assistance and support during the course of my research, as well as Dr. Gary Acton at the University of California-Davis, for his help and the use of the laboratory. I also want to thank Jane and R. Ken Williams for funding my research through the Jane and R. Ken Williams ’45 endowed chair.

Finally, thanks to my friends and family for their patience and unwavering belief that I could accomplish my goals.

TABLE OF CONTENTS

LIST OF FIGURES

LIST OF TABLES

1. INTRODUCTION

Apparent polar wander paths (APWPs) provide the basis for tectonic plate reconstructions and give insights into the motions of plates through geologic time. Because APWPs express the movement of a plate relative to the Earth's spin axis, they can indicate motion of plates relative to each another, latitudinal motion of the plate, movement of the plates relative to hotspots, and true polar wander (TPW) [Gordon, 1987; Besse and Courtillot, 2002]. To distinguish these various components of polar wander, detailed APWPs are required. Not all plates have a well-defined APWP, mainly due to sparse paleomagnetic pole data. This is especially true for the Pacific plate, whose outcrops are not easily accessible, because all but a tiny portion is underwater.

Paleomagnetic data from the Pacific plate are of four main types, each with uncertainties. Two types involve the modeling of crustal magnetic fields. Most such are from inversions of seamount magnetic anomalies which have provided much of the APWP constraint in the past [Gordon, 1982; Sager and Pringle, 1988; Sager and Koppers, 2000]. The other type of magnetic field modeling is determining the asymmetry (skewness) of marine magnetic anomalies, which is related to paleolatitude [Schouten and McCamy, 1972; Cande, 1976; Petronotis et al., 1992; Petronotis and Gordon, 1999].

This thesis follows the style and format of the *Journal of Geophysical Research.*

The other two types of data are from studies of azimuthally-unoriented cores. These data come from sediment cores (either piston cores or DSDP/ODP cores) and DSDP/ODP basalt cores. With few exceptions, these cores lack declination data [e.g., Cox and Gordon, 1984].

Most prior studies have focused on one data type or a limited time and many were done 15-20 years ago. As a result, the Pacific APWP is sparse and sometimes contradictory, making interpretation difficult (Fig. 1). Today, significantly more data are available, so refining the APWP is possible. We have compiled new data from (1) seamount magnetic anomaly inversions, (2) sediment cores and (3) basalt cores and (4) skewness data and combined them with existing data to calculate new paleomagnetic poles for a refined Pacific APWP for the latest Cretaceous and Early Cenozoic. The new mean paleomagnetic poles represent the Oligocene through Maastrichtian. We did not examine Miocene data due to the paucity of available data nor did we use older Cretaceous data because they have been compiled elsewhere [Sager, 2003; Sager, in press]. Because we use a larger data set than most previous investigators, we are able to divide the data into short time intervals, giving a detailed APWP.

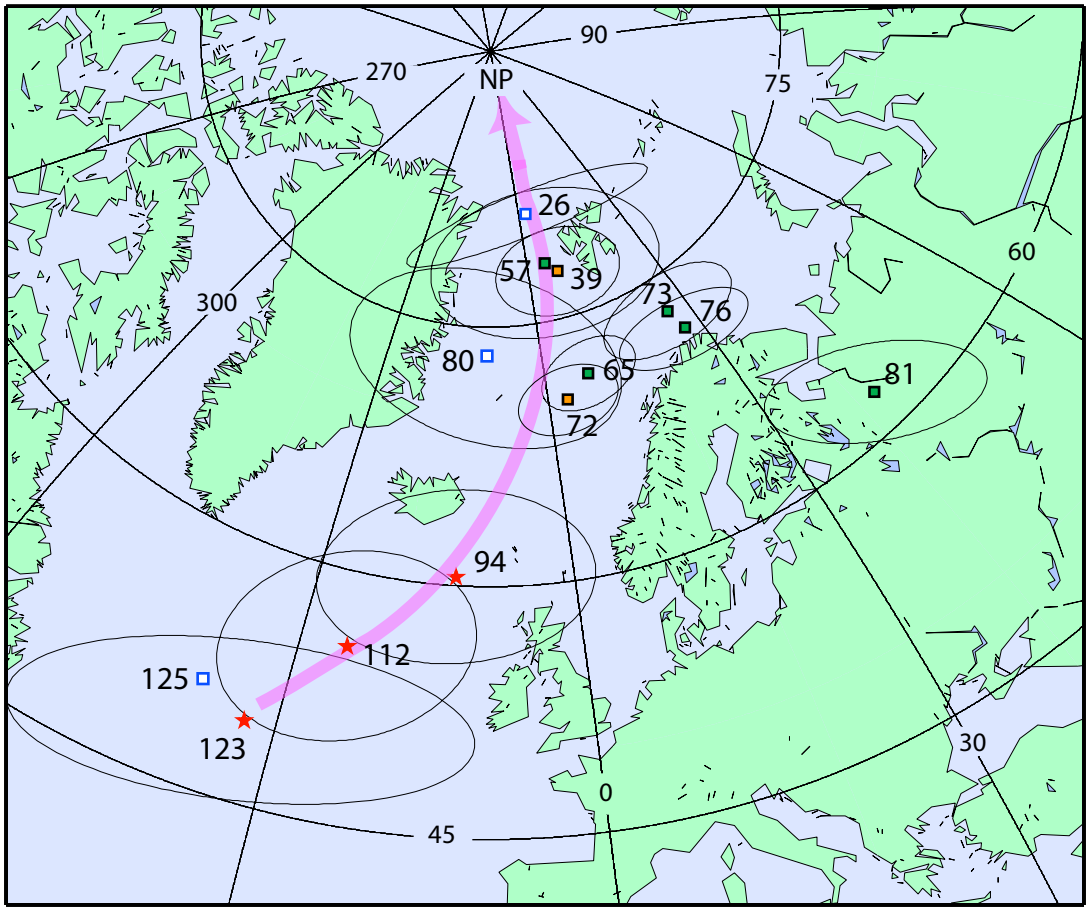

Figure 1. Pacific plate APWP prior to this study suggesting polar drift to the northeast, followed by a shift to the north in the Late Cretaceous. APWP modified from Sager [in press]. Open blue squares are poles incorporating diverse data sets (skewness, seamounts, sediment cores and basalt cores); red stars are poles from basalt cores only [Sager, in press]; filled green squares are skewness poles [Acton and Gordon, [1991, 1994], Petronotis et al. [1992, 1994], Vasas et al. [1994], and Petronotis et al. [1999]]; filled orange squares are seamount poles from Sager [1987] and Sager and Pringle [1988]. Numbers next to poles give age in Myr. Ellipses are 95% confidence regions.

2. DATA

2.1. Data Types

2.1.1. Crustal Magnetic Field Modeling

Because of the difficulty in obtaining fully-oriented paleomagnetic samples from the seafloor, many Pacific plate studies have addressed the scarcity of such data by using methods involving modeling of magnetic anomalies. Seamount magnetic anomaly models (SAMs) can be sources of paleomagnetic data since seamounts consist of basalt and usually produce a large magnetic anomaly at the sea surface. SAM modeling involves using an inversion of the magnetic anomaly and bathymetry to calculate a mean magnetization that produces an anomaly that mimics the observed anomaly. One seamount modeling technique assumes a homogeneous magnetization and results in a best least-squares fit to the magnetic anomaly [Vacquier, 1962; Richards et al., 1967]. A second, similar technique calculates both homogeneous and inhomogeneous magnetization components, minimizing the latter [Parker et al., 1987].

Both techniques are based on homogeneity assumptions which may be violated. Seamount magnetizations may not be homogeneous because the seamount formed during magnetic reversals, incorporating blocks of opposing polarity. Seamounts can also be affected by lithologic variations such as debris slides and hyaloclastites, for example, which are non-magnetic [e.g., Harrison et al., 1975]. Data from the least complex seamount magnetic anomalies may have magnetization models in which the anomalies closely fit a homogenous seamount model. In these cases, the SAMs produce high goodness of fit ratios (GFRs), where the GFR is the mean model residual divided

by the mean observed anomaly and small residuals lead to high GFRs. Because high GFRs are associated with seamounts that are generally homogeneous, the seamount's magnetic inversion can determine a meaningful mean magnetization vector [Richards et al., 1967; Sager, 1987]. These high GFR SAMs should produce paleoinclination and paleodeclination data suitable for consideration for paleomagnetic pole calculations. Seamount models with grossly complex magnetic anomalies, which give low GFRs, probably do not produce reliable mean magnetization vectors and are likely unsuitable.

Perhaps the most significant problem associated with SAM techniques is the assumption that the magnetization is entirely remanent. Several studies have shown that seamount magnetizations may include induced or viscous overprint components [e.g., Gee et al., 1988, 1989]. Because of the large change in latitude for most Pacific seamounts between paleo and present locations, such overprints can significantly change the magnetization direction, especially the paleoinclination. Unlike inclination, declination changes from overprints for Pacific seamounts are small. This difference results from the fact that the Pacific plate has not rotated greatly, so the change in horizontal magnetization direction is small. Thus, horizontal overprints from the present field should be nearly parallel (or antiparallel) to the original declination magnetization direction. This will change the calculated declinations a few degrees at most [Sager, 2003] and paleodeclination values from SAMs will suffer less bias from overprint errors.

Another common magnetic method is to model the skewness of seafloor magnetic anomalies, which is related to paleoinclination and paleolatitude [Acton and Gordon, 1991; Petronotis et al., 1994, Petronotis and Gordon, 1999]. Magnetic anomaly

skewness data are obtained from profiles of seafloor marine magnetic anomalies produced by seafloor spreading. Skewness in magnetic anomalies is related to the magnetic inclination projected on the plane perpendicular to anomaly strike (i.e., the "effective" inclination) [Schouten and McCamy, 1972; Cande, 1976]. Effective inclination determines a half great circle upon which a paleomagnetic pole should lie and the intersection of several such semi-circles is an estimate of the paleomagnetic pole position [Schouten and Cande, 1976]. Skewness is complicated in some cases by the mismatch of anomalies on opposing sides of a ridge, likely related to the crustal magnetic recording process [Dyment and Arkani-Hamed, 1995]. This anomaly mismatch results in skewness values that vary from those expected. To correct the mismatch, a factor known as "anomalous skewness" is applied. The anomalous skewness correction is estimated by averaging the skewness mismatch of age-equivalent anomalies on opposing sides of a ridge or over more than one ridge and assuming the mismatch is the same for all the surrounding ridges [Cande, 1976; Petronotis et al., 1992]. Although anomalous skewness can be calculated, its source is poorly understood and leads to uncertainty in the interpretation of skewness poles.

2.1.2. Azimuthally-Unoriented Cores

Many oceanic paleomagnetic data are determined from azimuthally-unoriented cores of oceanic sediment or basalt. Such cores produce discrete inclination (and rarely, absolute declination) measurements of the geomagnetic field at the time of deposition or emplacement. Although the azimuthally-unoriented core inclination data give a biased estimate of mean inclination, this error can be corrected [e.g., Cox and Gordon, 1984;

McFadden and Reid, 1982]. Paleoinclination measurements obtained from cores from a given site can be averaged to estimate the mean paleocolatitude, which is the angular distance between the paleomagnetic pole and the drill core site [Cox and Gordon, 1984].

For sediment cores, a major uncertainty is inclination shallowing, a phenomenon believed to be caused by compaction of the sediments during burial [e.g., Anson and Kodama, 1987]. Shallowing causes the measured inclination to be less than the inclination of the ambient field at deposition. The reasons for inclination shallowing are not completely understood and it is not yet possible to predict which sediments will be affected. As a result, some workers treat all sediment data as suspect [e.g., Gordon, 1990; Tarduno, 1990]. Attempts have been made to estimate shallowing using the anisotropy of magnetic susceptibility or anhysteretic remanent magnetization [e.g., Jelínek, 1977; Kodama and Sun, 1990; Jackson et al., 1991; Hodych and Bijaksana, 1993; Bijaksana and Hodych, 1997; Hodych et al., 1999; Weaver et al., 2004], but these techniques are labor intensive and have not been widely applied or tested.

Basalts are thought to be more reliable magnetic field recorders than sediments, because their inclinations are not compromised by inclination shallowing. However, a major difficulty has been obtaining a sufficient number of independent flow samples to average out secular variation [Cox and Gordon, 1984]. Not many DSDP or ODP holes penetrate deeply into the basaltic crust, so few sample more than several independent magnetic units. Consequently, a small number of single sites produce sufficient data to average secular variation. Nonetheless, such data can still be valuable when combined

with coeval data from other sites to calculate mean pole locations [e.g., Cox and Gordon, 1984; Sager, 2003; Sager, in press].

2.2. Data Set

2.2.1. Previously Published Data

Previously published paleomagnetic data of all four types are used in our analyses. SAM declination data have been taken from seamounts analyzed by Sager [1992], Sager and Koppers [2000], and Sager et al. [2005] (Fig. 2; Table 1). Skewness data have come from Acton and Gordon [1991], Acton and Gordon [1994], Petronotis et al., [1994], and Petronotis and Gordon [1999] (Table 1). Some publications show additional skewness poles documented from abstracts; however, these poles are only used here in illustrations to show trends because they are poorly documented. Piston core data come from Prince et al. [1980] and Epp et al. [1983]. These older piston cores (GPC-3, S68-24, K72-39, K78020, K78523, and K78023) were used because they produced paleocolatitudes in agreement with the newer DSDP and ODP data and the younger part of the data set is sparse without them. Other published sediment core data have been taken from DSDP/ODP Sites 199, 315A, 577, 577A, 585, and 585A (Fig. 2; Table 1). Data from sites 577 and 577A have been reanalyzed from published measurements [Bleil, 1985]. Basalt core data come from Midway Atoll, as well as DSDP and ODP Sites 63, 430A, 432A, 433C, 597, 871, 1205, and 1206 (Fig. 2; Table1). For consistency, data ages estimated from stratigraphy or magnetic polarity (Table 1) have been adjusted to the Gradstein et al. [2004] geomagnetic polarity time scale (GPTS).

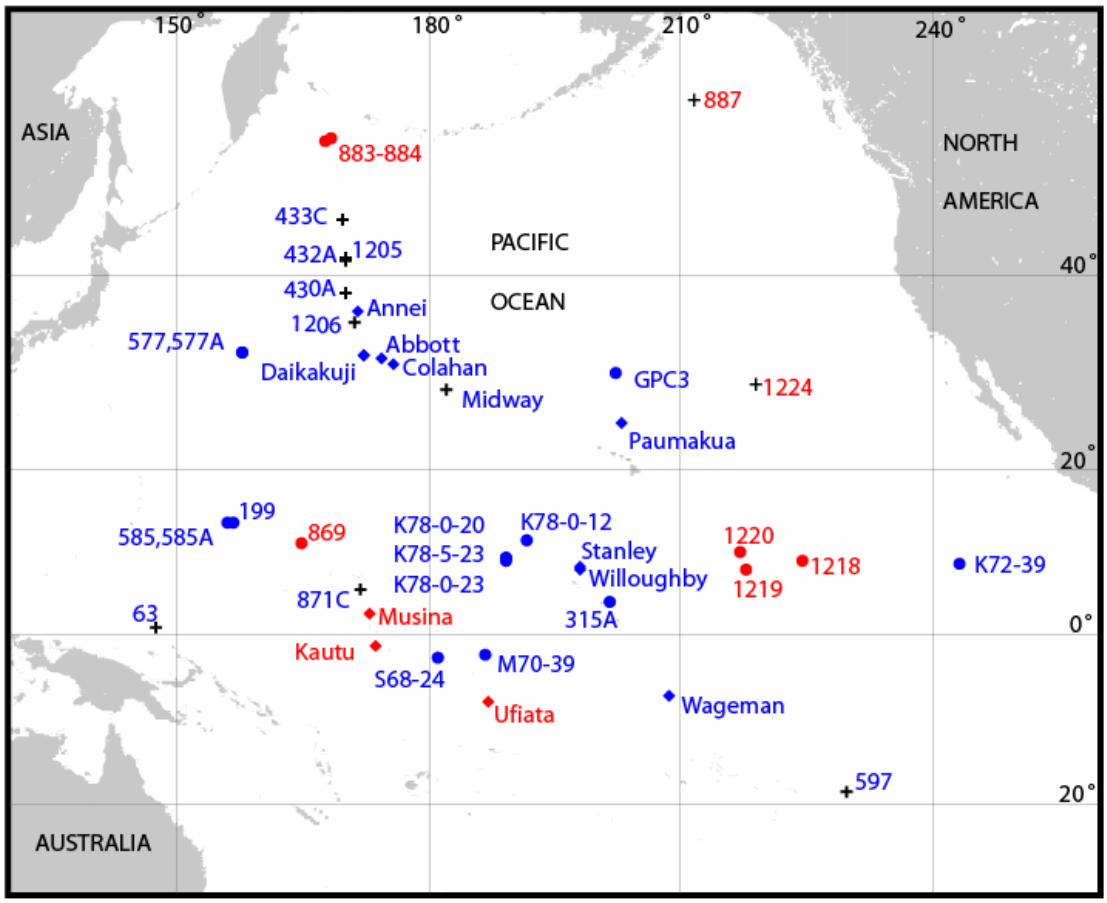

Figure 2. Locations of data sites from the Pacific Ocean. Red text denotes previously unpublished data, blue text is published data. Circles represent sediment core sites; diamonds are seamounts with SAM data; + are basalt core sites. Magnetic anomalies for effective inclination measurements (skewness) not shown, see Acton and Gordon [1991], Petronotis et al. [1994] and Petronotis and Gordon [1999] for data sites.

Table 1. Paleomagnetic data.

Sediment paleocolatitude data

Site	Site lat. (°N)	Site lon. (°E)	Colatitude (°)	Std. error (°)	Average age (Ma)	Age range (Ma)	Age type	Samples (N)	Pmag ref.	Age ref.
S68-24	-2.0	181.2	105.6	3.2	32.7	30.6-34.8	F	29	1,2	1,2
K72-39	8.5	243.1	91.7	3.0	30.6	27.8-33.4	F	62	1,2	1,2
K78020	9.2	189.2	87.9	3.0	26.1	24.0-28.2	F	48	1,2	1,2
K78523	9.2	189.3	88.0	3.0	30.9	28.5-33.3	F	74	1,2	1,2
K78023	9.1	189.3	90.9	3.0	26.4	24.2-28.6	F	84	1,2	1,2
ODP 1218	8.9	224.8	87.5	2.7	26.3	23.1-28.3	M	1668	3	3,4
ODP 1218	8.9	224.8	87.4	3.7	29.2	28.5-30.0	M	839	3	3,4
ODP 1219	7.8	218.0	92.9	3.1	32.0	30.4-34.0	M	1652	3	3,4
ODP 884B	51.5	168.3	48.8	9.3	30.0	26.0-34.0	F,M	49	5	5,7
ODP 869A	11.0	164.8	85.4	3.9	32.5	30.0-35.0	F	44	5	8,9
S68-24	-2.0	181.2	100.6	3.4	36.3	35.6-37.0	F	18	1,2	1,2
M70-39	-2.5	186.7	106.6	2.6	37.0	36.0-38.0	F	56	1,2	1,2
K78-0-12	11.4	191.8	93.1	2.4	47.5	46.0-49.0	F	57	1,2	1,2
ODP 883B	51.2	167.8	61.5	8.1	52.5	49.0-56.0	F	12	6	7
ODP 883B	51.2	167.8	53.9	9.2	41.8	36.5-47.1	F	28	6	7
DSDP 577	32.4	157.7	74.0	4.2	50.6	48.6-52.6	F	15	10	10
DSDP 577	32.4	157.7	76.4	4.6	54.7	52.6-56.8	F	16	10	10
DSDP 577A	32.4	157.7	74.5	5.0	51.3	49.4-53.2	F	21	10	10
DSDP 577A	32.4	157.7	74.7	5.3	55.8	53.1-58.5	F	8	10	10
ODP 1220 (c20r)	10.2	217.2	92.4	2.8	44.1	42.8-45.4	M	161	11	4
ODP 1220 (c20n)	10.2	217.2	94.5	3.8	42.2	41.6-42.8	M	772	11	4
ODP 884B(c20r-c22n)	51.5	168.3	49.7	7.5	45.7	42.8-48.6	F,M	26	5	5,7
ODP 884B(c19r)	51.5	168.3	64.5	6.3	41.2	40.7-41.7	F,M	11	5	5,7
DSDP 585, 585A	13.5	156.8	90.3	4.1	61.6	57.6-65.6	F	7	12	12
DSDP 577	32.4	157.7	75.8	4.3	57.7	56.7-58.7	F	13	10	10
DSDP 577	32.4	157.7	76.0	4.0	60.9	58.7-63.1	F	28	10	10
DSDP 577	32.4	157.7	78.6	3.9	64.1	63.1-65.1	F	47	10	10
DSDP 577	32.4	157.7	77.5	3.8	65.5	65.1-65.9	F	40	10	10
DSDP 577A	32.4	157.7	73.0	4.5	60.1	58.4-61.8	F	21	10	10
DSDP 577A	32.4	157.7	75.9	5.7	63.1	61.7-64.5	F	14	10	10
DSDP 577A	32.4	157.7	77.2	4.0	65.2	64.4-66.0	F	34	10	10
DSDP 199	13.5	156.2	95.9	4.1	62.0	56.0-68.0	F	9	13	14
DSDP 577	32.4	157.7	78.7	2.5	66.8	65.9-67.7	F	22	10	10
DSDP 577A	32.4	157.7	72.7	3.6	66.8	65.9-67.7	F	24	10	10
DSDP 577A	32.4	157.7	73.1	5.3	68.2	67.7-68.7	F	9	10	10
DSDP 585, 585A	13.5	156.8	91.3	2.2	68.0	65.0-71.0	M	15	10	10
DSDP 315A	4.2	201.5	98.9	3.8	70.0	68.3-71.7	F	25	15	15
GPC-3	30.3	202.2	78.9	3.5	67.5	64.5-70.5	F	12	16	16

Basalt paleocolatitude data

Site	Site lat. (°N)	Site lon. (°E)	Colatitude (°)	Std. error (°)	Average age (Ma)	Age range (Ma)	Age type	Samples (N)	Pmag ref.	Age ref.
Midway Reef Hole	28.3	182.6	71.3	4.9	27.7	27.7± 0.6	K	5	17,18	19
Midway Sand Island	28.2	182.6	75.7	7.2	27.7	27.7± 0.6	K	2	17,18	19
ODP 887D	54.4	211.6	56.2	7.5	27.4	27.4 ± 0.4	R	3	6	20
DSDP 597	-18.6	230.2	119.5	5.1	27.3	27.3 ± 0.8	F	7	21	21
DSDP 63	0.8	147.9	94.0	9.3	32.4	31.1-33.7	A	5	17,22	26,27
DSDP 1206 (Koko Smt)	35.3	171.6	68.5	4.1	49.1	49.1± 0.2	R	14	23	29
DSDP 430a	38.0	170.6	69.9	6.1	55.2	55.2 ± 0.7	R	3	24	30
DSDP 433C (Suiko Smt)	44.8	170.0	63.2	3.2	61.3	61.3 ± 0.5	R	20	24	31
DSDP 432a	41.3	170.4	57.7	8.3	56.2	56.2 ± 0.6	R	2	24	30
DSDP 1205 (Nintoku Gyt)	41.2	170.6	64.0	4.2	55.6	55.6 ± 0.2	R	22	23	29
ODP 871(Limalok Gyt)	5.6	172.3	98.9	5.2	68.3	68.3 ± 0.5	R	4	25	32
ODP 1224	27.9	219.0	83.1	4.6	46.1	43.8-46.3	A	5	5,28	33

Table 1. Continued.

Seamount declination data

Site	Site lat. (°N)	Site lon. (°E)	Pole lat. (°N)	Pole lon. (°E)	Declin. (°)	Std. error (°)	Average age (Ma)	Age range (Ma)	Age type	Pmag ref.	Age ref.
Stanley (ST)	8.2	198.1	75.6	356.5	5.3	10.6	39.3	39.3±1.5	R	35	34
Abbott (AB)	31.8	174.3	77.4	21.7	173.9	10.6	38.7	38.7±0.9	R	36	31
Colahan (CO)	31	176	78.2	20.5	354.8	10.6	38.8	38.8±0.2	R	37	31
Daikakuji E (DE)	32.1	172.4	80.7	332.8	183.4	10.6	46.7	46.7±0.2	R	37	31
Daikakuji W (DW)	32.1	172.3	69.7	50.2	341.8	10.6	46.7	46.7±0.2	R	37	31
Willoughby (WL)	7.9	198.1	78.2	14.6	0.7	10.6	39.3	39.3±1.1	R	35	34
Annei (AN)	36.3	171.6	62.0	312.8	197.6	10.6	52.0	49.0-55.0	S	37	37
Kautu (KA)	-1.4	173.6	78.1	10.3	-3.1	10.6	65.3	65.3±0.5	R	6	39
Paumakua (PA)	24.9	202.9	64.8	352.1	192.6	10.6	65.5	65.5±4.3	R	38	40
Musina (MU)	2.5	172.9	58.8	340.6	7.2	10.6	69.6	69.6±0.6	R	6	39
Wageman (WA)	-7.5	208.5	68.5	345.6	195.7	10.6	71.9	71.9±1.4	R	35	34

Magnetic anomaly skewness data

Site	Pole lat. (°N)	Pole lon. (°E)	95% Confidence Ellipse Maj. axis	Min. axis	Azi. (°)	Units (N)	Average age (Ma)	Age type	Pmag ref.	Age ref.
MMA 25r	78.2	4.8	3.7	2.4	93	131	57	A	41	41
MMA 27r-29r	73.2	10.2	2.1	1.4	69	32	64	A	42	42
MMA 32 (N. Farallon)	68.4	9.2	3.3	0.9	79	62	71	A	43	43
MMA 29r-31	73.2	4.6	3.8	2.4	68	15	68	A	42	42

References: 1. Epp et al. [1983]; 2. F. Theyer, pers. com.; 3. Lanci et al. [2005]; 4. Shipboard Scientific Party [2002]; 5. This study; 6. W. Sager, pers. com.; 7. Barron et al. [1995] ; 8.Shipboard Scientific Party [1993]; 9. Firth [1995]; 10. Bleil [1985]; 11. Parés and Lanci [2004]; 12. Ogg [1986]; 13. B. Keating, pers. com.; 14. Hekel [1973]; 15. Cockerham and Jarrard [1976]; 16. Prince et al. [1980]; 17. Cox and Gordon [1984]; 18. Grommé and Vine [1972]; 19. Dalrymple et al [1977]; 20. Keller et al. [1995]; 21. Sager and Horner-Johnson [in press]; 22. Marshall [1978]; 23. Tarduno et al. [2003]; 24. Kono [1980]; 25. Nakanishi and Gee [1995]; 26. Winterer et al. [1971]; 27. Bracey [1975]; 28. G. Acton, pers. com.; 29. Duncan and Keller [2004]; 30. Dalrymple et al. [1980]; 31. Sharp and Clague (2002); 32. Koppers et al. [2000]; 33. Stephen et al. [2003]; 34. Schlanger [1984]; 35. Sager and Keating [1984]; 36. Sager [1984]; 37. Sager et al. [2005]; 38. Sager [1992]; 39. Koppers and Staudigel [2005]; 40. Sager and Pringle [1988]; 41. Petronotis et al. [1994]; 42. Acton and Gordon [1991]; 43. Petronotis and Gordon [1999]

Age Codes: A= Anomaly, K= K/Ar, R= Ar/Ar, F= Fossil, M= Magnetostratigraphy, S= Age progression

2.2.2 New Data

Our study includes new data from two seamounts and seven ODP sites (Fig. 2; Table 1). Unpublished paleomagnetic SAM declinations from two new seamounts, Musina and Kautu of the Gilbert Ridge [Koppers and Staudigel, 2005] have been included in this study, as well as inclinations from three ODP Leg 199 sites 1218, 1219, and 1220 that were published elsewhere as magnetostratigraphy [Lanci et al., 2005; Parés and Lanci, 2004]. Site 1218 data include inclination measurements from chrons C6Cn.2r through C11n.2n; Site 1219 data include C11r through C13r, whereas Site 1220 data are limited to chrons C20n and C20r. These data were highly dense measurements from u-channel samples, which gave us over 5000 individual values. We measured discrete sediment samples from ODP Holes 884B and 869A to determine new paleocolatitudes for our data set (details in Appendix A; Table 1). Paleocolatitudes were also used from unpublished measurements from ODP Hole 883B sediment samples and basalt samples from ODP Hole 887D (Appendix A).

3. METHODS

Most of the data from seamounts, magnetic anomalies and basalt cores, as well as some from sediment cores, were collected and analyzed by others. Because it was impractical to remeasure or reanalyze these data, most were accepted as published. To make the data ages consistent, we adjusted the age to fit with a current GPTS [Gradstein et al., 2004]. Some published data [Bleil, 1985; Parés and Lanci, 2004; Lanci et al., 2005] were also subdivided into smaller age groups to limit the time span of the data groups to less than ~5 Myr. Unpublished existing data and newly calculated data (ODP Holes 869A and 884B) were also grouped by age, using stratigraphic age and polarity [Gradstein et al., 2004]. Once subdivided into age groups, mean core paleocolatitudes were calculated and corrected for the bias that results from averaging inclination-only data [Cox and Gordon, 1984]. We used the Cox and Gordon [1984] method because it provided an uncertainty estimate that takes into account both paleosecular variation and possible error from off- vertical borehole tilt [Cox and Gordon, 1984].

Because another method [McFadden and Reid, 1982] is widely used for correction of inclination-only data bias, we tested a subset of paleocolatitudes for consistency by calculating corrected paleocolatitudes using both the Cox and Gordon [1984] and McFadden and Reid [1982] methods. Overall, the results of the two methods were in good agreement, with the McFadden and Reid method [1982] producing slightly larger ($\leq 1°$) mean corrected paleocolatitudes than Cox and Gordon [1984] method. Even though the paleocolatitudes were nearly equivalent, uncertainty estimates for the McFadden and Reid method were smaller than those of the Cox and Gordon method.

The latter produced larger uncertainty estimates because it included uncertainty budgets for tilt and secular variation. We prefer the Cox and Gordon method because it gives a more conservative (i.e., larger) estimate of the pole uncertainties.

We combined paleocolatitudes and other data to determine best least-squares-fit paleomagnetic poles (discussed below) using the method of Gordon and Cox [1980]. For comparison, mean poles were calculated for sediment data only, basalt data only, and all data combined. Due to the small number of basalt data available, basalt pole calculations were only feasible for the Oligocene (30 Ma), Early Eocene (49 Ma) and Paleocene (61 Ma) poles (Table 2).

Poles calculated solely from azimuthally-unoriented core data often gave large aspect ratio error ellipses due to poor declination control. In an effort to improve constraints on pole longitude, we added SAM declination data to the pole calculations. SAM declinations were included in the Late and Early Eocene, Paleocene, and Maastrichtian poles. We used SAM declinations only, because of concern about bias of the calculated magnetization inclinations from induced or viscous magnetization [Gee et al., 1988, 1989; Sager, 2003]. To calculate a standard error for the declination data (required for the estimation of pole uncertainty), we used the standard deviation of the declinations (10.6°) as an approximation for the uncertainty of each declination.

In addition to colatitude and seamount declination data, we also included skewness data in our pole calculations. A skewness pole from anomaly 25r [Petronotis et al., 1994] was used as published. In contrast, we used subsets of skewness data from

Table 2. Calculated paleomagnetic poles.

Epoch/Stage Poles

Pole	Age (Ma)	Std. dev.	Data types	Pole lat. (°N)	Pole lon. (°E)	95% Confidence Ellipse Maj. axis	Min. axis	Azimuth (°)	Chi sq.	Degrees freedom
Oligocene	30		S	80.6	23.1	6.5	2.7	90	5.9	8
	28		B	76.4	34.4	16.2	7.5	104	1.3	3
	30		S B (ODP)	80.2	16.6	8.8	3.7	75	4.5	8
	30	2.5	S B	80.1	24.4	6.1	2.6	91	8.7	13
Late Eocene	40		S	75.5	21.7	17.8	4.3	103	6.7	3
	39	2.3	SD	75.9	17.3	10.2	4.3	99	7.5	7
Early Eocene	47		S	73.1	349.5	9.0	3.7	75	1.7	6
	49		B	69.0	39.9	20.8	7.1	117	0.3	1
	48		SB	73.2	359.7	8.3	3.3	84	5.6	9
	49	3.8	SBD	73.1	356.9	7.2	3.3	81	11.7	12
Paleocene	62		S	60.4	33.9	52.0	3.4	138	2.1	7
	59		B	9.3	108.8	172.0	6.0	136	0.4	1
	62		SB	50.9	268.6	42.9	3.0	34	2.8	10
	61	3.2	SBD	72.0	344.9	17.5	3.0	95	4.6	12
	62	3.0	SBDA	73.2	3.9	2.7	1.8	91	18.4	16
Maastrichtian	68		S	72.0	357.6	10.4	3.2	100	5.2	4
	69		SB	72.2	357.2	10.3	3.1	100	5.6	5
	68	1.5	SBD	72.4	350.2	8.8	3.1	94	6.4	8
	70	1.7	SBDA	69.4	8.6	3.3	1.3	83	19.3	12

Time Window Poles

Pole	Age (Ma)	Std. dev.	Data types	Pole lat. (°N)	Pole lon. (°E)	95% Confidence Ellipse Maj. axis	Min. axis	Azimuth (°)	Chi sq.	Degrees freedom
25 Ma	27	2.4	SB	81.8	13.9	6.4	1.4	63	9.5	25
30 Ma	29	2.6	SB	80.7	12.3	5.1	1.5	65	13.6	26
35 Ma	33	2.9	SBD	79.2	19.1	5.2	2.2	81	7.7	17
40 Ma	40	3.2	SBD	75.3	22.5	8.3	3.5	94	10.2	10
45 Ma	46	3.8	SBD	73.1	0.3	6.9	3.3	77	13.8	14
50 Ma	48	3.9	SBD	73.2	357.0	7.2	3.2	81	11.7	13
55 Ma	55	3.7	SBD	68.9	300.5	22.5	3.2	56	2.8	12
	57	2.4	SBDA	74.8	348.5	5.8	2.6	93	13.4	14
60 Ma	62	3.1	SBDA	73.0	5.8	2.7	1.7	91	19.8	20
	63	4.2	SBD	71.2	359.0	11.0	2.8	103	5.2	16
65 Ma	65	2.4	SBDA	72.1	4.0	2.5	1.6	91	14.4	21
	66	3.3	SBD	71.9	351.5	8.2	2.3	98	9.3	17
70 Ma	67	2.4	SBD	71.8	350.4	8.1	2.5	97	9.1	14
	67	3.2	SBDA	70.1	7.6	2.3	1.2	82	31.9	20
75 Ma	69	1.5	SBD	73.1	348.4	8.2	4.3	87	3.9	3
	70	1.5	SBDA	69.4	9.0	3.7	1.4	80	15.3	7

Data Type codes : S = sediment paleocolatitudes, B = basalt paleocolatitudes, D = seamount declinations, A = magnetic anomaly skewness

anomalies 27r-31 and 32 [Acton and Gordon, 1991; Petronotis and Gordon, 1999]. Effective inclination data from anomalies 27r-31 was split into two data sets because of the large age range, which included parts of the Paleocene and Maastrichtian. Effective inclinations for anomalies 27r-29r were used for the Paleocene pole calculations, whereas data from anomalies 29r-31were used in calculating the Maastrichtian pole. In the anomaly 32 data set, effective inclinations from the Pacific plate boundaries south of the equator were removed, so that only North Pacific data were used to calculate a skewness pole. This modification was done because the data from the South Pacific do not agree well with the North pacific data, unless significant anomalous skewness is assumed [Petronotis and Gordon, 1999]. Alternatively, this difference could be due to an unrecognized plate boundary in the southern Pacific plate [Acton and Gordon, 1994; Sager, in press].

In our final pole calculations, we excluded all of the skewness data because they cause the poles to shift and fall at the edges of the 95% confidence ellipses of poles calculated without skewness data. Furthermore, when the skewness data are included the χ^2 values of the poles are high, nearing the 95% confidence limit. We prefer poles without skewness data because they better represent the majority of the data and have χ^2 values that fall nearer to the middle of the 95% confidence limits for the appropriate degrees of freedom.

Pole age data were obtained from biostratigraphic zone and magnetostratigraphic chron estimates of the sediment cores [Gradstein et al., 2004], Ar^{40}/Ar^{39} radiometric

dating of basalt cores and most seamounts, and magnetic anomaly ages for skewness data and one seamount (Table 1).

Mean ages for each of the poles were calculated using weighted averages. The age data were weighted by their importances [Gordon and Cox, 1980], i.e., their weight in determining the location of the pole. The calculated datum importances were multiplied by the datum ages and then averaged to obtain the mean (Appendix A).

The data were grouped by age using stratigraphic epochs for the Paleogene poles and stratigraphic stage for the Maastrichtian pole. The Eocene data were further divided into late and early groups due to the long time span of this epoch.

In addition to grouping data by stratigraphic epoch, we also grouped in evenly-spaced time windows (Appendix A). The windows that worked best were 10 Myr in duration and spaced 5 Myr apart. This overlap in time allowed smoothing of the APWP by increasing data within each window. We prefer the poles calculated by stratigraphic epoch; however, because they are independent.

4. RESULTS

4.1. Paleomagnetic Poles

Combining these previously described data resulted in five mean paleomagnetic poles for the Oligocene through Maastrichtian (Table 2). The mean or combined poles, along with supplemental poles calculated from individual data types are shown in the figures on pages 19, 21, 23, 25, and 27, and in Table 2.

4.1.1. 30 Ma Oligocene Pole

The 30 Ma Oligocene pole (Fig. 3) was calculated from fifteen sediment and basalt paleocolatitudes (Table 2). SAM declination and effective inclination data are not available for this interval. Paleocolatitudes used to calculate the pole are from recent ODP cores as well as from DSDP and older piston cores (Table 1; Appendix A). The sediment pole calculated from ODP data agrees well with the sediment pole calculated from older piston/DSDP data, resulting in almost identical pole locations (Fig. 3). The basalt pole is located to the southeast of the sediment poles by 4-5° but its large 95% confidence ellipse encloses the latter. The combined pole calculated from both sediment and basalt data is located at 80.1°N, 24.4°E with a 95% confidence ellipse having major and minor semi-axes lengths of 6.1° and 2.6° and a major semi-axis azimuth of 91° (Fig. 3; Table 2). The combined pole age is 29.5 ±2.5 Ma (Appendix A).

4.1.2. 39 Ma Late Eocene Pole

The combined Late Eocene pole is located at 75.9°N, 17.3°E and has a 95% confidence ellipse with major and minor semi-axes of 10.2° and 4.3° and a major

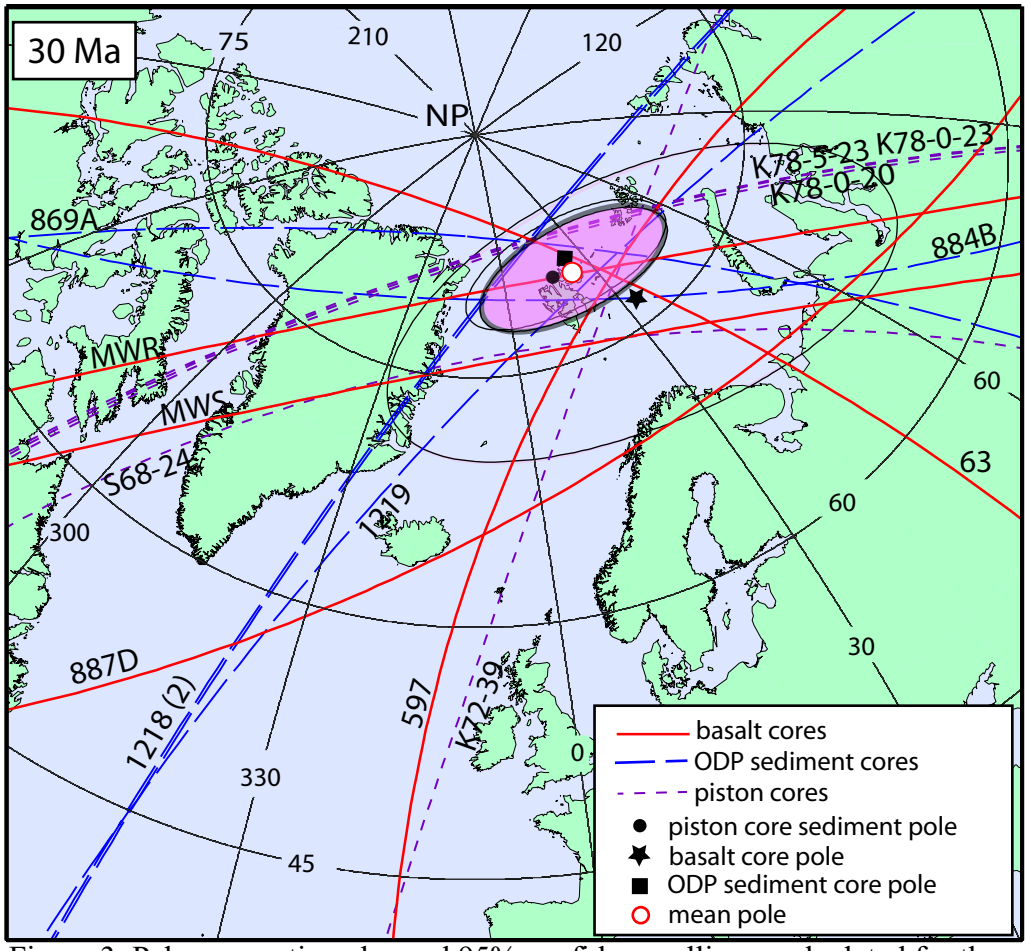

Figure 3. Paleomagnetic poles and 95% confidence ellipses calculated for the Oligocene epoch. Mean pole age is 30 Ma. Arcs represent loci of paleo-magnetic poles from azimuthally-unoriented cores. Red arcs are paleocolatitude arcs from basalt cores, long dashed blue lines are from ODP sediment cores; short dashed purple arcs denote sediment piston cores. Numbers give core names or DSDP/ODP site numbers (see Table 1). Open red circle represents mean pole from all data, filled square is pole calculated from ODP sediment cores only; filled black circle is pole calculated from DSDP/piston cores only; filled black star is basalt only pole.

semi-axis azimuth of 99° (Fig. 4; Table 2). The Late Eocene pole has an average age of 39.2 ± 2.3 Ma (Appendix A). The Late Eocene data group is composed of five piston and ODP sediment core paleocolatitudes and four SAM declinations. Poles were calculated for the sediment data only and for the sediment data and seamount declinations combined. Without the SAM data, the major semi-axis length of the uncertainty ellipse was 17.8°. Including the SAM data greatly reduced this uncertainty to 10.2°, but affected the combined pole location by less than 2° (Table 2).

4.1.3. 49 Ma Early Eocene Pole

The combined Early Eocene pole was calculated using paleocolatitudes from nine sediment and basalt cores and declinations from three SAMs. The combined pole for the Early Eocene is located at 73.1°N, 357.1°E and has a 95% confidence ellipse with a major semi-axis of 7.3°, a minor semi-axis of 3.3°, and an azimuth of 81° (Fig. 5; Table 2). The mean pole age is 48.6 ± 3.8 Ma (Appendix A). Some of the sediment cores in this time interval produced more than one mean paleocolatitude, so that overall, the mean pole is based on fourteen measurements of colatitude and declination (Table 2).

In addition to the combined pole calculated from sediment, basalt and SAM declinations, poles were also calculated from sediment only, basalt only, and sediment and basalt. Three of these four poles fall within a few degrees of each other, showing good agreement of the data (Table 2). The mean basalt pole is located ~15° east of the other poles; although its large 95% uncertainty ellipse encompasses the sediment and

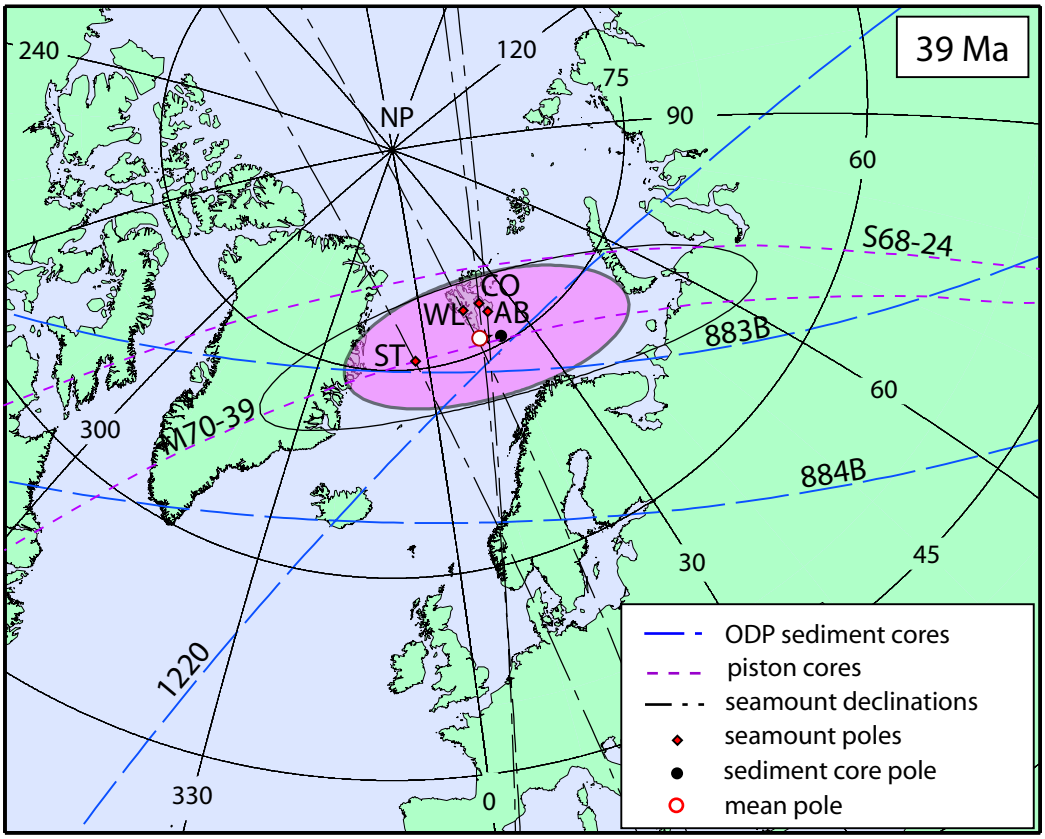

Figure 4. Paleomagnetic poles and 95% confidence ellipses calculated for the Late Eocene. Mean pole age is 39 Ma. Dash-dot arcs show declinations from seamount anomaly inversions (Table 1). Diamonds show seamount paleomagnetic pole locations (not used in calculations). Open red circle represents mean pole; filled black circle is pole calculated from ODP sediment and piston cores only. Other symbols as in Figure 3.

seamount data poles. The difference is mainly the result of having few basalt paleocolatitudes. In particular, the ODP Site 1224 paleocolatitude pulls the mean basalt pole eastward because it crosses the paleocolatitude arcs from Sites 430 and 1206 obliquely. The Site 1224 paleocolatitude has a large uncertainty because it was calculated from a small number (4) of independent units.

4.1.4. 61 Ma Paleocene Pole

Paleocene age data were used to calculate poles with and without skewness data. Two mean poles were calculated because the Paleogene and Maastrichtian skewness data plot to the east of other paleomagnetic data types of the same age. The Paleocene pole including skewness data is referred to as the combined pole with skewness and the pole without skewness is the combined pole without skewness. The combined pole with skewness has a mean age of 62 Ma and is located at 73.2°N, 3.9°E (Fig. 6; Table 2) and increases in age to 62.1 ± 3.0 Ma (Table A1). This pole was determined from data from twelve sediment and basalt paleocolatitudes from seven DSDP/ODP holes, two SAM declinations and skewness data from anomalies 25r and 27r-29r.

The combined pole without skewness has an average age of 61.1 ± 3.2 Ma located at 72.0°N, 344.9°E, 19.0° southwest of the pole including skewness. This combined pole without skewness has a 95% confidence ellipse with major and minor semi-axes of 17.5° and 3.0° and a major semi-axis azimuth of 95° (Fig. 6; Table 2, Appendix A). The 19.0° difference between these two Paleocene poles places the combined pole with skewness at the edge of the combined pole without skewness'

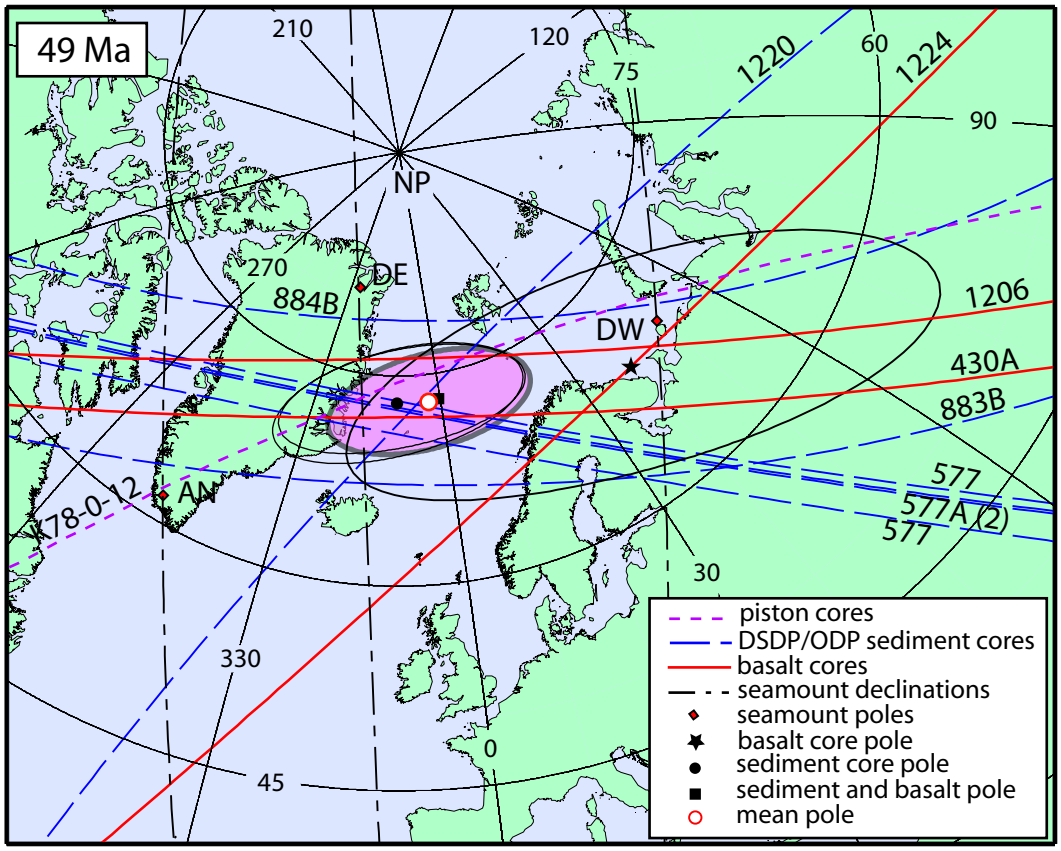

Figure 5. Paleomagnetic poles and 95% confidence ellipses calculated for the Early Eocene. Mean pole age is 49 Ma. Black filled square is pole calculated from basalt and sediment cores. Other lines and symbols are the same as for Figures 3 and 4; data from Table 1.

uncertainty ellipse, while the non-skewness pole is outside the uncertainties of the pole with skewness. We prefer the pole without skewness data because it is less dependent on the result of a single data type. Also, the skewness data cause the error ellipse to be unrealistically small. Poles were also plotted for the sediment and basalt data types individually. However, because the data sites for each type were located close together, their paleocolatitude arcs meet obliquely. This obliquity causes the sediment and basalt poles to have large error ellipses and plot away from the combined pole without skewness. The sediment pole plots to the east of the combined pole without skewness at 60.4°N, 33.9°E, but has an uncertainty ellipse large enough to include the combined pole. The basalt pole and its uncertainty ellipse plot off the map, with the pole located near the equator at 9.3°N, 108.8°E (Table 2).

4.1.5. 68 Ma Maastrichtian Pole

Two combined poles were also calculated for the Maastrichtian stage data to compare skewness data to the other data types. The 68 Ma combined paleomagnetic pole without skewness for the Maastrichtian stage includes three SAM declinations and seven sediment and basalt paleocolatitudes from six holes. This combined pole is located at 72.4°N, 350.2°E and has a 95% confidence ellipse with a major semi-axis of 8.8°, a minor semi-axis of 3.1°, and a major semi-axis azimuth of 94° (Fig. 7; Table 2). The combined pole age without skewness is 68.2 ± 1.5 Ma (Appendix A). In addition to the combined pole, sediment, and sediment plus basalt poles were calculated for the Maastrichtian. These poles both have locations inside the combined pole without

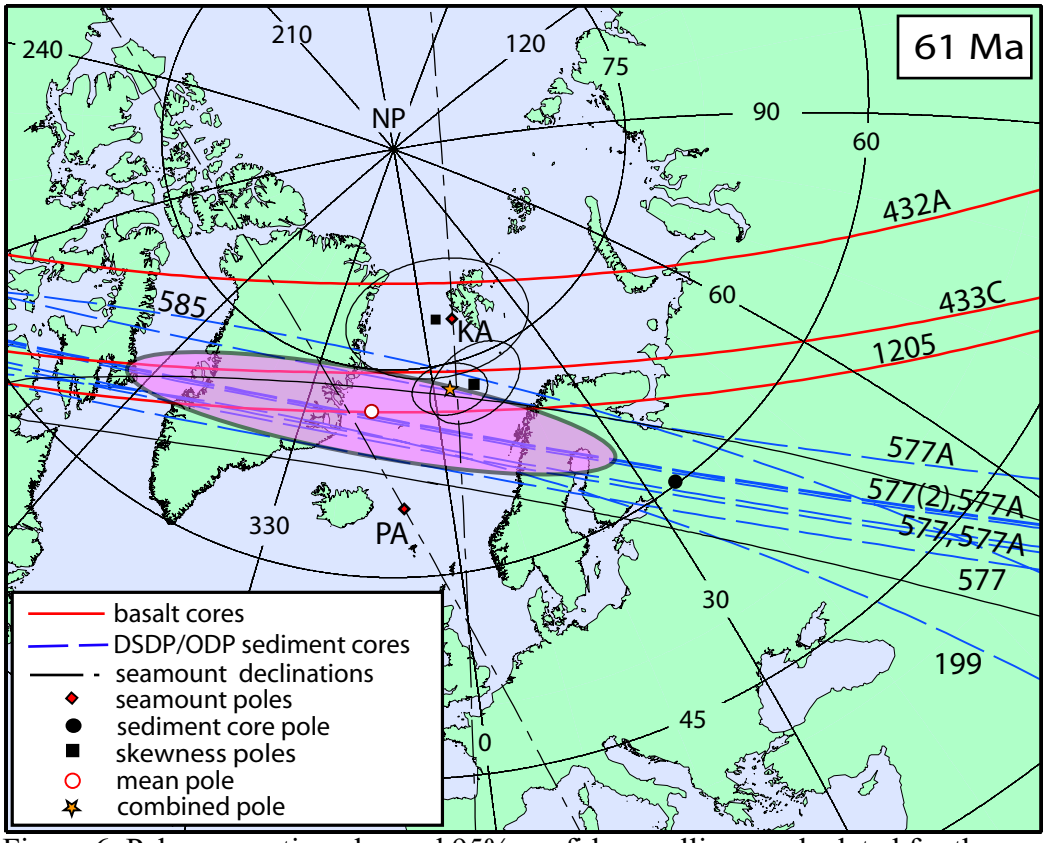

Figure 6. Paleomagnetic poles and 95% confidence ellipses calculated for the Paleocene epoch. Mean pole age 61 is Ma. Open red circle represents mean pole without skewness data, orange star is combined pole calculated from all data; filled black circle shows pole calculated from DSDP sediment cores; filled black squares are skewness poles recalculated from Petronotis et al. [1994] and Acton and Gordon [1991]; pole from basalt cores plots off of map. Other symbols and lines as in Figures 3 and 4.

skewness' 95% confidence ellipse at 72.0°N, 357.6°E and 72.2°N, 357.2°E, respectively (Table 2).

If we combine other data with skewness data from anomalies 29r-31 and 32, the pole position moves to 69.4°N, 8.6°E, southeast of the pole calculated without skewness data (Fig. 7; Table 2). The combined pole is also older than the mean pole with an average age of 69.6 ± 1.7 Ma (Table A1). Because the addition of the skewness data changes the pole location 18.6° to the southeast (Fig. 7), the combined pole with skewness falls at the edge of the combined pole without skewness' 95% confidence ellipse. The combined with skewness also has a large χ^2 value (at the edge of the 95% confidence limits) that indicates the skewness data violate the assumption that the data are χ^2 distributed; they do not correlate well with the other data. The combined pole with skewness also has an unrealistically small uncertainty ellipse. Due to the small uncertainties and the large effect of the skewness data on the pole locations, we prefer to use the combined poles excluding skewness data in the revised APWP.

4.2. New APWP

The five new mean paleomagnetic poles constitute a revised APWP for the Pacific plate for the Late Cretaceous to mid-Cenozoic (Figs. 1, 8). Combined with the 80 Ma pole from Sager [in press], we can now trace a detailed Late Cretaceous to mid-Cenozoic APWP from 80-30 Ma. We include the 80 Ma pole in this discussion because it is indistinguishable in location from many of the poles from this analysis. The revised

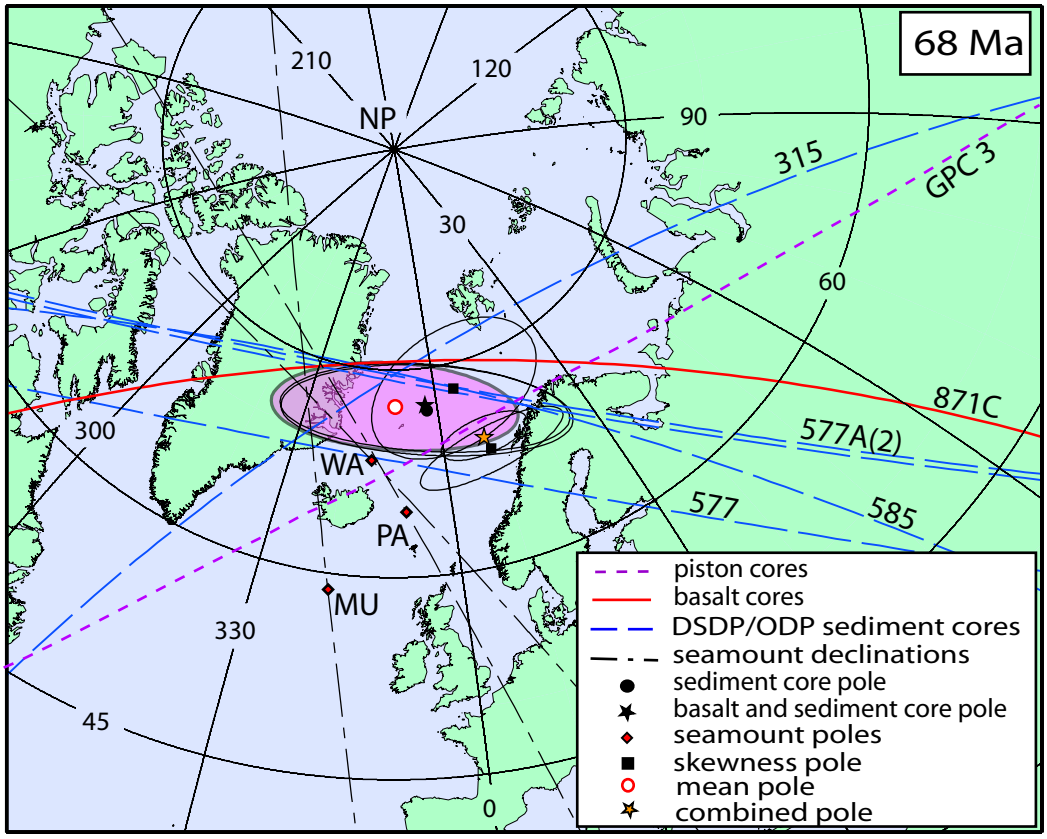

Figure 7. Paleomagnetic poles and 95% confidence ellipses calculated for the Maastrichtian stage. Mean pole age is 68 Ma. Open red circle represents mean pole without skewness data, orange star is combined pole calculated from all data; filled black squares are skewness poles modified from Acton and Gordon [1991] and Petronotis and Gordon [1999]; filled black circle is pole calculated from sediment cores only; filled black star is pole calculated from sediment and basalt cores. Other lines and symbols as in Figures 3 and 4.

APWP shows three phases of motion between 80 and 30 Ma (Fig. 8). Phase one of the APWP is a polar stillstand, in which there appears to be negligible polar drift from approximately 80 Ma until 49 Ma. Phase two (49 to 30 Ma) shows northeast polar drift. The data show this resumption of drift beginning sometime in the mid-Eocene, suggesting a change in Pacific plate motion during this time. Phase three begins at ~30 Ma, with the APWP shifting its polar drift direction from northeast (49-30 Ma) to north. This could possibly represent another shift in Pacific plate motion.

The time windowed APWP can be split into two paths prior to 50 Ma, one path calculated from all data and one path excluding the skewness data (Fig. 9; Table 2). In performing the time window analysis, a problem with the 55 Ma pole (excluding skewness data) was encountered. This 55 Ma pole plots far to the west of the other poles and has a significantly larger uncertainty. This discrepancy is an artifact caused by a window with few data from a limited area of the plate. In essence, the westward shift of the pole results from declination constraint being provided mainly by one seamount declination value (Annei seamount, Table 1).

The time window APWP without skewness data (excluding 55 Ma) is in good agreement with the APWP calculated from the five stratigraphic age poles. Because the time window poles contain a substantial data overlap between windows, adjacent poles are not independent. Because the five stratigraphic age poles are independent, it is a clearer representation of APWP trends and thus it is preferred.

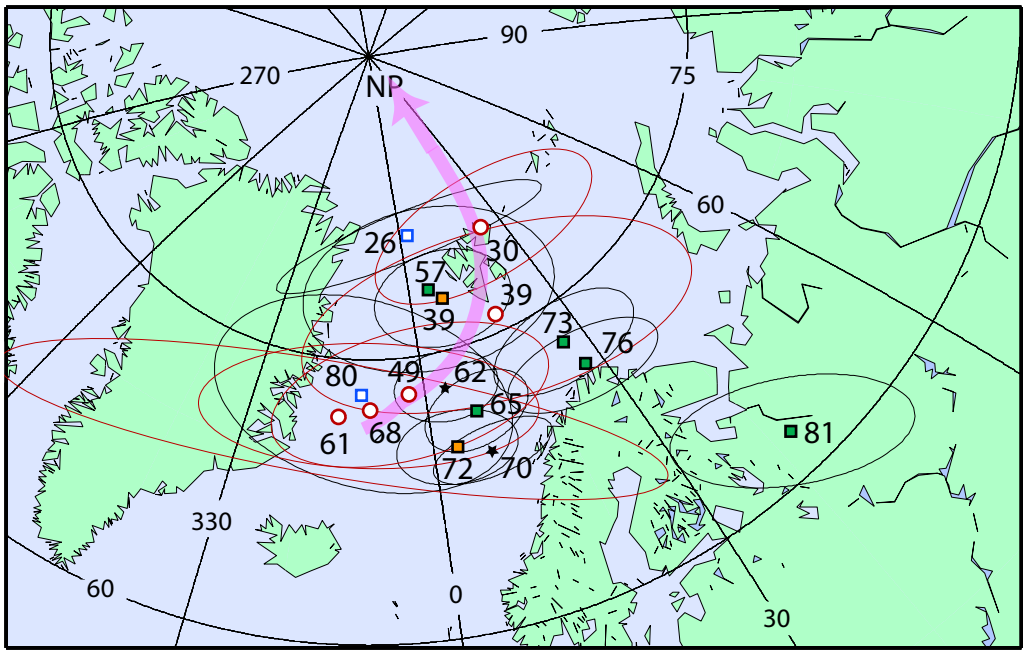

Figure 8. New APWP constructed from new mean paleomagnetic poles from this study (open red circles) and the 95% confidence ellipses (thin red ellipses). Mean poles combined with skewness are shown by filled black stars. Combined poles of Sager [in press] and Acton and Gordon [1994] denoted by open blue squares; filled green squares are skewness poles of Acton and Gordon [1991], Petronotis et al. [1994], Vasas et al. [1994] and Petronotis and Gordon [1999]; filled orange squares show seamount poles of Sager [1987] and Sager and Pringle [1988]; thin black ellipses are 95% confidence ellipses for combined, skewness, and seamount poles. Northward polar standstill can be observed in poles 80- 49 Ma.

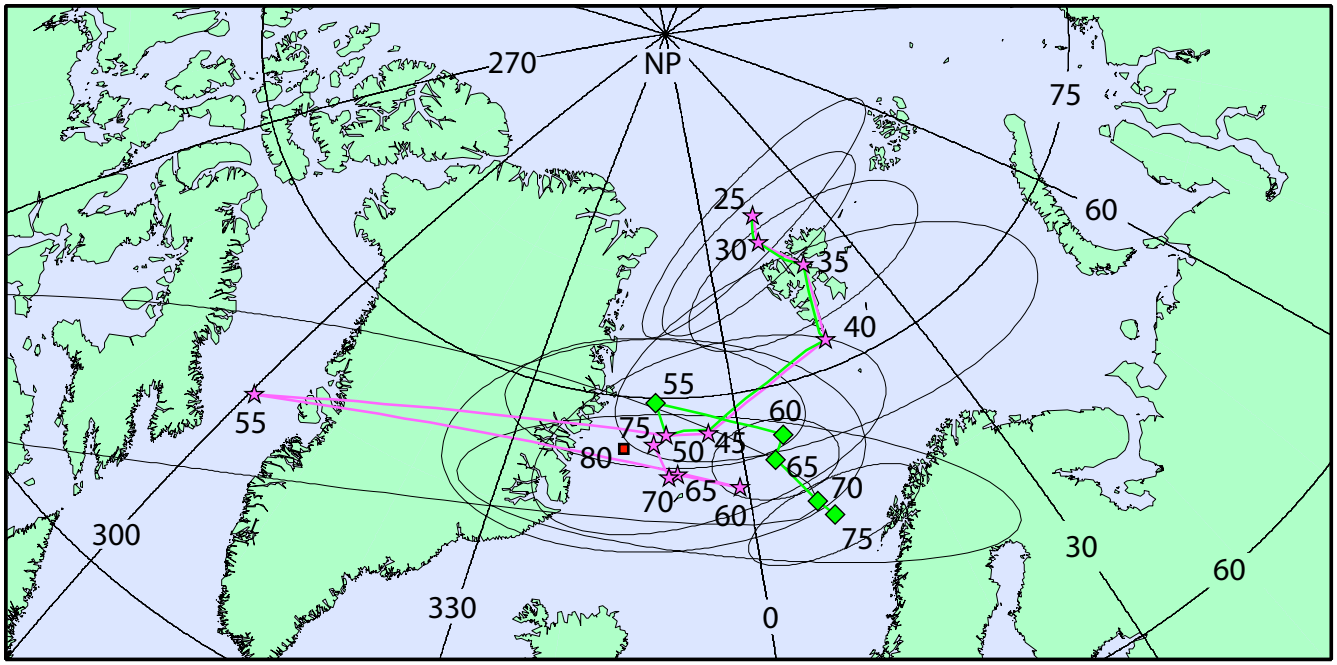

Figure 9. Time window (5 Myr center, 10 Myr width) APWP with paleomagnetic poles and selected 95% confidence ellipses for 25 to 75 Ma. Filled pink stars are poles that contain only sediment core, basalt core and seamount declination data; filled green diamonds are poles that also include skewness data. Plotted with combined 80 Ma pole from Sager [in press]. APWP diverges when skewness added prior to 50 Ma. Skewness poles are consistently located east of similar age non-skewness poles. 55 Ma pole is outlier artifact caused by sparse data in that window.

5. DISCUSSION

5.1. Paleomagnetic Data

Using a large data set consisting of sixty-five different estimates of the paleomagnetic pole, we have documented latest Cretaceous to mid-Cenozoic APW with unprecedented detail. Our calculations resulted in five independent poles (30, 39, 49, 61 and 68 Ma) determined from data groups spanning 26 to 72 Ma. The APWP suggests two significant changes in plate motion, one coincident with a change from stillstand (80-49 Ma) to northeast APW (49-30 Ma) and another from northeast to northward APW after ~30 Ma.

We had hoped to eliminate much of the older paleocolatitude data from the pole calculations due to poor documentation and the past use of blanket demagnetization techniques. In spite of this, in reexamining older data such as that from Epp et al. [1983], Prince et al. [1980], and Grommé and Vine [1972], we found the older data in good agreement with the newer data. Exclusion of the older data resulted in less robust pole calculations for the Oligocene and Late Eocene, and since the data agreed, the older data are retained.

Paleocolatitude estimates from sediment cores are distrusted by some authors [Tarduno, 1990; Gordon, 1990] due to the possibility of shallowing of the inclination from compaction [Anson and Kodama, 1987]. Because 58% of our data are from sediments, we could not ignore these data and still calculate a detailed APWP. Due to these concerns, we carefully examined the sediment paleocolatitude data for bias. In order to test our data for inclination shallowing, mean poles were calculated for data

from north and south of the equator because the paleocolatitudes from each hemisphere are biased in different directions.

When poles were calculated from stillstand (80-40 Ma) sediment data, 4° of separation (with overlapping 95% confidence ellipses) was observed between the northern and southern hemisphere sediment poles (Fig. 10). This separation translates into 2° mean paleolatitude difference (~ 4° inclination shallowing). The effects of the shallowing on our interpretation of the data are minimal for three reasons. First, because the sediment paleocolatitudes are averaged with others from across the equator, the bias from north and south will tend to offset. For example, the ratio of sediment paleocolatitudes from the northern to southern hemisphere ranges from a best of 3:2 in the Oligocene to a worst of 7:2 in the Paleocene. Second, the mean poles are not based solely on sediment data, but also include basalt paleocolatitudes that are not biased by inclination shallowing. Lastly, although this effect may change mean pole locations slightly, it is unlikely that the sediment paleocolatitudes result in the observed features of the APWP These findings suggest that, at least in this data set, inclination shallowing may not be as significant a problem as previously thought. However, it is important to note that many of our sediment cores come from low latitude sites where inclination shallowing tends to be small.

Because they come from azimuthally-unoriented cores, sediment and basalt paleocolatitude data both suffer from a lack of declination control which results in mean pole positions having large uncertainties perpendicular to a line between the site and the

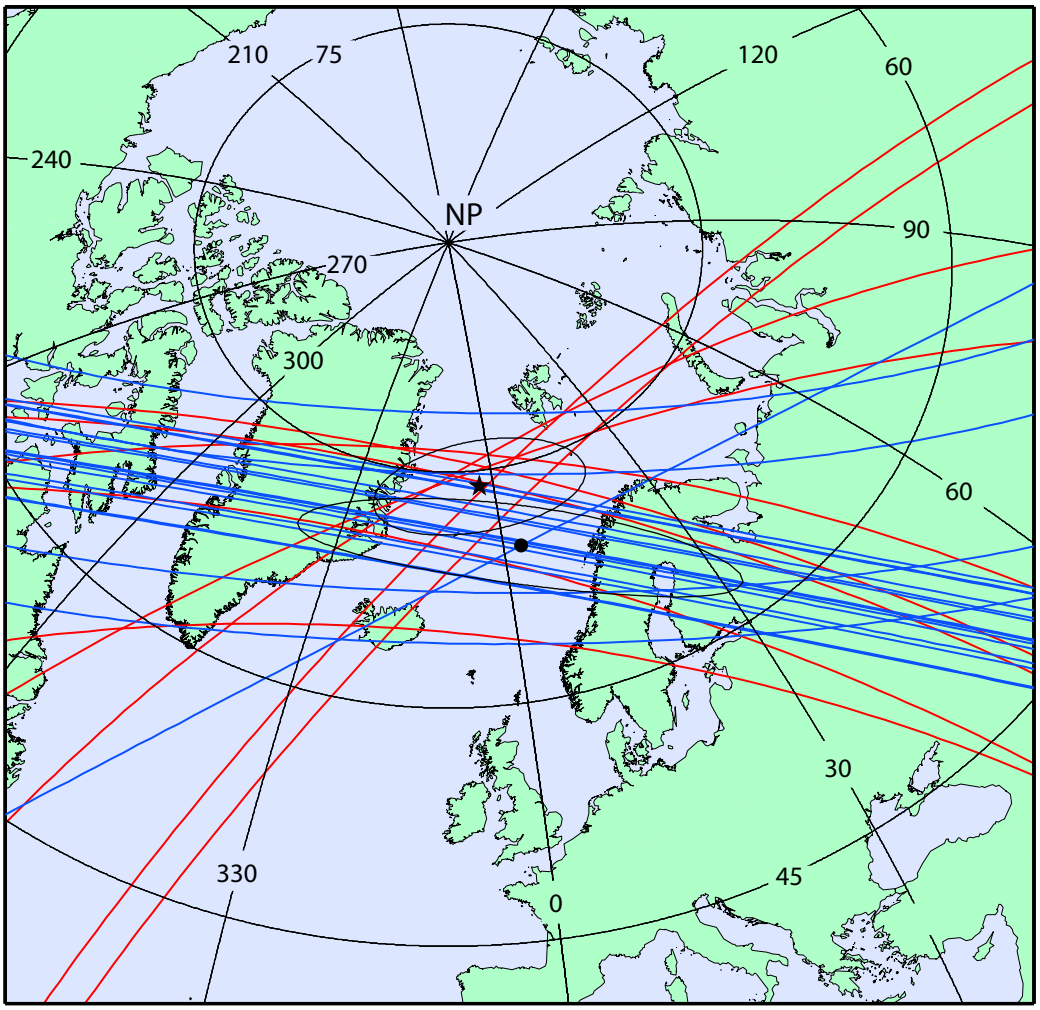

Figure 10. Paleomagnetic poles and 95% confidence ellipses for sediment paleo-colatitude data from the stillstand (40 Ma to 80 Ma). Blue lines are colatitudes < 90˚ (deposited north of the equator); red lines are sediment colatitudes > 90˚ (deposited south of the equator). Filled star is pole from southern hemisphere sediment colatitudes; filled circle represents pole for northern hemisphere sediment colatitudes. The difference in latitude between the northern and southern hemisphere poles is 4˚, with siginificant overlap in their uncertainties. The mean poles for the Early Eocene, Paleocene and Maastrichtian are located (latitudinally) between these two sediment poles.

pole. One way to overcome this problem is a data set of large longitudinal extent (e.g., the Oligocene data set). However, existing Pacific data are often limited in extent, coming from sites in the Western Pacific and resulting in high aspect ratio error ellipses with poor longitude control. Rather than accept this limitation, we used SAM declinations to decrease the uncertainties in pole longitude.

Although there are concerns about the fidelity of SAM data, the introduction of these data into the pole calculations never changes the pole location by more than a few degrees (i.e., the data agree well) whereas it helps reduce the longitude uncertainty considerably. Because we lacked a good estimate of standard error for the SAM declination (a quantity used to determine the uncertainty ellipse), we made an estimate (10.6°) from the distribution of declinations for all the SAMs included in the data set. The assignment of this uncertainty is arbitrary because there is not a theoretical or observational method to produce a better error estimate; however, we consider it to be conservatively large. A better estimate of SAM declination uncertainty is desirable, but currently not available. Our choice mainly affects the major semi-axes of the uncertainty ellipses, but does not significantly affect the APWP or our interpretation.

Although most of the data in this study are in good agreement, skewness data are notable outliers. Late Cretaceous skewness poles consistently plot to the east of the poles calculated from basalt, sediment and seamount data [Acton and Gordon, 1991; Petronotis et al., 1994; Petronotis and Gordon, 1999; Sager, 2003; Sager in press]. Because the skewness poles yield small uncertainty ellipses, the skewness poles tend to pull the combined poles to the east. The eastward offset trend increases with increasing

skewness pole age (Fig. 1, 8). The significance of this discrepancy is unclear since many of the uncertainty ellipses overlap significantly and some of the older skewness poles are poorly documented. This offset caused us to exclude skewness data for the calculation of the Paleocene and Maastrichtian combined poles.

5.2. New APWP

The revised APWP exhibits some important differences from previous APWPs of the Pacific plate. The most significant difference is the observation of three phases of polar motion from 80 Ma to 30 Ma, rather than a continuous north polar drift suggested by previous APWPs [Sager and Pringle, 1988; Parés and Moore, 2005].

The observed standstill between 80 and 49 Ma indicates that the Euler pole of rotation for the Pacific plate was located near the Earth's spin axis, implying that the Pacific plate experienced either no motion or only east-west motion during this period. Given the connection of the Pacific plate to subduction zones in the Western Pacific, the plate was likely moving rapidly, as it does today, with the motion being westward. Motion of the plate towards western Pacific subduction zones can be explained by having either ridge or transform margins on the Pacific's north, south and eastern margins during this time. Examination of the configuration of the Pacific's plate boundaries from magnetic anomalies and plate reconstructions shows this scenario is plausible [Engbretson et al., 1985; Lonsdale, 1988; Raymond et al., 2000; Lawver et al., 2003].

Changes in Pacific plate motion may be related to a clockwise northeastward propagation of the western Pacific's subduction boundary. During the Late Paleocene

and Early Eocene, subduction of the Pacific plate migrated from the western Pacific to the northeast as increasing amounts of the Kula plate were subducted by the Kuril-Kamchatka and Bering Sea subduction zones. This led to eventual destruction of the Pacific-Kula plate boundary during the mid-Eocene [Lonsdale, 1988; Harbert et al., 1998]. Once the Kula-Pacific ridge was subducted, the Pacific plate would have begun subduction in the Aleutian trench, pulling the plate more northward. This shift to northward pull on the Pacific plate is shown not only in the subduction zone migration from the Bering Sea to the Aleutian Trench (50- 55 Ma) [Scholl et al., 1986] but also as a change in Pacific-Farallon motion (49-53 Ma) [Atwater, 1989] and cessation of the Kula-Pacific spreading center [Byrne, 1979]. The onset of northward pull from subduction in the Aleutian trench apparently coincides with the transition from the first phase (standstill) to the second phase as APW resumed at ~49 Ma, tracking northeast.

The last phase of motion observed in the Pacific APWP begins with a shift to north drift after ~30 Ma. The exact timing of the shift is unclear, due to a lack of younger poles, but likely reflects a shift to modern plate motions. It is consistent with the APWP of Parés and Moore [2005]. This shift may be related to the subduction of the Pacific-Farallon ridge under the North American Plate and development of the San Andreas Fault transform boundary at ~33 Ma [Atwater, 1989; Norton, 1995].

This revised APWP demonstrates that each phase of APW can be linked to significant tectonic events and boundary reorganizations occurring at the edges of the Pacific, as expected with edge forces driving the plate and slab pull acting as the major

plate driving force. Prior Pacific APWPs lacked the detail between 80 and 30 Ma to delineate these transitions in Pacific plate motions.

5.3. Hotspot Motion

For years, the Emperor Chain was thought to record plate motion over the fixed Hawaiian-Emperor Hotspot. Specifically, the Emperor Chain has been viewed as evidence of rapid northward drift of the Pacific plate during the Late Cretaceous and Early Cenozoic. Indeed, this view has been so ingrained, it is included in most western Pacific tectonic models, in which the hotspot-predicted APWP shows significant northward Late Cretaceous and Early Cenozoic motion (~80 to 40 Ma) [Hilde, 1977; Morgan, 1971, 1972; Engebretson et al., 1984; Duncan and Clague, 1985; Engbretson et al., 1985; Fleitout and Moriceau, 1992; Wessel and Kroenke, 1997; Harada and Hamano, 2000; Raymond et al., 2000] (Figure 11A).

However, some authors have suggested that the Hawaiian-Emperor Chain does not show plate motion over a fixed hotspot [i.e., Molnar and Atwater, 1973; Norton, 1995; Tarduno and Cottrell, 1997; Raymond et al., 2000]. This is supported by recent paleomagnetic results from ocean drilling that imply significant southward motion of the hotspot [Tarduno et al., 2003]. The revised APWP also disagrees with the fixed hotspot model (before 39 Ma) and suggests that the north-south extent of the chain does not represent northward Pacific plate motion (Figure 11B). This discrepancy between the hotspot models and the APWP is result of the observed polar standstill (80 Ma to 49 Ma) coinciding with the formation of the Emperor Chain. The stillstand suggests negligible

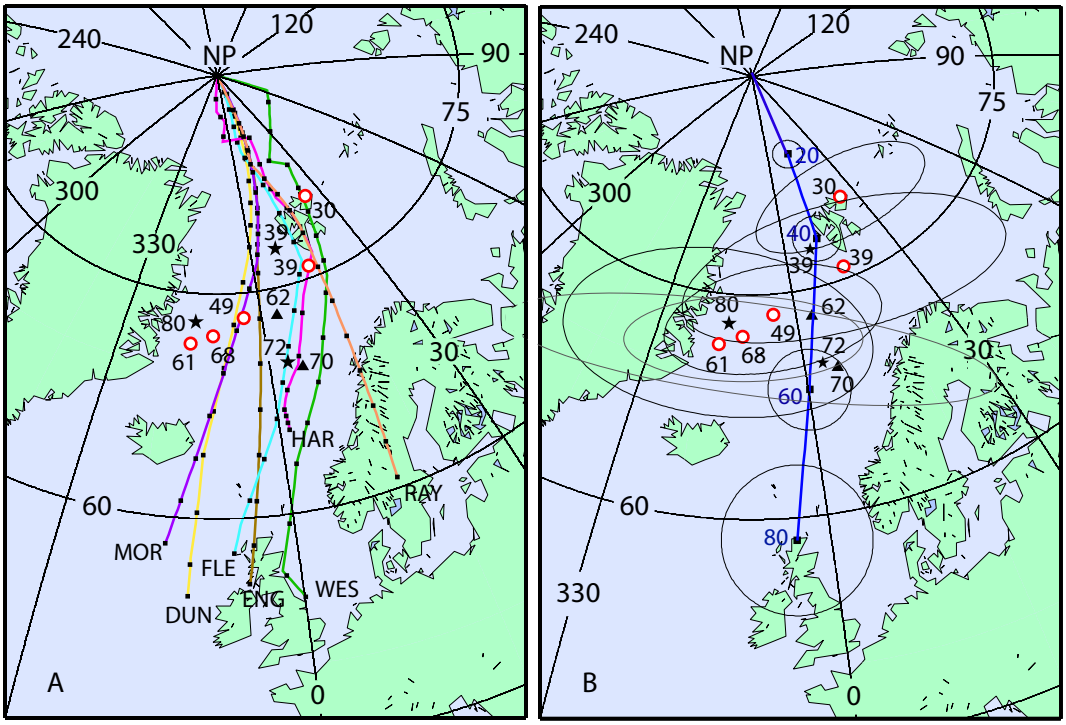

Figure 11. A) Paleomagnetic poles compared to published APWPs predicted for the Pacific plate from hotspot models. [Morgan, 1971, (MOR); Duncan and Clague, 1985, (DUN); Engebretson et al., 1985, (ENG); Fleitout and Moriceau,1992, (FLE); Wessel and Kroenke, 1997, (WES); Harada and Hamano, 2000, (HAR); Raymond et al., 2000, (RAY)]. Each dot along the APWPs represents 5 Myr. B) Paleomagnetic poles and average predicted hotspot track (calculated from average of models in (A) for the Pacific plate (filled blue squares). Circles at 20, 40, 60, and 80 Ma show α 95 confidence limits. Predicted hotspot tracks diverge from APWP during the 80-49 Ma stillstand.

northward motion of the plate during the formation of the Emperor Chain; therefore, the observed northward extent of the chain must have resulted from southward motion of the volcanic source. Alternatively, true polar wander (TPW), i.e., or changes in the hotspot latitude due to movement of the spin axis, could also contribute to the observed motion of the hotspot [Gordon and Cape, 1981].

The discrepancy of the fixed hotspot estimates (Figure 11), with paleomagnetic data suggests between 5° and 20°of hotspot drift [Harada and Hamano, 2000; Duncan and Clague, 1985; Wessel and Kroenke, 1997]. The fixed hotspot model calculated by Harada and Hamano [2000], corresponding the least amount of hotspot drift, most closely resembles the APWP calculated from the paleomagnetic data. This model's track may also indicate a northward stillstand prior to 65 Ma (Figure 11A) as its track from 65-70 Ma shows negligible motion. However, because Harada and Hamano's [2000] model is poorly constrained before 70 Ma, interpreting the hotspot model for this time period is problematic.

Although Tarduno et al. [2003] do not list specific drift estimates for motion of the hotspot over the last 80 Ma, Figure 3 of their paper suggests an average of 15° (8° to 19°) of drift between the latitude of Detroit seamount (76-81 Ma) and the latitude of the Hawaiian-Emperor bend (that of present day Hawaii). Tarduno et al. [2003] also give motion rates for two preferred models, A and B, of 57.7 ± 19.2 mm/yr and 43.1 ± 22.6 mm/yr, respectively. If these rates are applied to the north-south extent of the Emperor Chain (81 to 47 Ma) they give northward drift estimates of between 6° and 24°. Paleomagnetic data in this study indicate that the Hawaiian-Emperor Hotspot may have

moved south by 20° (the latitude extent of the Emperor Chain) from 81-47 Ma. Thus, our data are in agreement with the southward drift estimates of Tarduno et al. [2003]; however, our data suggest the higher estimates may be more accurate. Similar to Tarduno et al. [2003], our study suggests most hotspot motion occurred prior to 47 Ma, with small latitudinal change since that time.

6. CONCLUSIONS

Five paleomagnetic poles were calculated for the latest Cretaceous and Early Cenozoic for 30, 39, 49, 61 and 68 Ma. Improvement of the APWP was possible because it was compiled from a large data set consisting of sixty-five sediment core paleocolatitudes, basalt core paleocolatitudes, SAM declinations and magnetic anomaly skewness data. The first three data types showed relatively good agreement, with Late Cretaceous skewness data as notable outliers.

One significant result was the agreement of basalt core data with sediment core data paleocolatitudes. The agreement of these two data sources suggests that shallowing effects on sediments may be less severe than previously thought, at least in this data set [Tarduno, 1990; Gordon, 1990]. Our analysis suggests ~2° mean paleolatitude error and shallowing effects are mitigated here because sediment paleocolatitudes from both north and south of the equator are averaged, tending to cancel the shallowing errors. The inclusion of other data types in the pole calculations reduces the bias of inclination shallowing on the pole locations.

Because of the improved detail, three phases of APW motion were observed in the APWP. The first phase, a stillstand, was observed in the APWP from 80 to 49 Ma. In phase two, from 49 to 30 Ma, the APW resumed with motion to the northeast and phase three begins at 30 Ma with APW shifting from the northeast to the north. The stillstand indicates negligible northward motion, with probable motion to the west due to the subduction of the Pacific plate in western Pacific subduction zones. The end of the stillstand in the mid-Eocene is coincident with the connection of the Pacific plate into

the Aleutian trench and initiation of northward pull on the plate from subduction. The change in motion from northeast motion to northward drift at ~30 Ma may be related to the continued clockwise rotation of subduction or development of the eastern Pacific transform plate boundary with the North American plate.

The identification of the APW stillstand during the formation of the Emperor Chain suggests the Hawaiian hotspot drifted south ~20° since 81 Ma, with the majority of motion occurring before 47 Ma. This drift estimate is consistent with that made from ocean drilling cores from the Emperor Chain and argues against long term fixity of the Hawaiian hotspot.

REFERENCES

Acton, G. D. and R. G. Gordon, A 65 Ma paleomagnetic pole for the Pacific plate from the skewness of magnetic anomalies 27r-31, *Geophys. J. Intl.* 106, 407-420, 1991.

Acton, G. D. and R. G. Gordon, Paleomagnetic tests of Pacific plate reconstructions and implications for motion between hotspots, *Science* 263, 1246-1254, 1994.

Anson, G.L. and. K. P. Kodama, Compaction-induced inclination shallowing of the post-depositional remanent magnetization in a synthetic sediment, *Geophys. J. R. Astr. Soc.* 88, 673-692, 1987.

Atwater, T., Plate tectonic history of the northeast Pacific and western North America, in *The Geology of North America, Vol. N, The Eastern Pacific Ocean and Hawaii*, edited by E. L. Winterer, D. M. Hussong, and R.W. Decker, Geol. Soc. Am 21-72, 1989.

Barron, J.A., I.A. Basov, L. Beaufort, G. Dubuisson, A.Y. Gladenkov, J.J. Morley, M. Okada, G. Ólafsson, D.K. Pak, A.P. Roberts, V.V. Shilov, and R.J. Weeks, Biostratographic and magnetostratigraphic summary, *Proc. ODP Sci. Results 145,* edited by D.K. Rea, I.A. Basov, D.W. Scholl and J.F. Allan, Ocean Drilling Program, College Station, TX, 559-576, 1995.

Besse, J. and V. Courtillot, Apparent and true polar wander and the geometry of the geomagnetic field over the last 200 Myr, *J. of Geophys. Res*., 107, B11, 2300, doi: 10.1029/2000JB000050, 2002.

Bijaksana, S. and J.P. Hodych, Comparing remanence anisotropy and susceptibility anisotropy as predictors of paleomagnetic inclination shallowing in turbidites from the Scotian Rise, *Phys. Chem. Earth* 22, 189-193, 1997.

Bleil, U., The magnetostratigraphy of northwest Pacific sediments, Deep Sea Drilling Project Leg 86, in *Init. Repts. DSDP 86,* edited by G.R. Heath, L.H. Burckle, et al., US Govt. Printing Office, Washington, DC, 441-458, 1985.

Blow, R.A. and N. Hamilton, Effect of compaction on the acquisition of a detrital remanent magnetization in fine-grained sediments, *Geophys. J. R. Astr. Soc*. 52, 13-23, 1978.

Bracey, D. R., Reconnaissance survey of the Caroline Basin, *Geo. Soc. Am. Bull*. 86, 6, 775-7842002, 1975.

Byrne, T., Late Paleocene demise of the Kula-Pacific spreading center, *Geology* 7, 341-344, 1979

Cande, S.C., A paleomagnetic pole from Late Cretaceous marine magnetic anomalies in the Pacific, *Geophys J. R. Astron. Soc.*, 44, 547-566, 1976.

Cande, S.C. and D.V. Kent, A new geomagnetic polarity time scale for the Late Cretaceous and Cenozoic, *J. Geophys. Res*., 97, 13917-13951, 1995.

Cockerham R.S. and R.D. Jararrd, Paleomagnetism of some Leg 33 sediments and basalts, in *Init. Rep. DSDP 33*, edited by S.O. Schlanger, E.D. Jackson, et al., US Govt. Printing Office, Washington, DC, 631-644, 1976.

Cox, A. and R.G. Gordon, Paleolatitudees determined from paleomagnetic data from vertical cores, *Rev. Geophys. and Space Phys.*, 22-1, 47-72, 1984.

Dalrymple, G.B., D.A. Clague, and M.A. Lanphere, Revised age for Midway Volcano, Hawaiian Volcanic Chain, *Earth Planet. Sci. Let.* 37 (1), 107-116, 1977.

Dalrymple, G.B., M.A. Lanphere, D.A. Clague, Conventional and $^{40}Ar/^{39}Ar$ K-Ar ages of volcanic rocks from Ojin (Site 430), Nintoku (Site 432), and Suiko (Site 433) seamounts and the chronology of volcanic propagation along the Hawaiian-Emperor Chain, *Init. Repts. DSDP 55*, US Govt. Printing Office, Washington DC, 659-676, 1980.

Day, R., M..D. Fuller and V.A. Schmidt, Hysteresis properties of titanomagnetites: Grain size and composition dependence, *Phys. Earth Planet. Init.*,13, 260-267, 1977.

Deamer G.A. and K.P. Kodama, Compaction induced inclination shallowing in synthetic and natural clay-rich sediments, *J. Geophys. Res*. 95, 4511-4529, 1990.

Duncan, R.A. and D.A. Clague, Pacific plate motion recorded by linear volcanic chains, in *The Ocean Basins and Margins,* 7A, edited by A.E.M. Nairn, F.G. Stehli, and S. Uyeda, Plenum, New York, 1985.

Duncan, R.A. and R.A. Keller, Radiometric ages for basement rocks from the Emperor Seamounts, ODP Leg 197, [Online] *Geochem., Geophys., Geosys.* 5, Art. No. Q08L03 Aug 11 2004, 2004.

Dunlop, D.J., Magnetic mineralogy of heated and unheated red sediments by coercivity spectrum analysis, *Geophys. J. R. Astron. Soc.*, 27, 37-55, 1972.

Dyment, J. and J. Arkani-Hamed, Spreading-rate-dependent magnetization of the oceanic lithosphere inferred from the anomalous skewness of marine magnetic anomalies, *Geophys. J. Int*. 121, 789-804, 1995.

Engebretson, D.C., A.Cox, and R.G. Gordon, Relative motions between oceanic plates of the Pacific Basin, *J. Geophys. Res.*89 (B12), 10291-10310, 1984.

Engebretson, D.C., A. Cox, , and R.G. Gordon, Relative motions between oceanic and continental plates in the Pacific Basin, *Geo. Soc Am. Spec. Paper* 206, 1985.

Epp, D., W. W. Sager, F. Theyer, and S. R. Hammond, Hotspot-spin axis motion or magnetic far-sided effect?, *Nature* 303, 318-320, 1983.

Firth, J.V. Data report: Cenozoic calcareous nannofossils of Hole 869A, equatorial Pacific Ocean, *Proc. ODP Sci Results 143,* edited by E.L. Winterer, W.W. Sager, J.V. Firth, and J.M. Sinton, Ocean Drilling Program, College Station, TX, 567-570, 1995.

Fisher, A.T., K. Becker, P.D. Rabinowitz, J. Baldauf, and T.J.G. Francis, A guide to ODP tools for downhole measurements, Ocean Drilling Program, Texas A&M University, Technical Note 10, (http:www-odp.tamu.edu/publications/tnotes/tn10/10toc.html), 1993.

Fleitout, L., and C. Moriceau, Short-wavelength geoid, bathymetry and the convective pattern beneath the Pacific Ocean, *Geophys, J. Intl.* 110, 6-28, 1992.

Gee, J., L. Tauxe, , J.A. Hildebrand, H. Staudigel, and P. Lonsdale, Nonuniform magnetization of Jasper Seamount, *J. Geophys. Res.* 93 (B10) 12159-12175, 1988.

Gee. J., H. Staudigel, and L. Tauxe, Contriubution of induced magnetization to magnetization of seamounts, *Nature* 342, 170-173, 1989.

Gordon, R. G. and A.Cox, Calculating paleomagnetic poles for oceanic plates, *Geophys. J. R. Astr. Soc*., 63, 619-640, 1980.

Gordon, R.G. and C.D. Cape, Cenozoic latitudinal shift of the Hawaiian hotspot and its implications for true polar wander, *Earth Planet. Sci. Let.*, 55 (1), 37-47, 1981.

Gordon, R. G., The Late Maastrichtian paleomagnetic pole of the Pacific plate, *Geophys. J. R. Astr. Soc.* 70 (1), 129-140, 1982.

Gordon, R. G., Polar wandering and paleomagnetism, *Annu. Rev. Earth Planet. Sci*., 15, 567-593, 1987.

Gordon, R., Test for bias in paleomagnetically determined paleolatitudes from Pacific plate Deep Sea Drilling Project sediments, *J. Geophys Res.*, 95, B6, 8397-8404, 1990.

Gradstein, F.M., J.G. Ogg, A.G. mith, F.P. Agterberg, W. Bleeker, R.A. Cooper, V. Davydov, P. Gibbard, L.A. Hinnov, M.R. House, L. Lourens, H.P. Luterbacher, J. McArthur, M.J. Melchin, L.J. Robb, J. Shergold, M. Villeneuve, B.R. Wardlaw, J. Ali, H. Brinkhuis, F.J. Hilgen, J. Hooker, R.J. Howarth, A.H. Knoll, J. Laskar, S. Monechi, K.A. Plumb, J. Powell, I. Raffi, U. Röhl, P. Sadler, A. Sanfilippo, B. Schmitz, N.J. Shackleton, G.A. Shields, H.Strauss, J. Van Dam, T. van Kolfschoten, J. Veizer, and D. Wilson, *A Geologic Time Scale 2004*, Cambridge University Press, Cambridge, 589 p., 2004.

Grommé, S. and F.J. Vine, Paleomagnetism of Midway atoll lavas and northward movement of Pacific plate, *Earth Planet. Sci. Let.* 17 (1), 159-168, 1972.

Harada, Y.Y. and Y. Hamano, Recent progress on the plate motion relative to hotspots. in *The History and Dynamics of Global Plate Motion* ,edited by M. A. Richards, R. G. Gordon, and R.D. van der Hilst, *Geophys. Mono. 121*, AGU, 327-338, 2000.

Harbert, W., P. Kepezhinskas, K. Krylov, V. Grigoriev, S. Sokolov, M. Aleksuitin, A. Heiphetz, and P. Layer, Paleomagnetism and tectonics of the kamchatka region, northeastern Russia: Implications for development and evolution of the northwest Pacific Basin, *Polarforschung* 68, 297-308 , 1998 (publ. 2000).

Harrison, C.G.A., R.D. Jarrard, V. Vaquier, and R.L. Larson, Paleomagnetism of Cretaceous Pacific seamounts, *Geophys. J.R. Astr. Soc*., 42 (3), 859-882, 1975.

Hekel, H., Nannofossil biostratigraphy, Leg 20, DSDP, in *Init. Repts. DSDP 20*, edited by B.C. Heezen, I.D. MacGregor, et al., US Govt Printing Office, Washington, DC, 221-248, 1973.

Hilde, T.W.C., S. Uyeda, L. Kroenke, Evolution of western Pacific and its margin, *Tectonophysics* 38 (1-2), 145-165, 1977.

Hodych, J.P. and S. Bijaksana, Can remanence anisotropy detect paleomagnetic inclination shallowing due to compaction? A case study using Cretaceous deep-sea limestones, *J. Geophys. Res*. 98, 22429-22441, 1993.

Hodych, J. P., S. Bijaksana, and R. Pätzold, Using magnetic anisotropy to correct for paleomagnetic inclination shallowing in some magnetite-bearing deep-sea turbidites and limestones, *Tectonophysics,* 307, 191-205, 1999.

Hrouda, F., Magnetic-anisotropy of rocks and its application in geology and geophysics, *Geophysical Surveys* 5 (1), 37-82, 1982.

Jackson, M.J., S.K. Banerjee, J.A.Marvin, R. Lu, and W. Gruber, Detrital remanence inclination errors and anhysteretic remanence anisotropy: quantitative model and experimental results, *Geophys. J. Intl.* 104, 95-193, 1991.

Jelínek, V., *The Statistical Theory of Measuring Anisotropy of Magnetic Susceptibility of Rocks and its Applications*, 88 pp, Geofysika, Brno, Czechoslovakia, 1977.

Keller, R. A., R. A. Duncan, and M. R. Fisk, Geochemistry and $^{40}Ar/^{39}Ar$ Geochronology of basalts from ODP Leg 145 (north Pacific transect), *Proc. ODP, Sci. Results, 145,* edited by D.K. Rea, I.A. Basov, D.W. Scholl, and J.F. Allan, Ocean Drilling Program, College Station, TX 77843, 333-344, 1995.

Kirschvink, J.L., The least squares line and plane and the analysis of paleomagnetic data, *Geophys. J. R. Astr. Soc.* 62 (3), 699-718, 1980.

Kodama, K.P. and W. W. Sun, SEM and magnetic fabric study of a compacting sediment, *Geophys. Res. Let.*, 17, 795-798, 1990.

Kodama, K.P. and W. W. Sun, Magnetic anisotropy as a correction for compaction-caused paleomagnetic inclination shallowing, *Geophys. J. Intl.*, 111, 465-469, 1992.

Kono, M., Paleomagnetism of DSDP Leg 55 basalts and implications for the tectonics of the Pacific plate, *Init. Repts. DSDP 55*, US Govt. Printing Office, Washington, DC, 737-752, 1980.

Koppers, A.A. P., H. Staudigel, and J.R. Wijbrans, Dating crystalline groundmass separates of altered Cretaceous seamount basalts by the $^{40}Ar/^{39}Ar$ incremental heating technique, *Chemical Geology* 166, 1-2, 139-158, 2000.

Koppers, A.A.P., H. Staudigel, Asynchronous bends in Pacific seamount trails: A case for extensional volcanism, Science 307 (5711), 904-907, DOI: 10.1126/science.1107260, 2005.

Lanci, L., J.M. Parés, , J.E.T. Channell, and D.V. Kent, Oligocene magnetostratigraphy from equatorial Pacific sediments (ODP Sites 1218 and 1219, Leg 199), *Earth Planet. Sci. Let*. 237 (3-4), 617-634, 2005.

Lawver, L.A., I.W.D. Dalziel, L.M. Gahagan, K.M. Martin, and D.A. Campbell, The PLATES 2003 atlas of plate reconstructions (750 Ma to present day), PLATES progress Report No. 280-0703, UTIG Technical Report No. 190, University of Texas Institute of Geophysics, Austin, TX 78759, 97 pp., 2003.

Lonsdale, P., Paleogene history of the Kula plate: Offshore evidence and onshore implications, *Geo. Soc. Am. Bull.* 100, 733-754, 1988.

Marshall, M., The magnetic properties of some DSDP basalts from the north Pacific and inferences for Pacific plate tectonics, *J. of Geophys. Res.*, 83, B1, 289-308, 1978.

McFadden, P.L., and A. Reid, Analysis of paleomagnetic inclination data, *Geophys. J. R. Astr. Soc.* 69, 307-319, 1982.

Mendenhall, W. and T. Sincich, *A Second Course in Business Statistics: Regression Analysis*, Macmillan, New York, 859p., 1993.

Molnar, P., and T. Atwater, Relative motion of hot spots in the mantle, *Nature*, v. 246, p. 288-291, 1973

Morgan, W.J., Convection plumes in the lower mantle, *Nature* 230, 42-43, 1971.

Morgan, W.J., Deep mantle convection: Plumes and plate motions, *AAPG Bull.* 56, 203-213, 1972.

Nakanishi, M., and J. Gee, Paleomagnetic investigations of volcanic rocks: Paleolatitudes of the northwestern Pacific guyots, *Proc. ODP., Sci. Res. 144* edited by J.A. Haggerty, I. Premoli-Silva, F. Rack, , and M. K. McNutt, Ocean Drilling Program, College Station, TX 77843, 585-604, 1995.

Norton, I.O., Plate motions in the north Pacific: The 43 Ma nonevent, *Tectonics* 14 (5), 1080-1094, 1995.

Ogg, J.G., Paleolatitudes and magnetostratigraphy of Site 585, Mariana Basin western central Pacific, in *Init. Rep. DSDP 89* edited by R. Moberly, S.O. Schlanger, et al., US Govt. Printing Office, Washington DC, 629-646, 1986.

Pak, D.K and K.G. Miller, Isotopic and faunal record of Paleogene deep-water transitions in the north Pacific, in *Proc. ODP Sci. Results 145* edited by D.K. Rea, I.A. Basov, D.W. Scholl, and J.F. Allan, Ocean Drilling Program, College Station, TX, 265-281, 1995.

Parés, J. M. and L. Lanci, A Middle Eocene-Early Miocene magnetic polarity stratigraphy in equatorial Pacific sediments (ODP Site 1220), *Geophys. Mono. 145*, AGU, 131-140, 2004.

Parés, J.M. and T.C. Moore, New evidence for the Hawaiian hotspot plume motion since the Eocene, *Earth Planet. Sci. Let.* 237, 951-959, 2005.

Parker, R.L., L. Shure, and J. A. Hildebrand, The application of inverse theory to seamount magnetism, *Rev. Geophys*. 25:1−65, 1987.

Petronotis, K.E., R.G. Gordon, and G.D. Acton, Determining paleomagnetic poles and anomalous skewness from marine magnetic anomaly skewness data from a single plate, *Geophys. J. Intl.*109, 209-224, 1992.

Petronotis, K. E., R. G. Gordon, and G. D. Acton, A 57 Ma Pacific plate palaeomagnetic pole determined from a skewness analysis of crossings of marine magnetic anomaly 25r, *Geophys. J. Intl.* 118, 529-554, 1994.

Petronotis, K. E. and Gordon, R. G., A Maastrichtian paleomagnetic pole for the Pacific plate from a skewness analysis of marine magnetic anomaly 32. *Geophys. J. Intl.* 139, 227-247, 1999.

Prince, R.A., G.R. Heath, and M. Kominz, Paleomagnetic studies of central north Pacific sediment cores: Stratigraphy, sedimentation rates, and the origin of magnetic instability, *Geol. Soc. Am. Bull.*, Part II, 91,1789-1835, 1980.

Raymond, C. A., J. M Stock, and S. C. Cande, Fast Paleogene motion of the Pacific hotspots from revised global plate circuit constraints, in *The History and Dynamics of Global Plate Motion,* edited by M. A. Richards, R. G. Gordon, and R.D. van der Hilst, *Geophys. Mono. 121*, AGU, 359-375, 2000.

Richards, M. L., V. Vacquier, and G.D. Van Voorhis, Calculation of magnetization of uplifts from combining topographic and magnetic surveys, *Geophysics* 32, 678-707, 1967.

Sager, W. W., Paleomagnetism of Abbott Seamount and implications for the latitudinal drift of the Hawaiian hotspot, *J. Geophys. Res*. 89 (NB7), 6271-6284, 1984.

Sager , W. W., and B.H. Keating, Paleomagnetism of Line Islands seamounts: Evidence for Late Cretaceous and Early Tertiary volcanism, *J. Geophys. Res*., 89, B13, 11135-11151, 1984.

Sager, W. W., Late Eocene and Maastrichtian paleomagnetic poles for the Pacific plate: Implications for the validity of seamount paleomagnetic data, *Tectonophysics* 144, 301-314, 1987.

Sager, W. W. and M.S. Pringle, Mid-Cretaceous to Early Tertiary apparent polar wander path of the Pacific plate, *J. Geophys. Res*., 93, B10, 11753-11771, 1988.

Sager, W. W., Seamount age estimates from paleomagnetism and their implications for the history of volcanism on the Pacific plate, in *Geology and Offshore Mineral Resources of the Central Pacific Basin*, edited by B. Keating, and B. Bolton, Circum-Pacific Council for Energy and Mineral Resources, Earth Sci. Ser., vol. 14, Springer-Verlag, New York, 21-37, 1992.

Sager, W. W. and A.A.P. Koppers, Late Cretaceous polar wander of the Pacific plate: Evidence of a rapid true polar wander event, *Science*, 287, 455-459, 2000.

Sager, W. W., A Chron 33r paleomagnetic pole for the Pacific plate, *Geophys. Res. Lett.*, 30, DOI: 10.1029/2003GLO17964, 2003.

Sager, W. W., A. J. Lamarche and C. Kopp, Paleomagnetic modeling of seamounts near the Hawaiian-Emperor bend, *Tectonophysics*, 405, 121-140, 2005.

Sager, W.W., and B. Horner-Johnson, Paleomagnetism of basaltic rocks cored at ODP Site 1179: Implications for paleolatitude and the mid-cretaceous paleomagnetic pole, *Proc. ODP, Sci. Res. 191*, in press.

Sager, W. W., DSDP and ODP basalt core paleomagnetic poles for the Cretaceous Pacific plate: Implications for apparent polar wander and plate tectonics, *Phys. Earth and Planet. Int*., in press.

Schlanger, S. O., M.O. Garcia, B.H. Keating, J.J. Naughton, W.W. Sager, J.A. Haggerty and J.A. Philpotts, Geology and geochronology of the Line Islands, *J. Geophys. Res.* 89, 11201-11272, 1984.

Scholl, D.W., T.L. Vallier, and A.J. Stevenson, Terrane accretion, production and continental growth: A perspective based on the origin and tectonic fate of the Aleutian-Bering Sea region, *Geology* 14, 43-47, 1986.

Schouten, H., and K. McCamy, Filtering marine magnetic anomalies, *J. Geophys. Res.* 77, 7089-7099, 1972.

Schouten, H. and S.C. Cande, Paleomagnetic poles from marine magnetic anomalies, *Geophys. J. R. Astr. Soc.*, 44, 567-575, 1976.

Sharp, W.D. and D.A. Clague, An older slower Hawaii-Emperor bend (abstract), *EOS, Trans. AGU, Fall Mtg. Suppl.,* 83 (47), 2002.

Shipboard Scientific Party, Site 869, *Proc. ODP Sci. Results 143,* edited by E.L. Winterer, W.W. Sager, J.V. Firth, and J.M. Sinton, Ocean Drilling Program, College Station, TX, 297-348, 1993.

Shipboard Scientific Party, Leg 199 summary and Sites 1218, 1219, 1220, *Proc. ODP, Init. Repts.,199,* edited by M. Lyle, P.A. Wilson, T.R. Janecek, et al.[CD-ROM], Available from: Ocean Drilling Program, College Station TX 77845-9547, 2002.

Stephen, R.A., J. Kasahara, G.D. Acton, R.S. Cahoun, S. Haraguchi, et al., *Proc. ODP, Init. Repts.,200* [CD-ROM], Available from: Ocean Drilling Program, College Station, TX 77845-9547, 2003.

Tarduno, J.A., Absolute inclination values from deep sea sediments: A reexamination of the Cretaceous Pacific record, *Geophys. Res. Lett.* 17, 101-104, 1990.

Tarduno, J.A., and R.D. Cottrell, Paleomagnetic evidence for motion of the Hawaiian hotspot during formation of the Emperor Seamounts, *Earth Planet. Sci., Lett*. 153, 171-180, 1997.

Tarduno, J.A., R.A. Duncan, D.W. Scholl, R.D. Cottrell, B. Steinberger, T. Thordarson, B.C. Kerr, C.R. Neal, F.A. Frey, M. Torii, and C. Carvallo, The Emperor Seamounts: Southward motion of the Hawaiian hotspot plume in Earth's mantle (plus data supplement), *Science*, 301, 5636, 1064-1069, DOI: 10.1126/science.1086442, 2003.

Vacquier, V., A machine method for computing the magnitude and direction of a uniformly magnetized body from its shape and a magnetic survey, *Proc. Benedum Earth Magnetism Symp*., 123-137, 1962.

Vasas, S.M., R.G. Gordon, and K.E. Petronotis, New paleomagnetic poles for the Pacific plate from analysis of the shapes of anomalies 33n and 33r (abstract), *EOS, Trans. AGU, Fall Mtg. Suppl.*, 75, 203, 1994.

Weaver, R., A.P. Roberts, R. Flecker, D.I.M. Macdonald, Tertiary geodynamics of Sakhalin (NW Pacific) from anisotropy of magnetic susceptibility fabrics and paleomagnetic data, *Tectonophysics,* 379, 25-42, 2004.

Wessel, P. and A. Kroenke, A geometric technique for relocating hotspots and refining absolute plate motions, *Nature* 387, 365-369, 1997.

Winterer, E.L., W.R. Riedel, R.M. Moberly, Jr., J.M. Resig, L.W. Kroenke, et al., *Init. Rep. DSDP 7*, US Govt. Printing Office, Washington, DC, 27-48, 1971.

APPENDIX A

Having a large, diverse data set allowed us to improve constraint on both the mean pole locations and mean pole ages (Tables 2, A1, A2). In order to create such a data set, it was necessary to analyze sediment and basalt cores not included in previous paleomagnetic studies. This additional sediment and basalt core data came from DSDP Holes 577 and 577A, ODP Holes 869A, 883B, 884B, 887D, and ODP Sites 1218, 1219, 1220, and 1224.

Holes 884B and 869A

Our paleocolatitude data set includes new inclination measurements made from core samples of two ODP holes, 869A and 884B that had not been previously subjected to paleomagnetic analysis for this time period. Discrete sample paleomagnetic measurements were made on samples from the working halves of the ODP cores (Table A3, A4).

Oligocene and Eocene sections of cores from Holes 884B and 869A are composed of both hard and soft sedimentary rock facies such as nannofossil chalks and oozes, respectively. We sampled five hydraulic piston cores (APCs) from Hole 869A, taking two to three discrete samples from each core, depending upon the amount of intact core material. A total of 101 samples were taken from cores 143-869A-5H through 143-869A-9H. From Hole 884B, we sampled expanded core barrel (XCB) cores 145-884B-70X through 145-884B-87X, with approximately two samples coming from each core, for a total of 205 samples. The softer, less consolidated samples of Hole 869A were extracted using clear plastic sampling cubes. The harder, more consolidated

chalks and claystones of Hole 884B were sampled using a metal, mini-push coring device with the samples placed into the sampling cubes.

Methods

The core samples from holes 869A and 884B underwent natural remnant magnetization (NRM) analysis in the paleomagnetism laboratory at the University of California- Davis campus (UC Davis). In the lab, the samples were subjected to alternating field demagnetization (AFD) to remove secondary magnetization overprinting the primary magnetization (ChRM) gained at deposition. AFD was performed on a 2G Enterprises 755-1.65UC DC SQUID Superconducting (u-channel) Rock Magnetometer fitted with a discrete sample tray and interfaced with a PC for automated data acquisition [http://paleomag.geology.ucdavis.edu/instruments.htm]. Samples showing irregular results on the u-channel magnetometer due to low magnetic moment values were also run on an 2G Enterprises 760-3.0 AC SQUID Superconducting Rock Magnetometer (discrete sample cryogenic magnetometer) to augment the u-channel magnetometer results. The discrete cryogenic magnetometer is more sensitive but also more time consuming than the u-channel magnetometer, so only low intensity samples were run on the machine. The AFD was initially carried out on a few samples from each site in steps of 5 and 10 milliteslas (mT), with increasing field strength from 0 to 80 mT, to determine which steps were best at removing the magnetic overprint and maintaining the consistency of the resulting inclination values. The best demagnetization steps were 0 to 50 mT for 884B samples and 0 to 35 mT for 869A samples. The remaining samples underwent AFD at these demagnetization intervals.

ChRM data from Holes 869A and 884B produced by the magnetometers were evaluated by making orthogonal vector plots for each sample and analyzing the results using principal component analysis (PCA) [Kirschvink, 1980]. The PCA produced stable inclination and declination data that were graphed to show polarity shifts in the downcore sediment record (Fig. A1, A2). The polarity shifts were then compared to the ODP leg biostratigraphy reports [Firth, 1995; Barron et al., 1995] to determine an appropriate magnetostratigraphy and age range for the sediments in each core.

Once all of the stable inclination measurements were complete, the new data from ODP Legs 143 and 145 were inclination corrected and averaged into mean paleocolatitudes [Cox and Gordon, 1984].

A subset of the Hole 884B samples were analyzed for anisotropy of magnetic susceptibility (AMS) to look for indications that inclination shallowing influenced the sediment samples. The AMS analysis was performed at UC Davis on a KappaBridge KLY-2 Susceptibility Meter using the standard fifteen position/3 axis sample analysis [Jelínek, 1977]. The degree of AMS is important because it relates to inclination error [Kodama and Sun, 1992] and by measuring the AMS, the level of error in the inclination measurements can be evaluated [Blow and Hamilton, 1978; Deamer and Kodama, 1990; Kodama and Sun, 1992; Hodych et al., 1999]. Hole 869A samples did not undergo AMS analysis because they are weakly magnetic and were deposited close to the equator, where they should not be significantly affected by inclination shallowing.

This subset of samples from Hole 884B were also analyzed for inclination shallowing by measuring the anisotropy of anhysteretic remanent magnetization

(AARM) present. AARM was measured on the 2G Enterprises u-channel magnetometer at UC Davis. AARM analysis was performed using the Hodych et al. [1999] method, which uses a linear regression to evaluate values of the tangent of inclination [tan I] compared to ARM_{min}/ARM_{max} and K_{min}/K_{max} values. With consistent inclination shallowing, a linear regression correlation is found between tan I and ARM_{min}/ARM_{max} [Hodych et al. 1999; Mendenhall and Sincich, 1993]. This correlation shows that when ARM_{min}/ARM_{max} =1, the value of tan I can be used to estimate the inclination of the sediments prior to any shallowing effects, allowing for the quantification of the changes shallowing has caused in the sediments.

An examination of the types of magnetic carriers present in the sediments from Holes 884B and 869A was also performed using hysteresis loop analyses on a few representative samples from each hole. This hysteresis analysis was performed on the UC Davis Princeton MicroMag 2900 Alternating Gradient Magnetometer (MicroMag). Small subsamples, < 50 milligrams in size, were removed from the selected paleomagnetic sample cubes after the cubes underwent AFD. The MicroMag allowed measurements of sample bulk coercive force (H_c), as well as values of remanent (M_r) and saturation (M_s) magnetization.

A few samples from Hole 869A had magnetic intensities too weak to be measured on the MicroMag. These weak samples were instead analyzed using an isothermal remanent magnetization (IRM) pulse magnetizer to determine magnetic carrier coercivity [Dunlop, 1972]. The saturating magnetic (IRM) pulse was applied to the samples using the u-channel magnetometer and increased in steps from 0 to 1000

mT. IRM acquisition curves and hysteresis loop plots were compared to plots of known ferromagnetic minerals to determine the primary magnetic carriers in our samples [Dunlop, 1972; Day et al, 1977].

Results

The discrete paleomagnetic samples from Hole 884B measured for AMS produced corrected anisotropy degree (P`) values between 1.00 and 1.09. All but two of the samples from Hole 884B had values of P`≤ 1.05, and thus are considered weakly anisotropic [Hrouda, 1982; Weaver et al., 2004]. The two samples with larger P` (>1.05) values were classified as weakly to moderately anisotropic (Table A5).

Because the AMS results from Hole 884B showed that the sediments were weakly anisotropic, we used the method of Hodych et al. [1999] to attempt to quantify the inclination shallowing. Using the method of Hodych et al. [1999] and Mendenhall and Sincich [1993], the tan I versus ARM_{min}/ARM_{max} results indicated a predicted inclination of 56.0° +8°/-12.8° (95% confidence) for Hole 884B sediments and the tan I versus K_{min}/K_{max} analysis from Hole 884B indicated an inclination of 57.2° +6.9°/-12.0° (95% confidence) (Fig. A3; Tables A5, A6). Both of these results are higher than the calculated 50.2° ± 12.8° (95% confidence) mean remanence inclination of the discrete samples, suggesting that the sediment may have been affected by inclination shallowing. However, the mean remanence inclination calculated from the discrete sample inclinations is within the 95% confidence limits of the corrected site inclination, suggesting that the inclination shallowing is not significant. The large confidence limits of the predicted inclination are probably due to the scatter of inclinations. This data set

produced a low regression coefficient value (R = 0.12), a poor correlation that implies inclination shallowing is not consistent throughout the sediment samples from Hole 884B. Nevertheless, the estimated 6° of inclination shallowing from Hole 884B AARM analysis is the same order of magnitude as the 4° estimated from the difference between the stillstand sediment core paleocolatitude data (Fig. 10).

Hysteresis analysis on twenty samples from Hole 884B and one sample from Hole 869A characterized the primary magnetic remanence carrier for both holes as pseudo-single domain magnetite (Fig. A4; Table A7). The SIRM analysis performed on the remaining thirty-five samples from Hole 869A exhibited rapid magnetization saturation (Fig. A5; Table A8). This rapid saturation of the magnetic grains is characteristic of titanomagnetite, so this test also implies magnetite as the predominate magnetic carrier in the sediment of Hole 869A [Dunlop, 1972; Day et al, 1977].

NRM analysis of the demagnetized samples from Hole 869A resulted in forty-four inclination measurements suitable for calculating a mean paleocolatitude for the Early Oligocene [Kirschvink, 1980; Cox and Gordon, 1984]. The calculated paleocolatitude from Hole 869A, 85.4° ± 3.9°, has an average age of 32.5 ± 2.5 Ma. The paleocolatitude and age were determined from correlation of the magnetostratigraphy and biostratigraphy (Table 1; Fig. A6) [Shipboard Scientific Party, 1993; Firth, 1995; Gradstein et al., 2004]. For determination of magnetostratigraphy, we were unable to use inclinations to determine polarity because the sediments were deposited near the equator. Alternatively, we used declination reversals (flips of ~180°) to establish changes in the samples' magnetic polarity. However, before using the declination

measurements, they had to be azimuthally oriented. Core declination corrections were determined onboard during Leg 143 coring operations by the Shipboard Scientific Party [1993] using the multishot camera on the tensor tool [Fisher et al., 1993]. The corrected declinations and observed polarity reversals were consistent with the biostratigraphic zonations assigned to the core sections 143-869A-5H-1 through 143-869A-9H-7 by Firth [1995]. The magnetostratigraphy was matched to the time scale used for this study (Fig. A6) [Gradstein et al., 2004].

Correlation of the biostratigraphy and magnetostratigraphy from the demagnetized samples for Hole 884B was more complex than that for Hole 869A. This complexity was due to a slight disagreement between the biostratigraphy and the magnetic polarity of the Hole 884B discrete sediment samples taken from core sections 145-884B-71X-5 to 145-884B-72X-6 (~660 to 670 mbsf).

The biostratigraphy in the upper measured section of Hole 884B showed that the last occurrence of (LO) of the calcareous nannofossil *Reticulofenestra bisecta* of pelagic zonation NP 25 occured between 145-884B-70X-1, 0 cm and 145-884B-70X-1, 48 cm, giving this interval an age of 23.1 to 27.1 Ma [Barron et al., 1995; Gradstein et al., 2004]. The discrete samples from this section displayed reversed magnetic polarity, and matching the polarity with the biostratigraphy, this section was assigned to chron 8r (26.18 to 26.71 Ma). The biostratigraphy also gave the first occurrence (FO) of diatom *Rocella vigilans* and LO of calcareous nannofossil *Reticulofenestra umbilica* between sections 145-884B-70X-CC and 145-884B-71X-CC, making core section 145-884B-71X-7 up to 32.4 Ma in age [Shipboard Scientific Party, 1993; Pak and Miller, 1995;

Gradstein et al., 2004]. Thus, first and last occurrences in the biostratigraphy from cores 145-884B-70X to 145-884B-71X implied a minimum age interval of 26.7 Ma to 32.4 Ma, ~6 Myr.

The discrete samples from this section included both normal and reversed polarities, with several reversals observed downcore (Fig. A7). However, there were not enough recorded reversals for the magnetostratigraphy of core sections 145-884B-71X-1 through 145-884B-72X-6 to match the assigned biostratigraphic age range. The GPTS [Gradstein et al., 2004; Cande and Kent, 1995] for this time interval showed 11 reversals (chrons 9n to 12r) and the data only showed 7 reversals, indicating missing chron data. The lack of chrons supports the existence of an unconformity, but of unclear duration. Changes in the lithology of the core sections also suggested the presence of an unconformity in the lowermost part of core 145-884B-71X, however the exact timing and duration of the unconformity were not determined. Changes in sedimentation rates could have also occurred during this time, further complicating the magnetostratigraphy.

The Eocene-Oligocene boundary was observed in the sediments just prior to a zone of shallow inclination, and unclear polarity. Even though the polarity following this unclear zone was normal, polarity chron assignments in much of sections 145-884B-75X-5 to 145-884B-82X-4 were unclear because the inclinations were inconsistent. These core sections also showed signs of slumping and re-deposition, making conclusive polarity and age assignments problematic.

The older core sections (145-884B-83X-3 to 145-884B-87X-6) for Hole 884B in this study had polarity chron assignments much more consistent with the biostratigraphy. These core sections were assigned to chrons C19r through C22n, 40.7 to 49.4 Ma.

Because the slight disagreement between the biostratigraphy and GPTS made polarity chron assignments uncertain in the upper part of the measured section, two possible magnetic stratigraphies were designated for this portion of Hole 884B (145-884B-71X-5 through 145-884B-72X-6) (Fig. A7). The difference in the two magnetostratigraphies is minor, with both resulting in the same overall chron range for the upper section (C8r-C13n).

Even though the measured section of Hole 884B had a zone of unclear data, it produced three reasonable paleocolatitude values; one for the Oligocene and two for the Eocene (Table 1). Forty-nine samples were averaged to calculate the 884B Oligocene paleocolatitude of 48.8° ± 9.3° with an age of 30.0 Ma. The Eocene paleocolatitudes calculated for Hole 884B are 64.5° ± 6.3° for 41.2 Ma (11 samples) and 49.7°± 7.5° for 45.7 Ma (26 samples).

Hole 883B

Discrete sediment samples from Hole 883B core sections 145-883B-76X -1 to 145-883B -85X-3 produced two mean paleocolatitudes [Cox and Gordon, 1984] for the Late and Early Eocene poles. The paleocolatitude calculated for the Early Eocene is 61.5°± 8.1° with an average age of 52.5 ± 3.5 Ma. The Late Eocene paleocolatitude has an average age of 41.8 ± 5.3 Ma and is located at 53.9 ± 9.2° (Table 1) [Barron et al., 1995; Gradstein et al., 2004]. The samples from Hole 883B, like those from Holes 884B

and 869A were AF demagnetized up to 80 mT and underwent principle component analysis (PCA) to establish stable inclination values. We used the biostratigraphy of Barron et al. [1995] and the Gradstein et al. [2004] time scale to date the sediment samples to the early and mid to late Eocene. Because there were only limited samples (41 samples for entire Eocene epoch) from this hole, we did not complete a magnetostratigraphy separate from that done during the initial analysis of the hole on ODP Leg 145.

Hole 887D

Hole 887D basalt samples, like the sediment samples, were AF demagnetized and PC analyzed. These thirty discrete samples from core sections 145-887D-4R-1 through 145-887D-10R-2 represent five flows and three independent cooling units. Paleocolatitude analysis on the basalt samples using the Cox and Gordon [1984] method resulted in one paleocolatitude of 56.2° ± 7.5°. The basalt samples had an average radiometric age of 27.4 ± 0.4 Ma calculated by Keller et al. [1995].

Holes 577 and 577A

Sediment paleocolatitudes for Holes 577 and 577A were recalculated from the stable inclination data of Bleil [1985]. The original paleocolatitudes were calculated over large time spans and we wanted to limit the ages of the paleocolatitudes to a few million years. The inclination data were re-dated according to the time scale of Gradstein et al. [2004], and grouped into polarity chrons using the observed polarity reversals. The method of Cox and Gordon [1984] was used to calculate paleocolatitudes. Fourteen paleocolatitudes were calculated from Hole 577 and 577A

cores. These were not averaged because the paleocolatitudes were distinct values that increased with increasing age. The paleocolatitude values are listed in Table 1.

Sites 1218 and 1219

Discrete sample stable inclination data published as magnetostratigraphies in Lanci et al. [2005] were converted into paleocolatitudes and averaged using the Cox and Gordon [1984] method. Site 1218 and 1219 age data from Lanci et al. [2005] were adjusted to the Gradstein et al. [2004] time scale. In total, we used 2507 measurements for Site 1218 and 1652 measurements for Site 1219. The large number of measurements was a result of detailed u-channel inclination meansurements.

Two mean paleocolatitudes were calculated for Site 1218 and one for Site 1219 (Table 1). One of the Site 1218 paleocolatitudes is 87.5° ± 2.7° and has an average age of 26.3 +2.0/-3.2 Ma, calculated from 1668 inclination measurements. The second Site 1218 paleocolatitude, 87.4° ± 3.7° has an average age of 29.2 +0.8/-0.7, determined from 839 measurements of inclination. Site 1219 has a paleocolatitude value of 92.9° ± 3.1° with an age of 32.0 +2.0/-1.6 Ma, from 1652 measurements.

The large number of data from these two sites allowed us to calculate ages of these paleocolatitudes using weighted ages. The large amount of data from Sites 1218 and 1219 allowed for the calculation of colatitude values for individual chrons. However, it was not feasible to include all of these colatitude values in the pole calculations, because the large amount of data would have weighted or biased the pole calculations in favor of these two sites. In order to avoid any data bias, we decided to take the colatitudes of the individual chron colatitudes and average them into mean

colatitude values for the Early Oligocene (Sites 1218 and 1219) and Late Oligocene (Site 1218). To provide the best possible overall estimate of the data's mean age, ages of the individual colatitudes were weighted before they were included in the mean colatitude calculation. For example, a colatitude age calculated from 150 samples received more weight in determining the mean colatitude age than one that was calculated from only 50 samples. The data weighting is the cause of the uneven age uncertainties in the Site 1218 and 1219 mean paleocolatitudes.

Site 1220

Stable inclination data published in the magnetostratigraphy of Parés and Lanci [2004] for Site 1220 was used to calculate two Eocene paleocolatitudes. These paleocolatitudes were calculated using the method of Cox and Gordon [1984] and dated using the Gradstein et al. [2004] time scale. The first paleocolatitude, representing mid Eocene chron C20n, was calculated from 772 inclinations, resulting in a colatitude value of 94.5° ± 3.8° and of age 42.2 ± 0.6 Ma. The second Site 1220 paleocolatitude of 92.4° ± 2.8° was calculated from 161 inclinations. It represents mid-Eocene chron C20r with an age of 44.1± 1.3 Ma.

Site 1224

One hundred twenty-six discrete samples of basalt cored from Site 1224 produced stable inclination values after AF demagnetization. These samples were separated into five individual cooling units for which paleocolatitudes were calculated using the Cox and Gordon [1984] and McFadden and Reid [1982] methods. Both methods produced a paleocolatitude value of 83.1°, however the error estimates of the

two methods differed slightly, with the McFadden and Reid [1982] method estimating 5.9° error and the Cox and Gordon [1984] method estimating 4.6° error in the paleocolatitude. For consistency with the other paleocolatitude data, the Cox and Gordon error estimate was used in the pole calculations (Table 1). The average age of the Site 1224 paleocolatitude is 46.1 Ma, determined the marine magnetic anomaly age of the crust in which Site 1224 was drilled (Table 1) [Stephen et al., 2003].

Table A1. Paleomagnetic pole mean age calculations.

Oligocene	Site	Colatitude	Average age (Ma)	Importance (I)	age*I	Std. dev.
	S68-24	105.6	32.7	0.18	5.9	1.8
	K72-39	91.7	30.6	0.35	10.7	0.4
	K78020	87.9	26.1	0.15	3.9	1.8
	K78523	88.0	30.9	0.15	4.6	0.3
	K78023	90.9	26.4	0.15	4.0	1.5
	ODP 1218	87.5	26.3	0.25	6.6	2.6
	ODP 1218	87.4	29.2	0.13	3.8	0.0
	ODP 1219	92.9	32.0	0.15	4.8	0.9
	ODP 884B	48.8	30.0	0.03	0.9	0.0
	ODP 869A	85.4	32.5	0.2	6.5	1.8
	Midway Reef	71.3	27.7	0.07	1.9	0.2
	Midway Sand Is.	75.7	27.7	0.03	0.8	0.1
	887D avg	56.2	27.4	0.02	0.5	0.1
	Site 597	119.5	27.5	0.09	2.5	0.4
	Site 63	94.0	32.4	0.05	1.6	0.4
average age 29.5				2	29.5	2.5

Late Eocene	Site	Colatitude	Average age (Ma)	Importance (I)	age*I	Std. dev.
	ODP 883B	53.9	41.8	0.05	2.1	0.3
	ODP 884B	64.5	41.2	0.11	4.5	0.4
	ODP 1220	94.5	42.2	0.43	18.1	3.9
	S68-24	100.6	36.3	0.31	11.3	2.6
	M7039	106.6	37.0	0.46	17.0	2.2
	Abbott	83.9	41.5	0.15	6.2	0.8
	Stanley	95.3	39.3	0.17	6.7	0.0
	Colahan	84.8	38.5	0.17	6.5	0.1
	Willoughby	90.7	39.3	0.15	5.9	0.0
average age 39.2				2	39.2	2.3

Early Eocene	Site	Colatitude	Average age (Ma)	Importance (I)	age*I	Std. dev.
	ODP 1206	68.5	49.1	0.13	6.4	0.0
	ODP 883B	61.5	52.5	0.04	2.1	0.6
	ODP 884B	49.7	45.7	0.04	1.8	0.3
	DSDP 430A	69.9	55.2	0.06	3.3	2.6
	DSDP 577A	74.7	55.8	0.11	6.1	5.6
	DSDP 577A	74.5	51.3	0.13	6.7	0.9
	DSDP 577	76.4	54.7	0.15	8.2	5.4
	DSDP 577	74.0	50.6	0.18	9.1	0.7
	ODP 1220	92.4	44.1	0.46	20.3	9.5
	ODP 1224	83.1	46.1	0.16	7.4	1.0
	K78-0-12	93.1	47.5	0.32	15.2	0.4
	Daikakuji -East	93.4	46.7	0.07	3.3	0.3
	Daikakuji -West	71.8	46.7	0.07	3.3	0.3
	Annei	107.6	52.0	0.08	4.2	0.9
average age 48.6				2	48.6	3.8

Table A1. Continued.

Paleocene	Site	Colatitude	Average age (Ma)	Importance (I)	age*I	Std. dev.
with MMA skewness	DSDP 199	95.9	62.0	0.04	2.5	0.0
	DSDP 585	90.3	61.6	0.04	2.5	0.0
	DSDP 577	75.8	57.7	0.03	1.7	0.6
	DSDP 577	76.0	60.9	0.04	2.4	0.1
	DSDP 577	78.6	64.1	0.04	2.6	0.2
	DSDP 577	77.5	65.5	0.04	2.6	0.5
	DSDP 577A	73.0	60.1	0.03	1.8	0.1
	DSDP 577A	75.9	63.1	0.02	1.3	0.0
	DSDP 577A	77.2	65.2	0.04	2.6	0.4
	DSDP 433C	63.2	61.3	0.05	3.1	0.0
	DSDP 432A	57.7	56.2	0.02	1.1	0.7
	ODP 1205	64.0	55.6	0.03	1.7	1.3
	Paumakua	102.6	65.5	0.01	0.7	0.1
	Kautu	86.9	58.4	0.02	1.2	0.3
	MMA 25r	78.2/4.8	57.0	0.37	21.1	9.7
	MMA27r-29	73.1/7.7	64.0	1.18	75.5	4.1
average age 62.1				2	62.1	3.0

Paleocene	Site	Colatitude	Average age (Ma)	Importance (I)	age*I	Std. dev.
no MMA skewness	DSDP 199	95.9	62.0	0.1	6.2	0.1
	DSDP 585	90.3	61.6	0.1	6.2	0.0
	DSDP 577	75.8	57.7	0.08	4.6	0.9
	DSDP 577	76.0	60.9	0.09	5.5	0.0
	DSDP 577	78.6	64.1	0.1	6.4	0.9
	DSDP 577	77.5	65.5	0.1	6.6	2.0
	DSDP 577A	73.0	60.1	0.07	4.2	0.1
	DSDP 577A	75.9	63.1	0.05	3.2	0.2
	DSDP 577A	77.2	65.2	0.09	5.9	1.5
	DSDP 433C	63.2	61.3	0.25	15.3	0.0
	DSDP 432A	57.7	56.2	0.05	2.8	1.2
	ODP 1205	64.0	55.6	0.16	8.9	4.8
	Paumakua	102.6	65.5	0.29	19.0	5.7
	Kautu	86.9	58.4	0.47	27.4	3.3
average age 61.1				2	61.1	3.2

Maastrichtian	Site	Colatitude	Average age (Ma)	Importance (I)	age*I	Std. dev.
with MMA skewness	GPC3	78.9	67.5	0.03	2.0	0.1
	DSDP 577	78.7	66.8	0.12	8.0	1.0
	DSDP 577A	72.7	66.8	0.06	4.0	0.5
	DSDP 577A	73.1	68.2	0.03	2.0	0.1
	DSDP 585-585A	91.3	68	0.18	12.2	0.5
	DSDP 315A	98.9	70.35	0.02	1.4	0.0
	ODP 871	98.9	68.3	0.02	1.4	0.0
	Wageman	105.7	71.9	0.02	1.4	0.1
	Paumakua	102.6	65.5	0.02	1.3	0.3
	Musina	97.2	69.6	0.02	1.4	0.0
	MMA 32 (N.Far.)	68.4/9.2	71.1	1.1	78.2	2.3
	MMA 27r-31	73.2/4.6	68	0.38	25.8	1.0
average age 69.6				2	69.6	1.7

Table A1. Continued.

Maastrichtian	Site	Colatitude	Average age (Ma)	Importance (I)	age*I	Std. dev.
no MMA	GPC3	78.9	67.5	0.4	27.0	0.2
skewness	DSDP 577	78.7	66.8	0.28	18.7	0.6
	DSDP 577A	72.7	66.8	0.14	9.4	0.3
	DSDP 577A	73.1	68.2	0.06	4.1	0.0
	DSDP 585-585A	91.3	68.0	0.39	26.5	0.0
	DSDP 315A	98.9	70.4	0.38	26.7	1.7
	ODP 871	98.9	68.3	0.06	4.1	0.0
	Wageman	105.7	71.9	0.08	5.8	1.1
	Paumakua	102.6	65.5	0.09	5.9	0.7
	Musina	97.2	69.6	0.12	8.4	0.2
average age 68.2				2	68.2	1.5

Table A2. Age calculations for time window poles.

Pole	Site	Age (Ma)	Std. Dev.	Importance (I)	I*age
25 Ma					
	K72-39	30.6	1.49	0.13	3.97
	K78020	26.1	0.27	0.24	6.26
	K78523	30.9	3.35	0.24	7.42
	K78023	26.4	0.16	0.24	6.32
	ODP-1218	23.1	1.13	0.07	1.62
	ODP-1218	23.3	1.18	0.08	1.87
	ODP-1218	23.7	0.48	0.04	0.95
	ODP-1218	24.1	0.67	0.07	1.68
	ODP-1218	24.1	0.46	0.05	1.21
	ODP-1218	24.4	0.47	0.06	1.46
	ODP-1218	24.7	0.18	0.03	0.74
	ODP-1218	25.0	0.33	0.07	1.75
	ODP-1218	25.7	0.08	0.04	1.03
	ODP-1218	26.4	0.03	0.06	1.59
	ODP-1218	27.3	0.00	0.05	1.36
	ODP-1218	28.0	0.04	0.05	1.40
	ODP-1218	28.3	0.07	0.05	1.42
	ODP-1218	28.5	0.09	0.05	1.42
	ODP-1218	28.6	0.09	0.04	1.15
	ODP-1218	29.1	0.07	0.02	0.58
	ODP-1218	29.6	0.12	0.02	0.59
	ODP-1218	30.0	0.41	0.05	1.50
	ODP-884B	30.0	0.39	0.05	1.50
	Midway-Reef	27.7	0.03	0.12	3.32
	Midway-Sand	27.7	0.01	0.05	1.39
	887D-avg	27.4	0.00	0.01	0.27
	Site-597	27.5	0.00	0.02	0.55
			2.41	2.00	27.16
average age=	27.2				
uncertainty=	2.4				

Pole	Site	Age (Ma)	Std. Dev.	Importance (I)	I*age
30 Ma					
	s68-24	32.7	1.86	0.17	5.56
	K72-39	30.6	0.16	0.12	3.67
	K78020	26.1	1.52	0.14	3.65
	K78523	30.9	0.32	0.14	4.33
	K78023	26.4	1.30	0.14	3.69
	ODP-1218	25.0	1.74	0.09	2.25
	ODP-1218	25.7	0.67	0.05	1.29
	ODP-1218	26.4	0.70	0.08	2.11
	ODP-1218	27.3	0.27	0.06	1.64
	ODP-1218	28.0	0.12	0.06	1.68
	ODP-1218	28.3	0.07	0.06	1.70
	ODP-1218	28.5	0.06	0.07	1.99
	ODP-1218	28.6	0.04	0.06	1.72
	ODP-1218	29.1	0.00	0.03	0.87
	ODP-1218	29.6	0.00	0.05	1.48
	ODP-1218	30.0	0.03	0.07	2.10
	ODP-1219	30.4	0.03	0.03	0.91
	ODP-1219	30.9	0.09	0.04	1.24
	ODP-1219	32.2	0.32	0.04	1.29
	ODP-1219	33.6	0.86	0.05	1.68
	ODP-1219	34.3	1.18	0.05	1.71
	ODP-884B	30.0	0.01	0.03	0.90
	ODP 869A	32.5	1.83	0.19	6.18
	Midway-Reef	27.7	0.20	0.07	1.94
	Midway-Sand	27.7	0.09	0.03	0.83
	887D-avg	27.4	0.04	0.01	0.27
	Site-597	27.5	0.11	0.03	0.82
	Site 63	32.4	0.36	0.04	1.30
			2.64	2.00	29.40
average age=	29.4				
uncertainty=	2.6				

Table A2. Continued.

Pole	Site	Age (Ma)	Std. Dev.	Importance (I)	I*age
35 Ma					
	s68-24	32.7	0.06	0.16	5.23
	K72-39	30.6	1.67	0.22	6.72
	K78523	30.9	0.75	0.13	4.02
	ODP-1218	30.0	1.92	0.18	5.41
	ODP-1219	30.4	0.50	0.06	1.83
	ODP-1219	30.9	0.65	0.11	3.40
	ODP-1219	32.2	0.11	0.10	3.22
	ODP-1219	33.6	0.01	0.16	5.37
	ODP-1219	34.3	0.12	0.13	4.45
	ODP-884B	30.0	0.22	0.02	0.60
	ODP-869A	32.5	0.11	0.17	5.53
	Site 63	32.4	0.03	0.04	1.30
	s68-24	36.3	1.35	0.15	5.45
	m70-39	37.0	2.60	0.19	7.03
	ODP-883B	41.8	1.43	0.02	0.84
	Stanley	39.3	1.44	0.04	1.57
	Abbott	38.7	1.16	0.04	1.55
	Colahan	38.5	1.08	0.04	1.54
	Willoughby	39.3	1.44	0.04	1.57
			2.88	2.00	33.30
average age=	33.3				
uncertainty=	2.9				

Pole	Site	Age (Ma)	Std. Dev.	Importance (I)	I*age
40 Ma					
	s68-24	36.3	4.93	0.29	10.53
	m70-39	37.0	4.33	0.37	13.69
	ODP-883B	41.8	0.09	0.05	2.09
	ODP-1220	44.1	5.27	0.39	17.20
	ODP-1220	42.2	0.66	0.21	8.86
	ODP-1224	46.1	2.30	0.14	6.45
	ODP-884B	45.7	1.67	0.06	2.74
	ODP-884B	41.2	0.05	0.09	3.70
	Stanley	39.3	0.13	0.10	3.93
	Abbott	38.7	0.30	0.10	3.87
	Colahan	38.5	0.37	0.10	3.85
	Willoughby	39.3	0.13	0.10	3.93
			3.18	2.00	40.42
average age=	40.2				
uncertainty=	3.2				

Table A2. Continued.

Pole	Site	Age (Ma)	Std. Dev.	Importance (I)	I*age
45Ma					
	k78-0-12	47.5	0.47	0.31	14.73
	ODP-883B	52.5	1.55	0.04	2.10
	ODP-883B	41.8	0.61	0.03	1.25
	DSDP-577	50.6	3.74	0.20	10.12
	DSDP-577a	51.3	3.47	0.14	7.18
	ODP-1220	44.1	1.61	0.34	14.99
	ODP-1220	42.2	3.32	0.20	8.44
	ODP-1224	46.1	2.30	0.12	5.53
	ODP 884B	45.7	0.02	0.05	2.29
	ODP-884B	41.2	1.84	0.07	2.88
	ODP-1206	49.1	1.20	0.15	7.37
	Stanley	39.3	3.41	0.07	2.75
	Daikakuji -E	46.7	0.01	0.07	3.27
	Daikakuji-W	46.7	0.01	0.07	3.27
	Willoughby	39.3	3.41	0.07	2.75
	Annei	52.0	2.29	0.07	3.64
			3.82	2.00	46.27
average age=	46.3				
uncertainty=	3.8				

Pole	Site	Age (Ma)	Std. Dev.	Importance (I)	I*age
50 Ma					
	k78-0-12	47.5	0.29	0.32	15.20
	ODP-883B	52.5	0.49	0.03	1.58
	ODP-883B	41.8	1.34	0.03	1.25
	DSDP-577	54.7	5.39	0.14	7.65
	DSDP-577	50.6	0.79	0.17	8.60
	DSDP-577a	55.8	5.87	0.11	6.13
	DSDP-577a	51.3	0.94	0.12	6.15
	ODP-1220	44.1	8.68	0.46	20.29
	ODP-1224	46.1	2.30	0.16	7.38
	ODP 884B	45.7	0.30	0.04	1.83
	ODP-1206	49.1	0.05	0.12	5.89
	DSDP-430A	55.2	2.74	0.06	3.31
	Daikakuji -E	46.7	0.24	0.08	3.74
	Daikakuji-W	46.7	0.24	0.08	3.74
	Annei	52.0	1.01	0.08	4.16
			3.92	2.00	48.44
avergae age=	48.4				
uncertainty=	3.9				

Table A2. Continued.

Pole	Site	Age (Ma)	Std. Dev.	Importance (I)	I*age		Std. Dev.	Importance (I)	I*age
55 Ma with MMA						*55 Ma* no MMA			
	ODP-883B	52.5	0.48	0.02	1.05		0.16	0.03	1.58
	DSDP-577	54.7	0.52	0.07	3.83		0.00	0.10	5.47
	DSDP-577	50.6	2.76	0.06	3.04		1.61	0.09	4.55
	DSDP-577a	55.8	0.13	0.05	2.79		0.06	0.07	3.90
	DSDP-577a	51.3	1.50	0.04	2.05		0.90	0.07	3.59
	DSDP-430A	55.2	0.14	0.03	1.66		0.01	0.08	4.42
	DSDP 585	61.6	1.22	0.07	4.31		4.97	0.11	6.77
	DSDP 577	57.7	0.01	0.06	3.46		0.83	0.10	5.77
	DSDP 577	60.9	0.87	0.07	4.26		4.06	0.11	6.70
	DSDP 577A	60.1	0.43	0.06	3.60		2.46	0.09	5.40
	DSDP 199	62.0	1.49	0.07	4.34		5.15	0.10	6.20
	DSDP 432A	56.2	0.03	0.02	1.12		0.08	0.04	2.25
	ODP 1205	55.6	0.19	0.06	3.34		0.09	0.15	8.34
	Annei	52.0	1.74	0.06	3.12		6.87	0.86	44.72
	MMA 25r	57.8	0.20	1.26	72.80		0.00	0.00	0.00
			2.42	2.00	57.38		3.69	2.00	54.83
average age=	57.4					54.8			
uncertainty=	2.4					3.7			

Table A2. Continued.

Pole	Site	Age (Ma)	Std. Dev.	Importance (I)	I*age		Std. Dev.	Importance (I)	I*age
60 Ma with MMA						*60 Ma* no MMA			
	ODP-883B	52.5	0.92	0.01	0.53		2.22	0.02	1.05
	DSDP-577	54.7	1.67	0.03	1.64		4.91	0.07	3.83
	DSDP-577a	55.8	0.81	0.02	1.12		2.65	0.05	2.79
	DSDP-430A	55.2	0.48	0.01	0.55		2.45	0.04	2.21
	DSDP 585	61.6	0.01	0.04	2.46		0.22	0.10	6.16
	DSDP 577	57.7	0.58	0.03	1.73		2.27	0.08	4.62
	DSDP 577	60.9	0.06	0.04	2.44		0.41	0.09	5.48
	DSDP 577	64.1	0.16	0.04	2.56		0.10	0.09	5.77
	DSDP 577A	60.1	0.13	0.03	1.80		0.62	0.07	4.20
	DSDP 577A	63.1	0.02	0.02	1.26		0.00	0.04	2.52
	DSDP 577A	65.2	0.37	0.04	2.61		0.41	0.09	5.86
	DSDP 199	62.0	0.00	0.04	2.48		0.11	0.10	6.20
	DSDP-433C	61.3	0.03	0.05	3.07		0.45	0.15	9.20
	DSDP 432A	56.2	0.35	0.01	0.56		0.93	0.02	1.12
	ODP 1205	55.6	1.27	0.03	1.67		4.96	0.09	5.00
	GPC 3	67.5	1.46	0.05	3.38		11.40	0.57	38.48
	Paumakua	65.5	0.12	0.01	0.66		0.80	0.13	8.52
	Kautu	65.3	0.10	0.01	0.65		1.03	0.20	13.06
	MMA25r	57.8	6.74	0.36	20.80		0.00	0.00	0.00
	MMA 27r-29r	63.9	3.82	1.13	72.25		0.00	0.00	0.00
			3.09	2.00	62.10		4.24	2.00	63.03
average age=	62.1					63.0			
uncertainty=	3.1					4.2			

Table A2. Continued.

Pole	Site	Age (Ma)	Std. Dev.	Importance (I)	I*age		Std. Dev.	Importance (I)	I*age
65 Ma with MMA						*65 Ma* no MMA			
	DSDP 585	61.6	0.36	0.03	1.85		1.37	0.06	3.69
	DSDP 577	57.7	1.61	0.03	1.73		4.47	0.06	3.46
	DSDP 577	60.9	0.51	0.03	1.83		1.77	0.06	3.65
	DSDP 577	64.1	0.04	0.04	2.56		0.30	0.06	3.85
	DSDP 577A	60.1	0.75	0.03	1.80		1.97	0.05	3.00
	DSDP 577A	63.1	0.08	0.02	1.26		0.32	0.03	1.89
	DSDP 577A	65.2	0.00	0.03	1.95		0.08	0.06	3.91
	DSDP 199	62.0	0.28	0.03	1.86		1.13	0.06	3.72
	DSDP-433C	61.3	0.56	0.04	2.45		2.53	0.10	6.13
	Odp 871	68.3	0.21	0.02	1.37		0.16	0.04	2.73
	DSDP 577	66.8	0.25	0.08	5.34		0.03	0.15	10.02
	DSDP 577A	66.8	0.12	0.04	2.67		0.02	0.07	4.68
	DSDP 577A	68.2	0.20	0.02	1.36		0.10	0.03	2.05
	DSDP-585	68.0	0.97	0.11	7.48		0.56	0.20	13.60
	DSDP-315A	70.4	1.13	0.04	2.81		5.41	0.34	23.57
	GPC 3	67.5	0.24	0.04	2.70		0.47	0.35	23.29
	Paumakua	65.5	0.00	0.01	0.66		0.05	0.07	4.59
	Kautu	65.3	0.00	0.01	0.65		0.12	0.11	7.18
	Musina	69.6	0.21	0.01	0.70		1.18	0.11	7.66
	MMA 27r-29r	63.9	1.22	1.01	64.58		0.00	0.00	0.00
	MMA 29r-31	68.0	2.98	0.33	22.45		0.00	0.00	0.00
total			2.42	2.00	65.04		3.32	2.00	66.33
average age=	65.0					66.3			
uncertainty=	2.4					3.3			

Table A2. Continued

Pole	Site	Age (Ma)	Std. Dev.	Importance (I)	I*age		Std. Dev.	Importance (I)	I*age
70 Ma with MMA						*70 Ma* no MMA			
	DSDP-585	61.6	1.04	0.03	1.85		2.36	0.07	4.31
	DSDP 577	64.1	0.33	0.03	1.92		0.74	0.07	4.49
	DSDP 577	65.5	0.11	0.03	1.97		0.28	0.08	5.24
	DSDP 577A	65.2	0.16	0.03	1.95		0.34	0.07	4.56
	DSDP 199	62.0	0.88	0.03	1.86		2.01	0.07	4.34
	Odp 871	68.3	0.01	0.01	0.68		0.04	0.05	3.42
	DSDP 577	66.8	0.03	0.07	4.68		0.06	0.18	12.02
	DSDP 577A	66.8	0.01	0.03	2.00		0.03	0.09	6.01
	DSDP 577A	68.2	0.01	0.02	1.36		0.03	0.04	2.73
	DSDP-585	68.0	0.03	0.10	6.80		0.10	0.24	16.32
	DSDP-315A	70.4	0.17	0.02	1.41		3.12	0.35	24.62
	GPC 3	67.5	0.00	0.02	1.35		0.01	0.35	23.63
	Paumakua	65.5	0.04	0.01	0.66		0.24	0.07	4.59
	Wageman	71.9	0.20	0.01	0.72		1.24	0.06	4.31
	Kautu	65.3	0.05	0.01	0.65		0.47	0.11	7.18
	Musina	69.6	0.05	0.01	0.70		0.50	0.10	6.96
	MMA 27r-29r	63.9	7.78	0.64	40.92		0.00	0.00	0.00
	MMA 32	71.1	9.42	0.70	49.77		0.00	0.00	0.00
	MMA 29r-31	68.0	0.08	0.20	13.61		0.00	0.00	0.00
			3.19	2.00	67.43		2.41	2.00	67.36
average age=	67.4					67.4			
uncertainty=	3.2					2.4			
75 Ma with MMA						*75 Ma* no MMA			
	DSDP-585	68.0	0.94	0.24	16.32		0.72	0.74	50.32
	DSDP-315A	70.4	0.00	0.02	1.41		0.67	0.36	25.33
	GPC 3	67.5	0.18	0.03	2.03		0.86	0.39	26.33
	Wageman	71.9	0.07	0.02	1.44		1.87	0.22	15.82
	Musina	69.6	0.00	0.02	1.39		0.11	0.29	20.18
	MMA 32	71.1	1.52	1.23	87.45		0.00	0.00	0.00
	MMA 29r-31	68.0	1.66	0.44	29.94		0.00	0.00	0.00
			1.48	2.00	69.98		1.45	2.00	68.99
average age=	70.0					69.0			
	1.5					1.5			

Table A3. Principle Component Analysis Results of Leg 143 Hole 869A discrete sediment samples.

Sample 143-869A-	Demag. levels	Declination (deg)	Corrected dec. (deg)	Inclination (deg)	MAD	A/UA	Fit of plot	Depth (mbsf)	Used in Colatitude
05H1-027		ICA					F	38.47	N
05H1-055	15-35	1.7	123.7	43.3	6.6	A	B-	38.75	N
05H1-126	15-35	12.0	134.0	40.8	6.7	A	C	39.46	N
05H2-010		ICA					F	39.80	N
05H2-057	15-35	15.2	137.2	25.9	23.3	A	C	40.27	N
05H2-117		ICA					F	40.87	N
05H3-010		ICA					F	41.30	N
05H3-083		ICA					F	42.03	N
05H3-129	15-35	28.3	150.3	-4.2	9.8	A	C	42.49	N
05H4-024	15-35	31.6	153.6	-6.1	10.3	A	C	42.94	N
05H4-083	15-35	-19.1	102.9	-24.3	6.3	A	C	43.53	N
05H4-133		ICA					F	44.03	N
05H5-008		ICA					F	44.28	N
05H5-088	15-25	69.3	191.3	42.5	20.2	A	C	45.08	N
05H5-142	15-30	69.7	191.7	36.9	11.8	A	C	45.62	N
05H6-021		ICA					F	45.91	N
05H6-086	15-30	24.1	146.1	-6.5	10.2	A	B	46.56	Y
05H6-136		ICA					F	47.06	N
05H7-009		ICA					F	47.29	N
05H7-054		ICA					F	47.74	N
06H1-020	15-30	-13.3	135.7	-27.3	14.9	A	C-	47.90	N
06H1-086	15-25	-8.5	140.5	43.1	22.8	A	C	48.56	N
06H1-116	15-25	-4.5	144.5	3.5	24.7	A	C	48.86	N
06H2-020	15-25	28.4	177.4	19.3	24.2	A	C-	49.40	N
06H2-086		ICA					F	50.06	N
06H2-132	15-25	-10.7	138.3	23.0	20.9	A	C-	50.52	N
06H3-022	15-25	109.3	258.3	-23.2	5.0	A	C	50.92	N
06H3-078	15-25	-15.2	133.8	57.6	8.1	A	B-	51.48	Y
06H3-126	10 to 30	305.3	94.3	27.0	11.9	UA	C	51.96	N
06H4-011	15-30	6.9	155.9	29.1	13.1	A	C	52.31	N
06H4-061	20-40	-19.2	129.8	24.7	28.5	UA	C	52.81	N
06H4-125	15-30	26.3	175.3	18.8	18.9	A	C-	53.45	N
06H5-018	15-30	265.7	54.7	77.4	3.6	A	C	53.88	N
06H5-079	15-35	57.9	206.9	-76.6	12.5	A	C-	54.49	N
06H5-128	15-35	284.2	73.2	-19.9	7.8	A	B	54.98	Y
06H6-020	20,30,35	14.1	163.1	-7.6	11.3	UA	C	55.40	N
06H6-088	15-25,35	20.4	169.4	36.2	8.3	A	C	56.08	N
06H6-130	25-35	264.7	53.7	3.2	12.7	UA	B	56.50	Y
06H7-007		ICA					F	56.77	N
06H7-060	20-30	256.7	45.7	36.7	13.3	A	C	57.30	N
07H2-015	20-30	196.5	182.5	10.2	6.1	A	B	57.47	Y
07H2-064	15-35	186.8	172.8	7.6	5.2	UA	B	57.96	Y
07H2-134	15-35	197.7	183.7	13.0	2.8	A	B	58.66	Y
07H3-027	15-35	218.6	204.6	1.7	4.2	A	B	59.09	Y
07H3-084	15-25	214.9	200.9	9.9	1.0	A	B	59.66	Y
07H3-128	15-25	226.1	212.1	-0.4	1.0	A	B+	60.10	Y
07H4-012	15-25	234.7	220.7	8.5	0.5	A	B+	60.44	Y
07H4-075	20-35	233.0	219.0	10.5	4.6	UA	A	61.07	Y
07H4-083	15-25	234.2	220.2	11.3	1.9	UA	A	61.15	Y
07H4-125	15-25	232.3	218.3	7.3	1.0	A	B+	61.57	Y
07H5-018	15-25	232.3	218.3	12.7	1.8	A	B	62.00	Y

Table A3. Continued.

Sample 143-869A-	Demag. Levels	Declination (deg)	Corrected Dec. (deg)	Inclination (deg)	MAD	A/UA	Fit of plot	Depth (mbsf)	Used in Colatitude
07H5-070	15-25	151.5	137.5	13.4	14.4	A	C	62.52	N
07H5-114	15-30	140.3	126.3	8.2	15.6	A	C	62.96	N
07H6-023	15-25	160.4	146.4	49.6	10.1	A	C-	63.55	N
07H6-070		ICA					F	64.02	N
07H6-132		ICA					F	64.64	N
07H7-015	15-30	141.2	127.2	11.9	38.9	A	C-	64.97	N
07H7-075	20-30	158.0	144.0	20.7	8	A	C	65.57	N
07H7-140		ICA					F	66.22	N
07H8-014		ICA					F	66.46	N
07H8-054	15-30	119.4	105.4	14.7	7.5	A	B-	66.86	Y
08H2-018		ICA					F	66.93	N
08H2-071	15-30	82.0	75.0	13.9	4.3	A	B	67.46	Y
08H2-125		ICA					F	68.00	N
08H3-015	15-30	95.5	88.5	-7.1	11.8	A	C	68.40	N
08H3-047		ICA					F	68.72	N
08H3-088	20-35	93.0	86.0	-9.9	6.9	A	B	69.13	Y
08H4-049		ICA					F	70.24	N
08H4-088		ICA					F	70.63	N
08H4-131	15-25	119.6	112.6	47.3	8.3	A	C	71.06	N
08H5-017		ICA					F	71.42	N
08H5-082	15-25	165.2	158.2	14.8	7.9	A	C	72.07	N
08H5-122	15-30	162.2	155.2	3.7	17.5	A	C	72.45	N
08H6-017	15-35	206.6	199.6	-72.3	10.4	UA	B-	72.92	N
08H6-077	15-25	99.2	92.2	-2.2	8.4	A	C	73.52	N
08H6-125	15-35	133.0	126.0	14.9	4.3	UA	A	74.00	Y
08H7-020	15-35	122.3	115.3	21.7	6.5	UA	B	74.45	Y
08H7-082	20-35	126.2	119.2	-9.0	8.8	UA	A-	75.07	Y
08H7-120	15-35	128.7	121.7	7.8	3.3	A	B	75.45	Y
08H8-019	20-35	121.6	114.6	-0.7	1.9	A	B+	75.94	Y
08H8-063	15-35	127.0	120.0	-2.6	2.9	A	B	76.38	Y
09H1-024	15-35	188.4	163.4	-14.4	3.5	A	B	76.44	Y
09H1-071	15-35	180.4	155.4	7.6	2.7	A	B	76.91	Y
09H1-123	15-35	174.0	149.0	-1.6	5.3	UA	A	77.43	Y
09H2-016	15-30	-11.5	323.5	-1.9	3.2	UA	A	77.86	Y
09H2-059	15-35	-5.4	329.6	-0.9	3.7	UA	A	78.29	Y
09H2-123	15-30	11.0	346.0	-11.2	1.6	A	B	78.93	Y
09H3-030	20-40	-0.1	334.9	-13.3	4.9	UA	A	79.50	Y
09H3-068	15-35	4.2	339.2	5.2	1.1	UA	B	79.88	Y
09H3-124	15-25	8.9	343.9	0.9	1.5	A	B+	80.44	Y
09H4-014	15-35	17.2	352.2	-3.3	5.5	UA	B	80.84	Y
09H4-070	15-35	30.6	365.6	-9.8	3.1	UA	A	81.40	Y
09H4-135	15-35	15.1	350.1	1.9	4.6	UA	B+	82.05	Y
09H5-013	15-35	19.0	354.0	-8.7	2.2	UA	B+	82.33	Y
09H5-071	15-35	22.4	357.4	-2.4	1.2	A	A-	82.91	Y
09H5-120	15-35	17.2	352.2	-4.2	2	UA	B+	83.40	Y
09H6-018	15-35	16.5	351.5	-10.1	1.5	A	B+	83.88	Y
09H6-084	15-35	221.6	196.6	-6.9	8.7	A	B-	84.54	Y
09H6-123	15-35	197.7	172.7	23.7	3.9	UA	A	84.93	Y
09H7-017	15-35	220.4	195.4	-15.2	2.7	A	B	85.37	Y
09H7-063	20-35	24.0	359.0	-5.0	2.4	A	B-	85.83	Y

Abbreviations: ICA= Inconsistent analysis; A/UA= Anchored/Unanchored fit of plot to (0,0); MAD= Maximum Angular Deviation of PCA; Fit of plot= how well PCA stable inclination fits actual observed inclinations (range: A=excellent to F=poor). Declination corrections= Core 5H (+122 deg), Core 6H (+149 deg), Core 7H (+346 deg), Core 8H (+353 deg), Core 9H (+335 deg).

Table A4. Principle Component Analysis results of Leg 145 Hole 884B discrete sediment samples.

Sample 145-884B-	Demag. levels	Declination (deg)	Inclination (deg)	MAD	A/UA	Fit of plot	Depth (mbsf)	Used in colatitude
70X1-121	10-50	303.2	-33.6	2.8	A	B	643.21	N
70X1-147	5-50	51.2	-62.1	1.4	A	A-	643.47	Y
70X2-040	5-50	173.8	-61.4	2.8	UA	A-	643.90	Y
70X3-082	10-35	25.5	64.1	2.4	A	B	645.82	Y
70X3-133	5-35	70.6	61.7	2.1	A	B	646.33	Y
70X3-144	5-40	156.3	51.5	2.7	UA	B+	646.44	Y
70X4-008	15-40	161.6	50.0	2.7	UA	A-	646.58	Y
70X4-070	20-60	70.3	46.6	3.5	UA	B	647.20	Y
70X5-059	5-50	84.7	52.1	2.9	UA	A	648.59	Y
70X5-109	10-50	-36.8	71.9	1.6	UA	A	649.59	Y
70X6-041	5-50	198.5	54.8	1.1	UA	A	649.91	Y
70X6-120	5-50	194.8	53.8	1.1	A	A	650.70	Y
70X7-011	10-50	29.3	62.3	3.2	A	B+	651.11	Y
71X1-139	10-50	164.7	-61.2	1.9	UA	A	653.09	Y
71X2-133	10-50	172.2	-69.4	0.4	UA	A	654.53	Y
71X3-081	15-50	-17.3	-31.2	3.2	A	B+	655.51	Y
71X3-145	5-50	53.7	60.5	1.9	UA	A	656.15	Y
71X4-013	10-50	264.8	55.4	1.0	UA	A	656.33	Y
71X4-072	5-50	144.5	49.5	0.8	UA	A-	656.92	Y
71X5-114	10-50	127.4	-58.0	2.3	UA	A-	658.84	Y
71X6-081	5-50	-12.8	50.8	1.2	UA	A	660.01	Y
71X7-010	10-50	151.7	-55.4	2.0	UA	A	660.80	Y
72X1-015	10-60	166.0	-65.5	2.1	A	B+	661.45	Y
72X2-043	10-50	272.5	-63.3	2.8	A	B	663.23	Y
72X2-100	10-50	33.9	-57.6	2.2	UA	A-	663.80	Y
72X2-144	10-50	208.0	-69.2	2.9	UA	A-	664.24	Y
72X3-046	5-50	187.3	-65.3	2.3	UA	A	664.76	Y
72X3-144	5-50	258.8	-65.6	1.4	UA	A	665.74	Y
72X4-074	15-50	328.7	-66.6	2.4	A	B+	666.54	Y
72X4-131	10-50	90.2	-56.5	2.0	UA	B+	667.11	Y
72X5-019	10-50	146.4	60.3	0.7	UA	A-	667.49	Y
72X5-072	10-50	233.8	51.3	1.6	UA	A	668.02	Y
72X6-105	10-50	-84.0	60.3	1.3	UA	A	669.85	Y
72X6-129	10-50	-30.6	59.4	2.4	UA	A	670.09	Y
72X7-051	10-50	60.4	-51.1	1.8	UA	A	670.81	Y
73X1-084	10-60	215.8	-67.3	1.2	UA	A	671.84	Y
73X2-134	10-50	128.7	-42.2	2.2	UA	A-	673.84	Y
73X3-014	10-50	-2.3	-41.4	1.7	UA	A	674.14	Y
73X3-068	10-50	289.4	-54.8	1.3	UA	A-	674.68	Y
73X4-060	10-50	47.9	-49.4	1.1	A	B+	676.10	Y
73X4-123	10-50	28.4	-57.5	1.5	UA	A	676.73	Y
73X5-012	10-50	153.4	-50.1	1.6	UA	A	677.12	Y
74X1-105		ICA				F	681.65	N
74X1-129	15-40	130.6	72.1	2.9	A	B-	681.89	Y
74X2-022	15-40	164.6	41.9	5.4	A	B-	682.32	Y
74X2-111	15-35	133.4	72.0	6.1	A	C	683.11	N
74X3-071	15-30	101.6	-68.4	4.6	A	C	684.31	N
74X3-138	10-50	231.8	69.3	1.8	A	B	684.98	Y
74X4-020	10-50	103.7	70.3	1.8	UA	B+	685.30	Y
74X4-078	15-50	152.9	40.9	7.7	A	C	685.88	N
74X5-064	10-50	120.4	80.8	1.5	A	B+	687.24	N
74X6-020	10-50	294.6	-54.3	6.2	A	B-	688.30	Y

Table A4. Continued.

Sample 145-884B-	Demag. levels	Declination (deg)	Inclination (deg)	MAD	A/UA	Fit of plot	Depth (mbsf)	Used in colatitude
74X6-101	15-40	172.0	83.9	1.1	A	B	689.11	N
74X7-008	10-50	206.0	-68.1	1.3	A	B+	689.68	Y
75X1-096	10-50	197.5	76.3	3.2	A	B-	691.16	N
75X1-115	10-50	12.5	64.3	4.2	A	B	691.35	Y
75X2-113	10-50	170.5	49.1	4.8	A	B-	692.83	Y
75X3-067	5-40	236.5	69.8	3.4	A	B	693.87	Y
75X3-083		ICA				F	694.03	N
75X4-044	10-35	222.6	61.6	11.5	A	C	695.14	N
75X4-102	10-35	2.1	57.5	6.0	A	C	695.72	N
75X5-066	10-50	-14.9	84.7	2.2	A	B+	696.86	N
75X5-124	10-20,30-40	195.8	78.8	3.8	A	C	697.44	N
75X6-026		ICA				F	697.96	N
75X6-046		ICA				F	698.16	N
75X7-004		ICA				F	698.74	N
75X7-079	10-20,30-50	118.3	-30.5	2.3	A	B	699.49	N
76X1-041	5-35	62.6	55.0	4.8	A	C-	700.21	N
76X2-084	10-20,30-50	102.3	23.8	3.7	A	B-	702.14	N
76X3-086	10-20,30-50	-33.2	-8.6	5.8	A	C	703.66	N
76X4-027	15-40	-21.2	-4.7	3.2	A	B-	704.57	N
76X4-110	5-50	145.1	5.9	3.9	A	B	705.40	N
76X5-005	15-40	152.8	26.5	4.6	A	B-	705.85	N
76X6-071	15-40	29.0	53.8	3.0	A	B	708.01	N
76X6-106	10-50	-87.1	84.2	1.9	A	B+	708.36	N
76X7-009	10-50	258.6	65.4	1.3	A	B+	708.89	N
77X1-101	10-60	-58.8	42.5	6.9	A	C+	710.51	N
77X2-008	10-50	221.8	55.2	1.6	A	B+	711.08	N
77X2-144	15-50	84.5	-6.9	2.5	A	B	712.44	N
77X3-021	15-50	-43.6	-30.6	1.7	A	B+	712.71	N
77X4-122	15-50	200.7	54.7	3.3	UA	B-	715.22	N
77X5-056	5-30,40	189.6	39.9	2.3	A	B-	716.06	N
77X5-064	10-50	60.9	58.9	6.4	A	B-	716.14	N
77X6-023	15-35	131.7	36.4	4.3	A	B-	717.23	N
77X6-085	10-30	-85.2	46.7	1.5	A	B	717.85	N
77X6-142	10-50	311.0	41.8	2.3	UA	A-	718.42	N
78X1-086	10-50	171.7	-25.6	2.7	A	B	719.96	N
78X2-013	15-50	250.4	-46.7	4.2	A	B	720.73	N
78X2-091	10-50	279.7	-76.3	2.2	A	B+	721.51	N
78X3-048	10-50	203.4	-26.8	2.5	UA	A-	722.58	N
78X3-107	15-50	154.4	-36.9	4.5	UA	B+	723.17	N
78X4-143	15-40	42.9	-23.6	4.0	A	B-	725.03	N
78X5-027	5-35,50	26.6	-10.3	4.6	A	B	725.37	N
78X6-007	15-50	-12.5	18.5	1.9	A	B	726.67	N
79X1-022		ICA				F	729.02	N
79X1-108	15-50	-53.2	87.1	5.5	A	C-	729.88	N
79X2-028	20-40	103.4	52.2	10.5	A	C-	730.58	N
79X2-073	20-50	220.0	72.5	10.5	A	C-	731.03	N
79X3-010	20-40	163.0	43.7	5.6	A	C	731.90	N
79X3-054	15-25,35	204.3	-22.1	6.9	A	C	732.34	N
79X4-060	15-35	80.6	72.7	9.7	A	C-	733.90	N
79X4-124	15-40	55.0	-55.4	3.2	A	C+	734.54	N
79X5-082		ICA				F	735.62	N
79X5-120		ICA				F	736.00	N
79X6-081		ICA				F	737.11	N

Table A4. Continued.

Sample 145-884B-	Demag. levels	Declination (deg)	Inclination (deg)	MAD	A/UA	Fit of plot	Depth (mbsf)	Used in colatitude
79X7-011	20-50	211.2	32.7	2.6	A	B	737.91	N
79X7-041	25-40	196.7	-17.5	3.7	A	B-	738.21	N
80X1-046	25-40	66.4	-13.5	4.9	A	D	738.86	N
80X1-093	15-50	27.1	-44.0	4.2	A	C	739.33	N
80X2-072		ICA				F	740.62	N
80X2-128	20-60	-3.6	66.5	2.9	UA	B+	741.18	N
80X3-041	20-40	221.7	39.5	3.8	A	B-	741.81	N
80X3-077	15-40	192.3	49.1	2.5	A	B+	742.17	N
80X4-051	25-50	-5.2	68.7	13.8	A	C	743.41	N
80X4-116		ICA				F	744.06	N
80X5-086	20-60	135.0	66.0	10.6	A	C	745.26	N
80X5-120		ICA				F	745.60	N
80X6-063	25-60	150.5	67.7	11.0	A	C-	746.53	N
80X6-097	15-35	104.5	61.6	7.8	A	C	746.87	N
80X7-054	10-40	182.8	21.5	3.4	A	B	747.94	N
81X1-032	15-35	-35.6	32.2	4.9	A	C+	748.42	N
81X1-081	5-20	116.3	59.5	2.5	A	C	748.91	N
81X2-053	10-25	191.6	62.0	8.1	A	C-	750.13	N
81X2-081	10-40	192.2	21.9	2.4	A	B	750.41	N
81X3-051		ICA				F	751.61	N
81X3-102	10-30	132.4	62.4	5.5	A	C	752.12	N
81X4-071	20-50	195.2	62.8	9.1	A	C-	753.31	N
81X4-083	10-50	4.3	75.3	2.1	UA	A-	753.43	N
81X5-009	10-40	0.4	73.8	3.0	A	B	754.19	N
82X1-047		ICA				F	758.17	N
82X1-135	25-80	14.4	16.9	4.0	A	B-	759.05	N
82X2-023	15-40	25.5	74.8	3.2	A	B-	759.43	N
82X2-143	15-80	142.4	41.2	1.9	UA	A	760.63	N
82X3-090	15-80	249.0	57.3	1.2	A	B+	761.60	N
82X3-136	15-80	136.4	79.6	0.6	A	B+	762.06	N
82X4-005	15-80	-60.5	79.3	0.8	A	B++	762.25	N
82X4-068		ICA				F	762.88	N
82X5-060	20-80	241.1	-46.8	1.2	UA	A	764.30	N
82X5-101	20-80	282.3	-53.7	1.3	UA	B+	764.71	N
82X6-048	25-80	308.5	-19.3	0.8	UA	A	765.68	N
82X7-012	10-25	167.4	64.9	5.1	A	C	766.82	N
83X1-011	15-25	-46.6	44.9	3.8	A	C-	767.51	N
83X2-015	50-80	-1.5	-7.0	1.6	A	C	769.05	N
83X2-101	15-30	207.8	39.2	4.2	A	C	769.91	N
83X3-043	15-30	259.9	54.9	3.1	A	C	770.83	N
83X3-116	35-80	282.4	-41.3	2.9	A	B	771.56	Y
83X4-062	40-80	328.0	-40.8	0.7	A	B+	772.52	Y
83X4-072	25-80	353.3	-55.5	1.5	A	B-	772.62	Y
83X5-036	5-50	223.9	-48.8	1.0	UA	B+	773.76	Y
83X5-091	10-60	20.1	-43.0	1.1	UA	B	774.31	Y
83X6-015	20-80	87.0	-30.9	1.3	A	B	775.05	Y
83X6-070	15-80	-5.8	-39.3	0.3	A	B+	775.60	Y
83X7-014	35-80	140.0	-39.6	0.6	A	B+	776.54	Y
83X7-032	25-80	144.7	-35.4	0.7	A	B+	776.72	Y
84X1-101	30-80	217.1	-53.7	1.9	A	B	778.01	Y
84X1-116	25-80	35.0	-39.6	0.7	A	B+	778.16	Y
84X2-059	30-80	175.2	14.3	5.0	A	C	779.09	N
84X2-129	25-80	295.1	29.6	0.6	A	B+	779.79	N

Table A4. Continued.

Sample 145-884B-	Demag. levels	Declination (deg)	Inclination (deg)	MAD	A/UA	Fit of plot	Depth (mbsf)	Used in colatitude
84X3-031	15-80	116.0	10.6	0.9	A	B+	780.31	N
84X3-119	25-80	181.7	51.1	1.3	A	B-	781.19	N
84X4-061	30-80	11.4	55.3	4.1	A	C+	782.11	N
84X4-113	15-80	189.9	35.1	1.4	A	B+	782.63	N
84X5-045	10-35	36.2	59.5	2.4	A	B-	783.45	N
84X5-106	10-30	237.9	58.3	8.2	A	C	784.06	N
84X6-043	10-40	85.8	72.9	4.3	A	B-	784.93	N
84X6-123	10-35	293.8	-27.3	1.9	UA	B	785.73	N
84X7-026		ICA				F	786.26	N
85X1-029		ICA				F	786.99	N
85X1-062	10-25	222.3	65.3	0.7	A	C	787.32	N
85X2-014	15-50	125.6	-46.7	3.1	A	B	788.34	N
85X2-122	15-50	158.9	-50.9	3.3	A	B-	789.42	N
85X3-062	20-40	309.0	-34.8	3.6	A	B-	790.32	N
85X3-084	30-70	343.8	-69.4	1.3	A	B	790.54	Y
85X4-089	25-80	242.1	-57.0	1.7	A	B	792.09	Y
84X4-113	25-80	242.2	-56.5	1.7	A	B	792.33	Y
85X5-010	20-70	97.3	-60.0	2.1	A	B	792.80	Y
85X5-111	15-50	241.2	-63.6	0.8	A	B+	793.81	Y
85X6-050	15-50	90.1	-62.8	1.3	A	A-	794.70	Y
85X6-122	15-80	152.8	-56.2	1.1	UA	A	795.42	Y
85X7-031	10-80	141.9	-56.3	1.1	UA	A+	796.01	Y
86X1-120	15-40	257.1	-27.3	2.7	A	B+	797.60	Y
86X2-030	15-80	165.7	-56.7	0.9	UA	A+	798.20	Y
86X2-079	15-80	277.9	-66.1	0.8	UA	A+	798.69	Y
86X3-013	15-80	144.7	-56.7	1.1	UA	A	799.53	Y
86X3-081	15-80	135.8	-61.0	2.0	UA	A	800.21	Y
86X4-054	15-80	57.3	-56.9	0.6	UA	A	801.44	Y
86X4-135	10-40	253.7	66.6	1.6	A	B	802.25	Y
86X5-030	20-80	4.3	55.7	0.5	UA	A-	802.70	Y
86X5-128	20-70	156.7	55.7	2.2	A	B	803.68	Y
86X6-051		ICA				F	804.41	N
86X6-077	20-70	104.5	65.8	1.2	A	B+	804.67	Y
86X7-043	20-80	66.3	68.4	0.7	UA	B+	805.83	Y
87X1-025	25-50	233.4	50.4	2.9	A	B	806.35	Y
87X1-144	15-80	114.0	9.1	2.8	A	B-	807.54	N
87X2-022	20-70	267.4	49.6	4.5	A	B	807.82	Y
87X2-124	25-60	352.6	-60.2	4.4	A	B	808.84	Y
87X3-010	20-70	117.2	-24.8	1.7	A	B-	809.20	N
87X3-079	20-70	-48.0	51.1	2.8	A	B	809.89	Y
87X4-017	25-60	27.3	59.6	4.5	A	B	810.77	Y
87X4-140	25-60	268.9	53.8	6.7	A	B	812.00	Y
87X5-028	20-50	120.7	19.1	7.5	A	C	812.38	N
87X5-136	15-60	-16.4	39.6	5.6	A	C	813.46	N
87X6-008	25-50	278.8	40.0	4.6	A	B	813.68	Y
87X6-039	25-80	183.5	50.3	3.0	A	B	813.99	Y

Abbreviations: ICA= Inconsistent analysis; A/UA= Anchored/Unanchored fit of plot to (0,0); MAD= Maximum Angular Deviation of PCA; Fit of plot= quality of stable PCA inclination fit to actual observed inclinations (range: A=excellent to F=poor).

Table A5. Leg 145 Hole 884B magnetic susceptibility (AMS) data.

Hole	Sample #	Magnetic Susceptibility (10E-6 SI)			Anisotropy Factors							Anisotropy	Inclination	tan(Inc)	Susceptibilty
		K(max)	K(int)	K(min)	L	F	P	1/P	P`	T	q		(°)		ellipsoid
884B	70x1-147	631	626	620	1.007	1.014	1.021	0.979	1.022	0.359	0.385	Weak	-62.1	1.89	oblate
884B	70x3-144	749	740	725	1.002	1.032	1.034	0.967	1.038	0.900	0.052	Weak	51.5	1.26	oblate
884B	71x4-072	473	471	466	1.002	1.016	1.018	0.982	1.02	0.815	0.098	Weak	49.5	1.17	oblate
884B	72x2-100	701	696	692	1.002	1.017	1.019	0.981	1.021	0.759	0.129	Weak	-57.6	1.58	oblate
884B	73x3-014	730	726	722	1.006	1.007	1.014	0.986	1.014	0.044	0.631	Weak	-41.4	0.88	oblate
884B	73x5-012	319	317	315	1.002	1.014	1.016	0.984	1.017	0.808	0.102	Weak	-50.1	1.20	oblate
884B	74x1-105	1113	1108	1104	1.006	1.003	1.008	0.992	1.008	-0.349	1.020	Weak	UA		prolate
884B	75x1-115	1543	1539	1535	1.002	1.004	1.006	0.994	1.006	0.422	0.339	Weak	64.3	2.08	oblate
884B	76x1-041	1001	984	971	1.022	1.008	1.030	0.971	1.031	-0.467	1.166	Weak	55.0	1.43	prolate
884B	77x6-023	1826	1800	1769	1.002	1.043	1.046	0.956	1.052	0.894	0.055	Weak	36.4	0.74	oblate
884B	78x4-143	3118	3084	3036	1.009	1.023	1.031	0.970	1.032	0.449	0.324	Weak	-23.6	0.44	oblate
884B	79x5-082	2518	2466	2366	1.002	1.078	1.080	0.926	1.092	0.947	0.028	Moderate	UA		oblate
884B	81x2-081	1203	1184	1149	1.008	1.048	1.056	0.947	1.061	0.717	0.156	Weak/Mod	59.5	1.70	oblate
884B	83x5-091	1381	1374	1360	1.003	1.016	1.019	0.981	1.021	0.675	0.178	Weak	-43.0	0.93	oblate
884B	85x4-089	1626	1603	1563	1.002	1.045	1.047	0.955	1.053	0.913	0.046	Weak	-57.0	1.54	oblate
884B	85x7-031	1211	1202	1188	1.003	1.019	1.022	0.978	1.024	0.695	0.167	Weak	-56.3	1.50	oblate
884B	86x5-030	2142	2111	2058	1.001	1.044	1.044	0.958	1.051	0.972	0.014	Weak	55.7	1.47	oblate
884B	86x7-043	2256	2234	2190	1.004	1.035	1.040	0.962	1.044	0.776	0.121	Weak	68.4	2.53	oblate
884B	87x2-124	1512	1492	1460	1.005	1.032	1.038	0.963	1.041	0.728	0.149	Weak	-60.2	1.75	oblate
884B	87x6-039	1404	1383	1344	1.004	1.040	1.045	0.957	1.05	0.804	0.105	Weak	50.3	1.20	oblate

Table A6. ARM (min) /ARM (max) analysis of selected Hole 884B samples.

Sample	Int. (Z) (A/m)	Int. (X) (A/m)	Int. (Y) (A/m)	Average X/Y	I(Z)/I(X)	I(Z)/I(Y)	ARM (min) ARM (max)	ARM ^2	Dev. ARM	Var. ARM	Inc. (I) (deg)	tan (I)	Dev. tan(I)	Var. tan(I)	Dev (ARM)* Dev tan (I)
884B70X1-147	5.63E-04	6.06E-04	6.02E-04	6.04E-04	0.929	0.935	0.932	0.869	-0.004	2.00E-05	-62.1	1.89	0.56	0.31	-2.49E-03
884B70X3-144	5.63E-04	6.00E-04	5.98E-04	5.99E-04	0.937	0.940	0.939	0.881	0.002	4.09E-06	51.5	1.26	-0.07	0.01	-1.50E-04
884B71X4-072	4.74E-04	4.99E-04	4.99E-04	4.99E-04	0.951	0.951	0.951	0.904	0.014	1.98E-04	49.5	1.17	-0.16	0.03	-2.26E-03
884B72X2-100	5.63E-04	6.00E-04	5.98E-04	5.99E-04	0.937	0.940	0.939	0.881	0.002	4.09E-06	-57.6	1.58	0.24	0.06	4.94E-04
884B73X3-014	7.48E-04	7.80E-04	7.80E-04	7.80E-04	0.960	0.960	0.960	0.921	0.023	5.32E-04	-41.4	0.88	-0.45	0.20	-1.04E-02
884B73X5-012	3.47E-04	3.62E-04	3.58E-04	3.60E-04	0.960	0.969	0.964	0.930	0.028	7.58E-04	-50.1	1.20	-0.14	0.02	-3.73E-03
884B75X1-115	6.40E-04	6.49E-04	6.51E-04	6.50E-04	0.987	0.984	0.985	0.971	0.048	2.34E-03	64.3	2.08	0.75	0.56	3.61E-02
884B76X1-041	5.94E-04	5.96E-04	6.18E-04	6.07E-04	0.996	0.960	0.978	0.956	0.041	1.68E-03	55.0	1.43	0.10	0.01	3.96E-03
884B77X6-023	1.38E-03	1.56E-03	1.55E-03	1.55E-03	0.887	0.894	0.891	0.794	-0.046	2.11E-03	36.4	0.74	-0.59	0.35	2.73E-02
884B78X4-143	1.53E-03	1.61E-03	1.59E-03	1.60E-03	0.952	0.966	0.959	0.919	0.022	4.75E-04	-23.6	0.44	-0.89	0.80	-1.95E-02
884B81X2-081	4.02E-04	4.42E-04	4.37E-04	4.40E-04	0.908	0.919	0.914	0.835	-0.023	5.43E-04	21.9	0.40	-0.93	0.86	2.17E-02
884B83X5-091	3.99E-04	4.19E-04	4.22E-04	4.21E-04	0.951	0.945	0.948	0.898	0.011	1.18E-04	-43.0	0.93	-0.40	0.16	-4.34E-03
884B85X4-089	4.16E-04	4.42E-04	4.42E-04	4.42E-04	0.942	0.941	0.942	0.887	0.005	2.23E-05	-57.0	1.54	0.21	0.04	9.84E-04
884B85X7-031	2.57E-04	2.74E-04	2.78E-04	2.76E-04	0.937	0.922	0.929	0.864	-0.008	5.63E-05	-56.3	1.50	0.17	0.03	-1.26E-03
884B86X5-030	4.55E-04	5.01E-04	4.98E-04	5.00E-04	0.906	0.913	0.910	0.828	-0.027	7.31E-04	55.7	1.47	0.13	0.02	-3.64E-03
884B86X7-043	6.09E-04	6.56E-04	6.53E-04	6.55E-04	0.928	0.933	0.930	0.866	-0.006	4.02E-05	68.4	2.53	1.19	1.43	-7.58E-03
884B87X2-124	4.43E-04	4.81E-04	4.86E-04	4.84E-04	0.921	0.912	0.916	0.839	-0.021	4.24E-04	-60.2	1.75	0.41	0.17	-8.54E-03
884B87X6-039	5.61E-04	6.33E-04	6.47E-04	6.40E-04	0.886	0.867	0.877	0.768	-0.060	3.63E-03	50.3	1.20	-0.13	0.02	7.65E-03
Std dev. Tan I=		0.546													
mean tan I=		1.331													
sum tan I=		23.966													
sum ARM (min/max)=		16.863													
sum (ARM min/max)^2=		15.811													
mean ARM min/max=		0.937													
SS(xx)=		1.37E-02													
SS (yy)=		5.07													
SS (xy)=		3.44E-02													
R =		0.130													
mean I=		50.24													
Std dev. I=		12.82													

Table A7. Hysteresis analysis data for selected samples from Holes 884B and 869A.

Hole	Sample	Mr/Ms	Hcr/Hc	Mass (mg)	Mineral	Grain type
869A	5H1-027	0.390	2.001	56	Magnetite	PSD
884B	70X1-121	0.227	2.109	26	Magnetite	PSD
884B	70X2-040	0.208	2.344	44	Magnetite	PSD
884B	70X6-041	0.214	2.381	10	Magnetite	PSD
884B	71X1-139	0.234	2.33	14	Magnetite	PSD
884B	72X1-015	0.212	2.361	36	Magnetite	PSD
884B	72X7-051	0.191	2.673	15	Magnetite	PSD
884B	73X1-084	0.220	2.284	50	Magnetite	PSD
884B	73X3-068	0.221	2.281	35	Magnetite	PSD
884B	74X3-138	0.232	2.336	14	Magnetite	PSD
884B	75X1-096	0.256	2.265	50	Magnetite	PSD
884B	75X3-083	0.196	2.489	37	Magnetite	PSD
884B	76X4-110	0.125	3.241	30	Magnetite	PSD
884B	77X4-122	0.261	2.225	24	Magnetite	PSD
884B	78X5-066	0.210	2.508	48	Magnetite	PSD
884B	79X5-120	0.216	2.183	45	Magnetite	PSD
884B	80X5-120	0.203	2.619	9	Magnetite	PSD
884B	81X4-083	0.328	N/A	23	Magnetite	PSD
884B	83X2-015	0.404	1.737	41	Magnetite	PSD/SD
884B	86X2-030	0.170	2.276	55	Magnetite	PSD
884B	86X4-056	0.170	2.238	50	Magnetite	PSD

Abbreviations : Mr = remanent magnetization, Ms = saturation magnetization, Hc = bulk coercivity, Hcr = coercivity of remanence, PSD = pseudo-single domain, SD = single domain.

Table A8. IRM acquistion data for Leg 143 Hole 869A.

SIRM Pulse	Sample Intensities (A/m)		Sample Intensities (A/m)		Sample Intensities (A/m)		Sample Intensities (A/m)		Sample Intensities (A/m)	
(mT)	Actual	Normalized	Actual	Normalized	Actual	Normalized	Actual	Normalized	Actual	Normalized
	5H1-055	5H1-055	5H2-057	5H2-057	5H3-083	5H3-083	5H4-083	5H4-083	5H5-008	5H5-008
0	4.22E-07	6.94E-04	9.92E-08	1.23E-04	2.32E-07	3.88E-04	3.50E-07	7.92E-04	1.50E-07	2.83E-04
1	1.98E-06	3.26E-03	2.46E-06	3.05E-03	1.85E-06	3.08E-03	1.15E-06	2.60E-03	1.61E-06	3.04E-03
5	1.45E-05	2.38E-02	2.02E-05	2.50E-02	1.43E-05	2.39E-02	8.66E-06	1.96E-02	1.27E-05	2.39E-02
10	4.68E-05	7.70E-02	6.42E-05	7.95E-02	4.58E-05	7.64E-02	2.88E-05	6.52E-02	4.04E-05	7.64E-02
15	8.70E-05	1.43E-01	1.18E-04	1.46E-01	8.46E-05	1.41E-01	5.50E-05	1.24E-01	7.47E-05	1.41E-01
20	1.37E-04	2.25E-01	1.82E-04	2.26E-01	1.33E-04	2.21E-01	8.84E-05	2.00E-01	1.17E-04	2.21E-01
25	1.99E-04	3.27E-01	2.65E-04	3.28E-01	1.93E-04	3.22E-01	1.31E-04	2.96E-01	1.71E-04	3.23E-01
30	2.54E-04	4.18E-01	3.39E-04	4.19E-01	2.49E-04	4.14E-01	1.70E-04	3.85E-01	2.20E-04	4.16E-01
35	3.12E-04	5.13E-01	4.17E-04	5.17E-01	3.08E-04	5.14E-01	2.11E-04	4.77E-01	2.71E-04	5.12E-01
40	3.64E-04	5.99E-01	4.85E-04	6.01E-01	3.60E-04	6.00E-01	2.48E-04	5.61E-01	3.17E-04	5.98E-01
50	4.40E-04	7.24E-01	5.85E-04	7.25E-01	4.37E-04	7.28E-01	3.04E-04	6.88E-01	3.85E-04	7.28E-01
60	4.88E-04	8.03E-01	6.49E-04	8.04E-01	4.85E-04	8.08E-01	3.41E-04	7.71E-01	4.28E-04	8.09E-01
70	5.20E-04	8.55E-01	6.93E-04	8.58E-01	5.17E-04	8.62E-01	3.66E-04	8.28E-01	4.57E-04	8.63E-01
80	5.41E-04	8.90E-01	7.19E-04	8.90E-01	5.37E-04	8.95E-01	3.84E-04	8.69E-01	4.76E-04	8.98E-01
90	5.55E-04	9.13E-01	7.38E-04	9.14E-01	5.49E-04	9.15E-01	3.94E-04	8.91E-01	4.87E-04	9.19E-01
100	5.63E-04	9.26E-01	7.46E-04	9.23E-01	5.57E-04	9.29E-01	4.02E-04	9.10E-01	4.94E-04	9.32E-01
120	5.73E-04	9.42E-01	7.63E-04	9.45E-01	5.67E-04	9.45E-01	4.11E-04	9.30E-01	5.02E-04	9.48E-01
140	5.77E-04	9.49E-01	7.64E-04	9.45E-01	5.70E-04	9.50E-01	4.15E-04	9.39E-01	5.05E-04	9.53E-01
160	5.84E-04	9.61E-01	7.76E-04	9.61E-01	5.77E-04	9.62E-01	4.20E-04	9.50E-01	5.10E-04	9.63E-01
180	5.84E-04	9.61E-01	7.75E-04	9.59E-01	5.77E-04	9.62E-01	4.22E-04	9.55E-01	5.11E-04	9.65E-01
200	5.90E-04	9.70E-01	7.84E-04	9.71E-01	5.83E-04	9.71E-01	4.26E-04	9.64E-01	5.15E-04	9.72E-01
220	5.89E-04	9.69E-01	7.80E-04	9.66E-01	5.82E-04	9.70E-01	4.27E-04	9.66E-01	5.15E-04	9.72E-01
240	5.94E-04	9.77E-01	7.88E-04	9.76E-01	5.86E-04	9.77E-01	4.30E-04	9.73E-01	5.18E-04	9.78E-01
260	5.93E-04	9.75E-01	7.87E-04	9.75E-01	5.87E-04	9.78E-01	4.31E-04	9.75E-01	5.18E-04	9.79E-01
300	5.95E-04	9.79E-01	7.88E-04	9.76E-01	5.88E-04	9.80E-01	4.33E-04	9.80E-01	5.20E-04	9.82E-01
350	5.97E-04	9.82E-01	7.90E-04	9.78E-01	5.90E-04	9.84E-01	4.34E-04	9.82E-01	5.22E-04	9.86E-01
400	5.99E-04	9.85E-01	7.92E-04	9.81E-01	5.92E-04	9.87E-01	4.36E-04	9.86E-01	5.23E-04	9.88E-01
450	6.01E-04	9.88E-01	7.95E-04	9.85E-01	5.93E-04	9.88E-01	4.37E-04	9.89E-01	5.24E-04	9.90E-01
500	6.02E-04	9.90E-01	7.98E-04	9.88E-01	5.95E-04	9.92E-01	4.38E-04	9.91E-01	5.25E-04	9.91E-01
550	6.02E-04	9.90E-01	7.95E-04	9.85E-01	5.94E-04	9.91E-01	4.38E-04	9.91E-01	5.25E-04	9.92E-01
600	6.02E-04	9.90E-01	7.97E-04	9.87E-01	5.96E-04	9.93E-01	4.39E-04	9.93E-01	5.26E-04	9.93E-01
700	6.06E-04	9.97E-01	8.06E-04	9.98E-01	5.98E-04	9.98E-01	4.41E-04	9.98E-01	5.28E-04	9.98E-01
800	6.07E-04	9.98E-01	8.06E-04	9.99E-01	5.99E-04	9.99E-01	4.41E-04	9.98E-01	5.29E-04	9.99E-01
900	6.08E-04	1.00E+00	8.08E-04	1.00E+00	6.00E-04	1.00E+00	4.42E-04	1.00E+00	5.29E-04	1.00E+00
1000	6.05E-04	9.95E-01	8.02E-04	9.93E-01	5.97E-04	9.96E-01	4.41E-04	9.98E-01	5.28E-04	9.97E-01

Table A8. Continued.

SIRM Pulse	Sample Intensities (A/m)		Sample Intensities (A/m)		Sample Intensities (A/m)		Sample Intensities (A/m)		Sample Intensities (A/m)	
(mT)	Actual	Normalized	Actual	Normalized	Actual	Normalized	Actual	Normalized	Actual	Normalized
	5H6-021	5H6-021	5H7-009	5H7-009	6H1-020	6H1-020	6H2-086	6H2-086	6H3-126	6H3-126
0	2.46E-07	5.12E-04	1.34E-07	3.06E-04	1.17E-06	1.94E-03	6.57E-07	8.15E-04	2.69E-07	4.53E-04
1	1.35E-06	2.81E-03	1.27E-06	2.91E-03	3.30E-06	5.43E-03	3.16E-06	3.92E-03	5.21E-06	8.77E-03
5	1.06E-05	2.21E-02	9.95E-06	2.27E-02	1.48E-05	2.44E-02	1.78E-05	2.20E-02	2.52E-05	4.24E-02
10	3.43E-05	7.14E-02	3.13E-05	7.15E-02	4.76E-05	7.83E-02	5.54E-05	6.87E-02	7.87E-05	1.32E-01
15	6.44E-05	1.34E-01	5.77E-05	1.32E-01	9.36E-05	1.54E-01	1.11E-04	1.38E-01	1.56E-04	2.62E-01
20	1.03E-04	2.15E-01	9.07E-05	2.07E-01	1.39E-04	2.29E-01	1.65E-04	2.04E-01	2.32E-04	3.90E-01
25	1.53E-04	3.18E-01	1.34E-04	3.06E-01	2.04E-04	3.37E-01	2.42E-04	3.00E-01	3.42E-04	5.75E-01
30	1.98E-04	4.13E-01	1.74E-04	3.96E-01	2.72E-04	4.49E-01	3.23E-04	4.01E-01	4.45E-04	7.48E-01
35	2.46E-04	5.13E-01	2.17E-04	4.96E-01	3.32E-04	5.46E-01	3.92E-04	4.87E-01	5.42E-04	9.11E-01
40	2.88E-04	5.99E-01	2.56E-04	5.84E-01	3.84E-04	6.33E-01	4.56E-04	5.65E-01	6.26E-04	1.05E+00
50	3.51E-04	7.31E-01	3.16E-04	7.21E-01	4.62E-04	7.62E-01	5.47E-04	6.78E-01	7.53E-04	1.27E+00
60	3.90E-04	8.12E-01	3.55E-04	8.10E-01	5.12E-04	8.43E-01	6.05E-04	7.50E-01	8.30E-04	1.40E+00
70	4.15E-04	8.65E-01	3.81E-04	8.70E-01	5.48E-04	9.04E-01	6.50E-04	8.06E-01	8.86E-04	1.49E+00
80	4.31E-04	8.99E-01	3.98E-04	9.08E-01	5.68E-04	9.35E-01	6.72E-04	8.34E-01	9.15E-04	1.54E+00
90	4.40E-04	9.17E-01	4.07E-04	9.29E-01	5.77E-04	9.50E-01	6.84E-04	8.48E-01	9.32E-04	1.57E+00
100	4.47E-04	9.32E-01	4.12E-04	9.41E-01	5.90E-04	9.72E-01	7.01E-04	8.69E-01	9.48E-04	1.60E+00
120	4.53E-04	9.45E-01	4.19E-04	9.55E-01	5.94E-04	9.79E-01	7.05E-04	8.75E-01	9.56E-04	1.61E+00
140	4.58E-04	9.55E-01	4.20E-04	9.58E-01	6.00E-04	9.89E-01	7.13E-04	8.84E-01	9.66E-04	1.63E+00
160	4.61E-04	9.61E-01	4.24E-04	9.68E-01	6.04E-04	9.95E-01	7.18E-04	8.91E-01	9.71E-04	1.63E+00
180	4.64E-04	9.68E-01	4.24E-04	9.67E-01	6.07E-04	1.00E+00	7.23E-04	8.96E-01	9.76E-04	1.64E+00
200	4.66E-04	9.71E-01	4.28E-04	9.76E-01	6.10E-04	1.01E+00	7.26E-04	9.00E-01	9.80E-04	1.65E+00
220	4.68E-04	9.76E-01	4.27E-04	9.74E-01	6.14E-04	1.01E+00	7.34E-04	9.10E-01	9.86E-04	1.66E+00
240	4.69E-04	9.78E-01	4.30E-04	9.81E-01	6.18E-04	1.02E+00	7.39E-04	9.16E-01	9.90E-04	1.67E+00
260	4.71E-04	9.82E-01	4.30E-04	9.81E-01	6.16E-04	1.01E+00	7.33E-04	9.09E-01	9.88E-04	1.66E+00
300	4.73E-04	9.85E-01	4.30E-04	9.82E-01	6.18E-04	1.02E+00	7.39E-04	9.16E-01	9.94E-04	1.67E+00
350	4.75E-04	9.89E-01	4.32E-04	9.85E-01	6.23E-04	1.03E+00	7.43E-04	9.22E-01	9.98E-04	1.68E+00
400	4.76E-04	9.92E-01	4.33E-04	9.89E-01	6.26E-04	1.03E+00	7.47E-04	9.26E-01	1.00E-03	1.69E+00
450	4.77E-04	9.94E-01	4.34E-04	9.91E-01	6.22E-04	1.03E+00	7.43E-04	9.21E-01	9.99E-04	1.68E+00
500	4.77E-04	9.94E-01	4.35E-04	9.92E-01	6.24E-04	1.03E+00	7.44E-04	9.23E-01	1.00E-03	1.68E+00
550	4.77E-04	9.95E-01	4.34E-04	9.90E-01	6.28E-04	1.03E+00	7.50E-04	9.31E-01	1.01E-03	1.69E+00
600	4.78E-04	9.96E-01	4.35E-04	9.93E-01	6.25E-04	1.03E+00	7.46E-04	9.25E-01	1.00E-03	1.69E+00
700	4.78E-04	9.96E-01	4.37E-04	9.98E-01	6.30E-04	1.04E+00	7.53E-04	9.34E-01	1.01E-03	1.70E+00
800	4.79E-04	9.97E-01	4.38E-04	9.99E-01	6.30E-04	1.04E+00	7.54E-04	9.35E-01	1.01E-03	1.70E+00
900	4.79E-04	9.98E-01	4.38E-04	1.00E+00	6.27E-04	1.03E+00	7.49E-04	9.29E-01	1.01E-03	1.70E+00
1000	4.80E-04	1.00E+00	4.37E-04	9.97E-01	6.27E-04	1.03E+00	7.50E-04	9.30E-01	1.01E-03	1.70E+00

Table A8. Continued.

SIRM Pulse	Sample Intensities (A/m)		Sample Intensities (A/m)		Sample Intensities (A/m)		Sample Intensities (A/m)		Sample Intensities (A/m)	
(mT)	Actual	Normalized	Actual	Normalized	Actual	Normalized	Actual	Normalized	Actual	Normalized
	6H4-061	6H4-061	6H5-128	6H5-128	6H6-130	6H6-130	6H7-060	6H7-060	7H2-064	7H2-064
0	2.25E-07	5.10E-04	1.97E-07	3.72E-04	3.29E-07	6.87E-04	5.86E-07	1.34E-03	4.34E-07	1.25E-03
1	2.81E-06	6.36E-03	2.66E-06	5.03E-03	2.42E-06	5.06E-03	3.31E-06	7.56E-03	1.42E-06	4.10E-03
5	1.34E-05	3.05E-02	1.32E-05	2.49E-02	1.18E-05	2.47E-02	1.69E-05	3.86E-02	7.67E-06	2.22E-02
10	4.21E-05	9.55E-02	4.34E-05	8.19E-02	3.88E-05	8.10E-02	5.37E-05	1.23E-01	2.33E-05	6.73E-02
15	8.30E-05	1.88E-01	8.68E-05	1.64E-01	7.81E-05	1.63E-01	1.06E-04	2.43E-01	4.31E-05	1.25E-01
20	1.24E-04	2.81E-01	1.30E-04	2.46E-01	1.18E-04	2.46E-01	1.59E-04	3.62E-01	6.81E-05	1.97E-01
25	1.85E-04	4.19E-01	1.92E-04	3.63E-01	1.76E-04	3.67E-01	2.34E-04	5.35E-01	9.91E-05	2.86E-01
30	2.42E-04	5.50E-01	2.49E-04	4.70E-01	2.29E-04	4.78E-01	3.04E-04	6.94E-01	1.30E-04	3.76E-01
35	2.99E-04	6.78E-01	3.06E-04	5.78E-01	2.82E-04	5.89E-01	3.71E-04	8.47E-01	1.64E-04	4.74E-01
40	3.50E-04	7.93E-01	3.56E-04	6.72E-01	3.27E-04	6.82E-01	4.29E-04	9.80E-01	1.98E-04	5.72E-01
50	4.27E-04	9.69E-01	4.35E-04	8.22E-01	3.97E-04	8.29E-01	5.19E-04	1.18E+00	2.46E-04	7.11E-01
60	4.74E-04	1.07E+00	4.86E-04	9.18E-01	4.40E-04	9.18E-01	5.72E-04	1.30E+00	2.74E-04	7.92E-01
70	5.08E-04	1.15E+00	5.24E-04	9.90E-01	4.69E-04	9.79E-01	6.09E-04	1.39E+00	2.95E-04	8.53E-01
80	5.24E-04	1.19E+00	5.46E-04	1.03E+00	4.85E-04	1.01E+00	6.29E-04	1.44E+00	3.02E-04	8.73E-01
90	5.34E-04	1.21E+00	5.60E-04	1.06E+00	4.96E-04	1.04E+00	6.40E-04	1.46E+00	3.13E-04	9.05E-01
100	5.43E-04	1.23E+00	5.74E-04	1.08E+00	5.05E-04	1.05E+00	6.51E-04	1.49E+00	3.18E-04	9.19E-01
120	5.47E-04	1.24E+00	5.85E-04	1.10E+00	5.13E-04	1.07E+00	6.58E-04	1.50E+00	3.23E-04	9.34E-01
140	5.51E-04	1.25E+00	5.94E-04	1.12E+00	5.19E-04	1.08E+00	6.64E-04	1.51E+00	3.26E-04	9.42E-01
160	5.53E-04	1.25E+00	6.01E-04	1.13E+00	5.24E-04	1.09E+00	6.67E-04	1.52E+00	3.28E-04	9.48E-01
180	5.56E-04	1.26E+00	6.06E-04	1.15E+00	5.27E-04	1.10E+00	6.70E-04	1.53E+00	3.30E-04	9.54E-01
200	5.58E-04	1.27E+00	6.11E-04	1.15E+00	5.30E-04	1.11E+00	6.74E-04	1.54E+00	3.34E-04	9.65E-01
220	5.61E-04	1.27E+00	6.16E-04	1.16E+00	5.32E-04	1.11E+00	6.77E-04	1.54E+00	3.30E-04	9.54E-01
240	5.64E-04	1.28E+00	6.19E-04	1.17E+00	5.34E-04	1.11E+00	6.79E-04	1.55E+00	3.34E-04	9.65E-01
260	5.62E-04	1.27E+00	6.20E-04	1.17E+00	5.36E-04	1.12E+00	6.79E-04	1.55E+00	3.34E-04	9.65E-01
300	5.64E-04	1.28E+00	6.25E-04	1.18E+00	5.39E-04	1.12E+00	6.82E-04	1.56E+00	3.38E-04	9.77E-01
350	5.68E-04	1.29E+00	6.30E-04	1.19E+00	5.41E-04	1.13E+00	6.85E-04	1.56E+00	3.38E-04	9.77E-01
400	5.69E-04	1.29E+00	6.32E-04	1.19E+00	5.42E-04	1.13E+00	6.87E-04	1.57E+00	3.38E-04	9.77E-01
450	5.68E-04	1.29E+00	6.33E-04	1.19E+00	5.43E-04	1.13E+00	6.86E-04	1.57E+00	3.43E-04	9.91E-01
500	5.69E-04	1.29E+00	6.34E-04	1.20E+00	5.44E-04	1.14E+00	6.88E-04	1.57E+00	3.44E-04	9.94E-01
550	5.71E-04	1.29E+00	6.37E-04	1.20E+00	5.45E-04	1.14E+00	6.89E-04	1.57E+00	3.42E-04	9.88E-01
600	5.70E-04	1.29E+00	6.37E-04	1.20E+00	5.46E-04	1.14E+00	6.89E-04	1.57E+00	3.43E-04	9.91E-01
700	5.72E-04	1.30E+00	6.39E-04	1.21E+00	5.47E-04	1.14E+00	6.92E-04	1.58E+00	3.45E-04	9.97E-01
800	5.72E-04	1.30E+00	6.40E-04	1.21E+00	5.47E-04	1.14E+00	6.92E-04	1.58E+00	3.46E-04	1.00E+00
900	5.71E-04	1.30E+00	6.40E-04	1.21E+00	5.48E-04	1.14E+00	6.92E-04	1.58E+00	3.44E-04	9.94E-01
1000	5.71E-04	1.29E+00	6.40E-04	1.21E+00	5.48E-04	1.14E+00	6.92E-04	1.58E+00	3.45E-04	9.97E-01

Table A8. Continued.

SIRM Pulse	Sample Intensities (A/m)		Sample Intensities (A/m)		Sample Intensities (A/m)		Sample Intensities (A/m)		Sample Intensities (A/m)	
(mT)	Actual	Normalized	Actual	Normalized	Actual	Normalized	Actual	Normalized	Actual	Normalized
	7H3-084	7H3-084	7H4-075	7H4-075	7H5-070	7H5-070	7H6-070	7H6-070	7H7-075	7H7-075
0	2.32E-07	5.63E-04	4.36E-07	7.80E-04	7.85E-08	2.17E-04	1.85E-07	4.34E-04	3.00E-07	6.55E-04
1	2.04E-06	4.95E-03	2.22E-06	3.97E-03	1.81E-06	5.01E-03	2.43E-06	5.71E-03	2.27E-06	4.97E-03
5	8.96E-06	2.17E-02	1.17E-05	2.09E-02	1.03E-05	2.85E-02	1.22E-05	2.85E-02	1.23E-05	2.68E-02
10	2.77E-05	6.72E-02	3.67E-05	6.57E-02	2.99E-05	8.27E-02	3.44E-05	8.09E-02	3.57E-05	7.81E-02
15	5.12E-05	1.24E-01	6.92E-05	1.24E-01	5.33E-05	1.47E-01	6.13E-05	1.44E-01	6.46E-05	1.41E-01
20	8.09E-05	1.96E-01	1.10E-04	1.97E-01	8.16E-05	2.26E-01	9.37E-05	2.20E-01	9.99E-05	2.18E-01
25	1.18E-04	2.87E-01	1.59E-04	2.84E-01	1.16E-04	3.20E-01	1.33E-04	3.12E-01	1.43E-04	3.12E-01
30	1.55E-04	3.75E-01	2.06E-04	3.68E-01	1.48E-04	4.10E-01	1.74E-04	4.08E-01	1.84E-04	4.02E-01
35	1.95E-04	4.74E-01	2.58E-04	4.62E-01	1.84E-04	5.08E-01	2.16E-04	5.06E-01	2.29E-04	5.00E-01
40	2.36E-04	5.73E-01	3.09E-04	5.54E-01	2.17E-04	6.00E-01	2.54E-04	5.96E-01	2.70E-04	5.90E-01
50	2.93E-04	7.11E-01	3.82E-04	6.85E-01	2.64E-04	7.30E-01	3.10E-04	7.27E-01	3.31E-04	7.23E-01
60	3.25E-04	7.88E-01	4.24E-04	7.59E-01	2.90E-04	8.02E-01	3.40E-04	7.99E-01	3.63E-04	7.93E-01
70	3.50E-04	8.49E-01	4.55E-04	8.15E-01	3.09E-04	8.56E-01	3.63E-04	8.53E-01	3.87E-04	8.45E-01
80	3.61E-04	8.76E-01	4.72E-04	8.46E-01	3.19E-04	8.83E-01	3.76E-04	8.83E-01	4.02E-04	8.78E-01
90	3.72E-04	9.02E-01	4.87E-04	8.72E-01	3.27E-04	9.06E-01	3.85E-04	9.05E-01	4.12E-04	9.01E-01
100	3.77E-04	9.14E-01	4.96E-04	8.88E-01	3.32E-04	9.20E-01	3.92E-04	9.21E-01	4.19E-04	9.16E-01
120	3.86E-04	9.37E-01	5.09E-04	9.12E-01	3.39E-04	9.38E-01	3.98E-04	9.36E-01	4.25E-04	9.29E-01
140	3.90E-04	9.46E-01	5.17E-04	9.26E-01	3.42E-04	9.48E-01	4.03E-04	9.46E-01	4.31E-04	9.42E-01
160	3.95E-04	9.57E-01	5.24E-04	9.38E-01	3.45E-04	9.56E-01	4.06E-04	9.54E-01	4.34E-04	9.48E-01
180	3.94E-04	9.56E-01	5.28E-04	9.45E-01	3.47E-04	9.60E-01	4.08E-04	9.59E-01	4.38E-04	9.57E-01
200	3.99E-04	9.67E-01	5.32E-04	9.53E-01	3.49E-04	9.67E-01	4.11E-04	9.66E-01	4.40E-04	9.62E-01
220	3.98E-04	9.64E-01	5.34E-04	9.56E-01	3.49E-04	9.66E-01	4.12E-04	9.68E-01	4.43E-04	9.68E-01
240	4.02E-04	9.74E-01	5.38E-04	9.64E-01	3.52E-04	9.74E-01	4.15E-04	9.74E-01	4.44E-04	9.71E-01
260	4.02E-04	9.75E-01	5.40E-04	9.67E-01	3.52E-04	9.75E-01	4.15E-04	9.76E-01	4.46E-04	9.75E-01
300	4.06E-04	9.85E-01	5.45E-04	9.76E-01	3.55E-04	9.84E-01	4.18E-04	9.82E-01	4.48E-04	9.78E-01
350	4.05E-04	9.83E-01	5.48E-04	9.81E-01	3.56E-04	9.85E-01	4.20E-04	9.86E-01	4.51E-04	9.85E-01
400	4.05E-04	9.83E-01	5.48E-04	9.82E-01	3.55E-04	9.84E-01	4.20E-04	9.87E-01	4.52E-04	9.89E-01
450	4.10E-04	9.95E-01	5.53E-04	9.90E-01	3.59E-04	9.94E-01	4.23E-04	9.92E-01	4.53E-04	9.90E-01
500	4.11E-04	9.96E-01	5.54E-04	9.92E-01	3.59E-04	9.95E-01	4.23E-04	9.93E-01	4.53E-04	9.91E-01
550	4.07E-04	9.88E-01	5.52E-04	9.89E-01	3.57E-04	9.89E-01	4.23E-04	9.93E-01	4.55E-04	9.94E-01
600	4.10E-04	9.95E-01	5.55E-04	9.94E-01	3.59E-04	9.94E-01	4.24E-04	9.95E-01	4.55E-04	9.95E-01
700	4.12E-04	9.99E-01	5.57E-04	9.98E-01	3.60E-04	9.98E-01	4.25E-04	9.98E-01	4.56E-04	9.96E-01
800	4.12E-04	1.00E+00	5.58E-04	1.00E+00	3.61E-04	1.00E+00	4.25E-04	9.99E-01	4.56E-04	9.98E-01
900	4.10E-04	9.94E-01	5.57E-04	9.98E-01	3.60E-04	9.96E-01	4.25E-04	9.99E-01	4.57E-04	1.00E+00
1000	4.12E-04	9.98E-01	5.58E-04	1.00E+00	3.60E-04	9.98E-01	4.26E-04	1.00E+00	4.58E-04	1.00E+00

Table A8. Continued.

SIRM Pulse	Sample Intensities (A/m)		Sample Intensities (A/m)		Sample Intensities (A/m)		Sample Intensities (A/m)		Sample Intensities (A/m)	
(mT)	Actual	Normalized	Actual	Normalized	Actual	Normalized	Actual	Normalized	Actual	Normalized
	7H8-054	7H8-054	8H2-018	8H2-018	8H3-088	8H3-088	8H4-049	8H4-049	8H5-017	8H5-017
0	4.71E-07	1.06E-03	1.16E-06	3.61E-03	2.99E-07	9.47E-04	1.16E-07	2.89E-04	1.34E-07	4.03E-04
1	2.14E-06	4.82E-03	1.75E-06	5.44E-03	2.04E-06	6.45E-03	2.53E-06	6.30E-03	1.70E-06	5.10E-03
5	1.22E-05	2.74E-02	9.78E-06	3.03E-02	8.91E-06	2.82E-02	1.28E-05	3.18E-02	9.61E-06	2.88E-02
10	3.57E-05	8.03E-02	2.38E-05	7.37E-02	2.19E-05	6.93E-02	3.09E-05	7.69E-02	2.36E-05	7.07E-02
15	6.42E-05	1.44E-01	4.34E-05	1.35E-01	4.10E-05	1.30E-01	5.63E-05	1.40E-01	4.35E-05	1.30E-01
20	9.85E-05	2.21E-01	6.97E-05	2.16E-01	6.69E-05	2.12E-01	8.97E-05	2.23E-01	7.05E-05	2.11E-01
25	1.40E-04	3.14E-01	1.01E-04	3.14E-01	9.77E-05	3.09E-01	1.30E-04	3.24E-01	1.04E-04	3.11E-01
30	1.83E-04	4.12E-01	1.27E-04	3.96E-01	1.26E-04	3.98E-01	1.68E-04	4.17E-01	1.32E-04	3.97E-01
35	2.27E-04	5.12E-01	1.64E-04	5.08E-01	1.62E-04	5.13E-01	2.14E-04	5.34E-01	1.72E-04	5.17E-01
40	2.67E-04	6.02E-01	1.88E-04	5.82E-01	1.88E-04	5.94E-01	2.45E-04	6.09E-01	1.99E-04	5.97E-01
50	3.26E-04	7.33E-01	2.27E-04	7.05E-01	2.28E-04	7.21E-01	2.94E-04	7.32E-01	2.43E-04	7.28E-01
60	3.58E-04	8.04E-01	2.54E-04	7.89E-01	2.55E-04	8.07E-01	3.27E-04	8.13E-01	2.71E-04	8.13E-01
70	3.81E-04	8.58E-01	2.71E-04	8.41E-01	2.71E-04	8.58E-01	3.46E-04	8.62E-01	2.88E-04	8.64E-01
80	3.95E-04	8.87E-01	2.82E-04	8.76E-01	2.81E-04	8.89E-01	3.59E-04	8.95E-01	2.99E-04	8.96E-01
90	4.04E-04	9.09E-01	2.90E-04	9.00E-01	2.89E-04	9.15E-01	3.68E-04	9.16E-01	3.06E-04	9.17E-01
100	4.10E-04	9.22E-01	2.96E-04	9.18E-01	2.94E-04	9.30E-01	3.74E-04	9.30E-01	3.11E-04	9.31E-01
120	4.17E-04	9.39E-01	3.00E-04	9.32E-01	2.98E-04	9.42E-01	3.79E-04	9.43E-01	3.15E-04	9.44E-01
140	4.22E-04	9.49E-01	3.04E-04	9.43E-01	3.00E-04	9.50E-01	3.83E-04	9.53E-01	3.18E-04	9.53E-01
160	4.25E-04	9.57E-01	3.07E-04	9.52E-01	3.03E-04	9.58E-01	3.86E-04	9.60E-01	3.20E-04	9.60E-01
180	4.28E-04	9.62E-01	3.07E-04	9.54E-01	3.02E-04	9.55E-01	3.86E-04	9.61E-01	3.21E-04	9.63E-01
200	4.30E-04	9.67E-01	3.11E-04	9.64E-01	3.06E-04	9.67E-01	3.89E-04	9.69E-01	3.23E-04	9.69E-01
220	4.31E-04	9.69E-01	3.10E-04	9.63E-01	3.06E-04	9.67E-01	3.90E-04	9.70E-01	3.24E-04	9.71E-01
240	4.33E-04	9.75E-01	3.12E-04	9.67E-01	3.06E-04	9.67E-01	3.91E-04	9.73E-01	3.25E-04	9.74E-01
260	4.35E-04	9.78E-01	3.14E-04	9.74E-01	3.08E-04	9.75E-01	3.93E-04	9.79E-01	3.27E-04	9.79E-01
300	4.37E-04	9.84E-01	3.14E-04	9.76E-01	3.09E-04	9.77E-01	3.94E-04	9.81E-01	3.27E-04	9.82E-01
350	4.39E-04	9.86E-01	3.18E-04	9.86E-01	3.12E-04	9.88E-01	3.97E-04	9.88E-01	3.30E-04	9.88E-01
400	4.39E-04	9.87E-01	3.17E-04	9.84E-01	3.10E-04	9.81E-01	3.96E-04	9.85E-01	3.29E-04	9.88E-01
450	4.42E-04	9.93E-01	3.18E-04	9.86E-01	3.11E-04	9.83E-01	3.97E-04	9.87E-01	3.30E-04	9.90E-01
500	4.42E-04	9.94E-01	3.20E-04	9.92E-01	3.13E-04	9.91E-01	3.99E-04	9.93E-01	3.31E-04	9.94E-01
550	4.41E-04	9.92E-01	3.18E-04	9.87E-01	3.10E-04	9.81E-01	3.97E-04	9.88E-01	3.30E-04	9.90E-01
600	4.43E-04	9.96E-01	3.18E-04	9.88E-01	3.11E-04	9.83E-01	3.97E-04	9.89E-01	3.30E-04	9.90E-01
700	4.44E-04	9.98E-01	3.20E-04	9.92E-01	3.13E-04	9.90E-01	3.99E-04	9.94E-01	3.32E-04	9.95E-01
800	4.44E-04	1.00E+00	3.20E-04	9.94E-01	3.13E-04	9.91E-01	4.00E-04	9.96E-01	3.32E-04	9.96E-01
900	4.44E-04	9.98E-01	3.22E-04	1.00E+00	3.16E-04	1.00E+00	4.02E-04	1.00E+00	3.33E-04	1.00E+00
1000	4.45E-04	1.00E+00	3.22E-04	1.00E+00	3.16E-04	9.99E-01	4.02E-04	1.00E+00	3.34E-04	1.00E+00

Table A8. Continued.

SIRM Pulse	Sample Intensities (A/m)		Sample Intensities (A/m)		Sample Intensities (A/m)		Sample Intensities (A/m)		Sample Intensities (A/m)	
(mT)	Actual	Normalized	Actual	Normalized	Actual	Normalized	Actual	Normalized	Actual	Normalized
	8H6-125	8H6-125	8H7-082	8H7-082	8H8-063	8H8-063	9H1-024	9H1-024	9H2-059	9H2-059
0	4.27E-07	6.90E-04	2.93E-07	6.42E-04	2.95E-07	6.95E-04	6.67E-07	2.43E-03	8.17E-07	1.10E-03
1	3.49E-06	5.64E-03	2.40E-06	5.26E-03	2.23E-06	5.25E-03	1.38E-06	5.04E-03	4.38E-06	5.90E-03
5	1.81E-05	2.92E-02	1.25E-05	2.74E-02	1.14E-05	2.68E-02	5.61E-06	2.04E-02	1.80E-05	2.42E-02
10	4.48E-05	7.23E-02	3.10E-05	6.80E-02	2.82E-05	6.65E-02	1.89E-05	6.88E-02	6.22E-05	8.37E-02
15	8.31E-05	1.34E-01	5.81E-05	1.27E-01	5.30E-05	1.25E-01	3.55E-05	1.29E-01	1.14E-04	1.53E-01
20	1.35E-04	2.17E-01	9.57E-05	2.10E-01	8.72E-05	2.05E-01	5.73E-05	2.09E-01	1.79E-04	2.41E-01
25	1.98E-04	3.19E-01	1.43E-04	3.12E-01	1.30E-04	3.06E-01	7.83E-05	2.85E-01	2.41E-04	3.25E-01
30	2.50E-04	4.04E-01	1.82E-04	3.98E-01	1.66E-04	3.92E-01	1.09E-04	3.97E-01	3.28E-04	4.41E-01
35	3.24E-04	5.23E-01	2.38E-04	5.21E-01	2.18E-04	5.13E-01	1.38E-04	5.02E-01	4.04E-04	5.44E-01
40	3.72E-04	6.01E-01	2.74E-04	6.00E-01	2.52E-04	5.93E-01	1.60E-04	5.83E-01	4.63E-04	6.23E-01
50	4.53E-04	7.30E-01	3.34E-04	7.31E-01	3.08E-04	7.26E-01	2.01E-04	7.31E-01	5.63E-04	7.58E-01
60	5.03E-04	8.11E-01	3.70E-04	8.12E-01	3.44E-04	8.10E-01	2.23E-04	8.10E-01	6.16E-04	8.29E-01
70	5.34E-04	8.61E-01	3.93E-04	8.62E-01	3.65E-04	8.60E-01	2.37E-04	8.63E-01	6.54E-04	8.81E-01
80	5.53E-04	8.93E-01	4.08E-04	8.94E-01	3.79E-04	8.94E-01	2.46E-04	8.95E-01	6.76E-04	9.10E-01
90	5.66E-04	9.13E-01	4.16E-04	9.11E-01	3.88E-04	9.14E-01	2.50E-04	9.10E-01	6.82E-04	9.18E-01
100	5.75E-04	9.28E-01	4.23E-04	9.26E-01	3.94E-04	9.29E-01	2.54E-04	9.25E-01	6.91E-04	9.31E-01
120	5.83E-04	9.40E-01	4.29E-04	9.40E-01	4.00E-04	9.42E-01	2.57E-04	9.36E-01	7.00E-04	9.42E-01
140	5.88E-04	9.49E-01	4.33E-04	9.49E-01	4.04E-04	9.51E-01	2.60E-04	9.48E-01	7.07E-04	9.52E-01
160	5.93E-04	9.57E-01	4.36E-04	9.56E-01	4.07E-04	9.58E-01	2.63E-04	9.59E-01	7.15E-04	9.62E-01
180	5.95E-04	9.61E-01	4.40E-04	9.63E-01	4.09E-04	9.63E-01	2.64E-04	9.61E-01	7.14E-04	9.62E-01
200	5.99E-04	9.67E-01	4.41E-04	9.67E-01	4.11E-04	9.68E-01	2.66E-04	9.69E-01	7.21E-04	9.71E-01
220	6.01E-04	9.70E-01	4.44E-04	9.72E-01	4.12E-04	9.72E-01	2.67E-04	9.73E-01	7.24E-04	9.74E-01
240	6.03E-04	9.73E-01	4.45E-04	9.76E-01	4.14E-04	9.75E-01	2.67E-04	9.72E-01	7.22E-04	9.72E-01
260	6.05E-04	9.77E-01	4.46E-04	9.78E-01	4.15E-04	9.79E-01	2.68E-04	9.75E-01	7.24E-04	9.74E-01
300	6.08E-04	9.81E-01	4.49E-04	9.84E-01	4.17E-04	9.83E-01	2.69E-04	9.80E-01	7.27E-04	9.80E-01
350	6.11E-04	9.86E-01	4.50E-04	9.87E-01	4.19E-04	9.88E-01	2.71E-04	9.85E-01	7.30E-04	9.83E-01
400	6.12E-04	9.88E-01	4.52E-04	9.91E-01	4.19E-04	9.88E-01	2.71E-04	9.88E-01	7.32E-04	9.86E-01
450	6.14E-04	9.91E-01	4.54E-04	9.94E-01	4.21E-04	9.92E-01	2.72E-04	9.90E-01	7.34E-04	9.88E-01
500	6.15E-04	9.92E-01	4.54E-04	9.94E-01	4.22E-04	9.94E-01	2.72E-04	9.90E-01	7.34E-04	9.88E-01
550	6.15E-04	9.92E-01	4.55E-04	9.96E-01	4.21E-04	9.92E-01	2.73E-04	9.95E-01	7.39E-04	9.95E-01
600	6.15E-04	9.93E-01	4.55E-04	9.97E-01	4.21E-04	9.93E-01	2.73E-04	9.92E-01	7.35E-04	9.90E-01
700	6.17E-04	9.96E-01	4.56E-04	9.99E-01	4.23E-04	9.97E-01	2.73E-04	9.94E-01	7.39E-04	9.95E-01
800	6.18E-04	9.98E-01	4.56E-04	1.00E+00	4.23E-04	9.98E-01	2.73E-04	9.95E-01	7.38E-04	9.94E-01
900	6.19E-04	1.00E+00	4.56E-04	1.00E+00	4.24E-04	1.00E+00	2.75E-04	1.00E+00	7.43E-04	1.00E+00
1000	6.20E-04	1.00E+00	4.56E-04	1.00E+00	4.24E-04	1.00E+00	2.74E-04	9.96E-01	7.39E-04	9.95E-01

Table A8. Continued.

SIRM Pulse	Sample Intensities (A/m)		Sample Intensities (A/m)		Sample Intensities (A/m)		Sample Intensities (A/m)		Sample Intensities (A/m)	
(mT)	Actual	Normalized	Actual	Normalized	Actual	Normalized	Actual	Normalized	Actual	Normalized
	9H3-030	9H3-030	9H4-014	9H4-014	9H5-120	9H5-120	9H6-084	9H6-084	9H7-063	9H7-063
0	9.02E-07	7.44E-04	1.29E-06	5.07E-04	1.34E-06	1.19E-03	3.59E-07	2.50E-04	1.13E-06	5.22E-04
1	7.36E-06	6.07E-03	1.47E-05	5.78E-03	6.04E-06	5.35E-03	8.90E-06	6.19E-03	1.28E-05	5.92E-03
5	3.14E-05	2.59E-02	6.36E-05	2.50E-02	2.57E-05	2.28E-02	3.72E-05	2.59E-02	5.47E-05	2.52E-02
10	1.06E-04	8.72E-02	2.18E-04	8.54E-02	8.60E-05	7.61E-02	1.23E-04	8.55E-02	1.84E-04	8.47E-02
15	1.93E-04	1.59E-01	4.01E-04	1.57E-01	1.58E-04	1.40E-01	2.23E-04	1.56E-01	3.37E-04	1.55E-01
20	3.04E-04	2.51E-01	6.35E-04	2.49E-01	2.54E-04	2.25E-01	3.54E-04	2.47E-01	5.36E-04	2.47E-01
25	4.08E-04	3.36E-01	8.53E-04	3.35E-01	3.47E-04	3.08E-01	4.78E-04	3.33E-01	7.26E-04	3.35E-01
30	5.53E-04	4.56E-01	1.16E-03	4.53E-01	4.82E-04	4.27E-01	6.56E-04	4.57E-01	9.96E-04	4.59E-01
35	6.79E-04	5.60E-01	1.42E-03	5.58E-01	6.04E-04	5.35E-01	8.14E-04	5.67E-01	1.23E-03	5.68E-01
40	7.71E-04	6.35E-01	1.61E-03	6.33E-01	6.94E-04	6.15E-01	9.25E-04	6.44E-01	1.40E-03	6.48E-01
50	9.32E-04	7.68E-01	1.95E-03	7.66E-01	8.58E-04	7.60E-01	1.12E-03	7.83E-01	1.71E-03	7.87E-01
60	1.02E-03	8.37E-01	2.13E-03	8.36E-01	9.44E-04	8.36E-01	1.23E-03	8.55E-01	1.86E-03	8.57E-01
70	1.07E-03	8.82E-01	2.25E-03	8.81E-01	9.97E-04	8.83E-01	1.29E-03	8.95E-01	1.95E-03	8.99E-01
80	1.10E-03	9.10E-01	2.32E-03	9.09E-01	1.03E-03	9.13E-01	1.32E-03	9.22E-01	2.01E-03	9.25E-01
90	1.12E-03	9.23E-01	2.35E-03	9.23E-01	1.05E-03	9.28E-01	1.35E-03	9.38E-01	2.03E-03	9.37E-01
100	1.13E-03	9.35E-01	2.38E-03	9.35E-01	1.06E-03	9.40E-01	1.36E-03	9.48E-01	2.05E-03	9.48E-01
120	1.15E-03	9.46E-01	2.41E-03	9.46E-01	1.07E-03	9.51E-01	1.38E-03	9.58E-01	2.07E-03	9.57E-01
140	1.16E-03	9.55E-01	2.43E-03	9.55E-01	1.08E-03	9.59E-01	1.38E-03	9.64E-01	2.09E-03	9.64E-01
160	1.17E-03	9.63E-01	2.46E-03	9.64E-01	1.09E-03	9.66E-01	1.39E-03	9.68E-01	2.10E-03	9.70E-01
180	1.17E-03	9.66E-01	2.46E-03	9.66E-01	1.09E-03	9.69E-01	1.40E-03	9.73E-01	2.11E-03	9.72E-01
200	1.18E-03	9.72E-01	2.48E-03	9.72E-01	1.10E-03	9.74E-01	1.40E-03	9.76E-01	2.12E-03	9.77E-01
220	1.18E-03	9.75E-01	2.49E-03	9.76E-01	1.10E-03	9.77E-01	1.41E-03	9.79E-01	2.12E-03	9.80E-01
240	1.18E-03	9.75E-01	2.49E-03	9.76E-01	1.10E-03	9.78E-01	1.41E-03	9.81E-01	2.13E-03	9.81E-01
260	1.19E-03	9.78E-01	2.49E-03	9.77E-01	1.11E-03	9.80E-01	1.41E-03	9.83E-01	2.13E-03	9.81E-01
300	1.19E-03	9.82E-01	2.50E-03	9.82E-01	1.11E-03	9.85E-01	1.42E-03	9.86E-01	2.14E-03	9.86E-01
350	1.20E-03	9.85E-01	2.51E-03	9.86E-01	1.12E-03	9.88E-01	1.42E-03	9.90E-01	2.14E-03	9.89E-01
400	1.20E-03	9.88E-01	2.52E-03	9.88E-01	1.12E-03	9.90E-01	1.42E-03	9.91E-01	2.15E-03	9.91E-01
450	1.20E-03	9.92E-01	2.53E-03	9.91E-01	1.12E-03	9.92E-01	1.43E-03	9.94E-01	2.15E-03	9.93E-01
500	1.20E-03	9.91E-01	2.53E-03	9.91E-01	1.12E-03	9.92E-01	1.43E-03	9.93E-01	2.15E-03	9.93E-01
550	1.21E-03	9.95E-01	2.53E-03	9.94E-01	1.12E-03	9.95E-01	1.43E-03	9.94E-01	2.16E-03	9.96E-01
600	1.20E-03	9.93E-01	2.53E-03	9.93E-01	1.12E-03	9.94E-01	1.43E-03	9.96E-01	2.16E-03	9.94E-01
700	1.21E-03	9.96E-01	2.54E-03	9.95E-01	1.12E-03	9.96E-01	1.43E-03	9.97E-01	2.16E-03	9.97E-01
800	1.21E-03	9.96E-01	2.54E-03	9.96E-01	1.13E-03	9.97E-01	1.43E-03	9.98E-01	2.16E-03	9.97E-01
900	1.21E-03	1.00E+00	2.55E-03	1.00E+00	1.13E-03	1.00E+00	1.43E-03	9.98E-01	2.17E-03	1.00E+00
1000	1.21E-03	9.99E-01	2.54E-03	9.99E-01	1.13E-03	9.99E-01	1.44E-03	1.00E+00	2.17E-03	1.00E+00

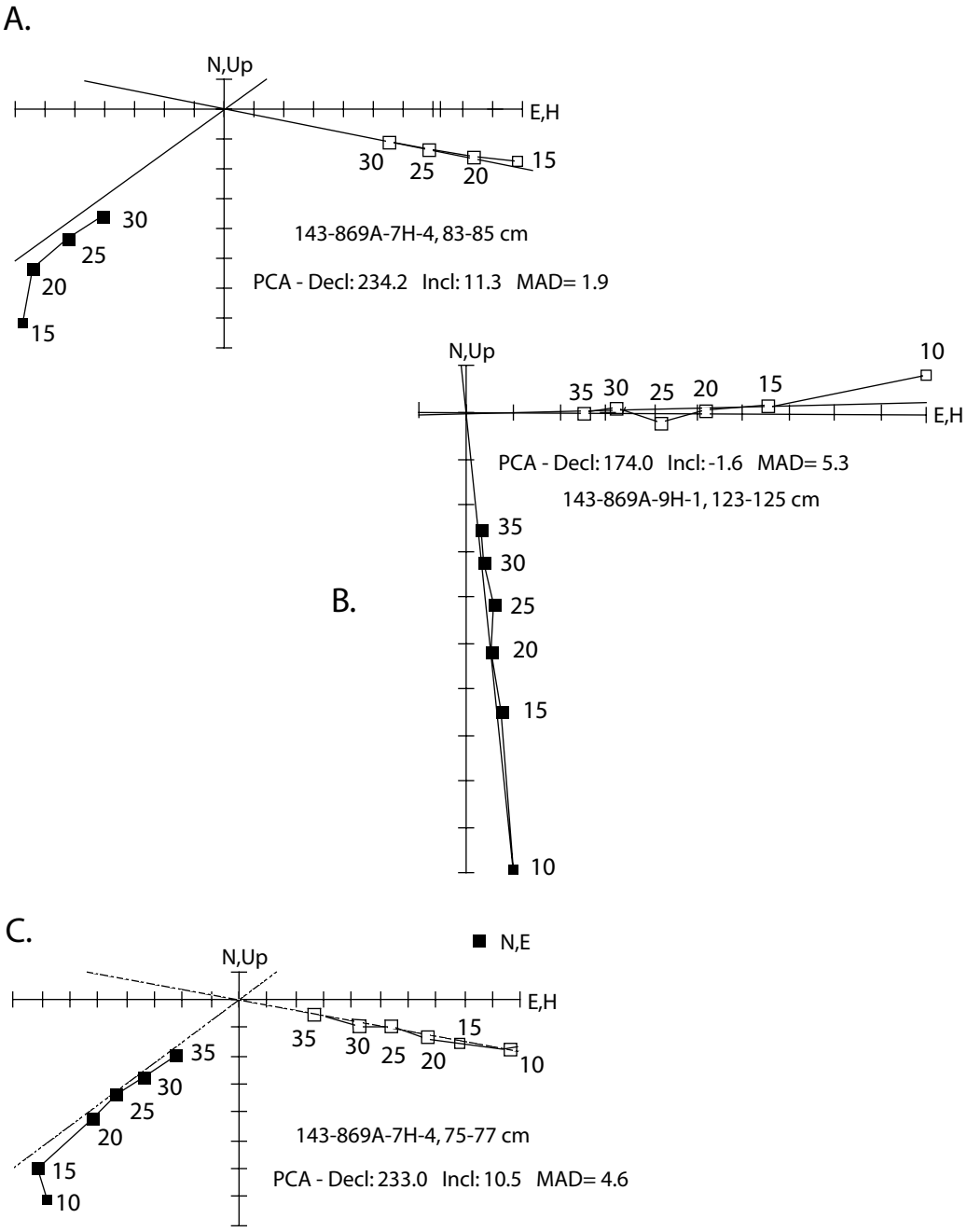

Figure A1. Zijderveld diagrams showing principal component analysis of three Hole 869A samples (unanchored); squares denote AF demagnetization steps in milliteslas (mT); open squares are vertical plane; solid squares are horizontal plane. A) Sample 143-869A-7H-4, 83-85 cm; B) Sample 143-869A-9H-1, 123-125 cm; C) Sample 143-869A-7H-4, 75-77 cm.

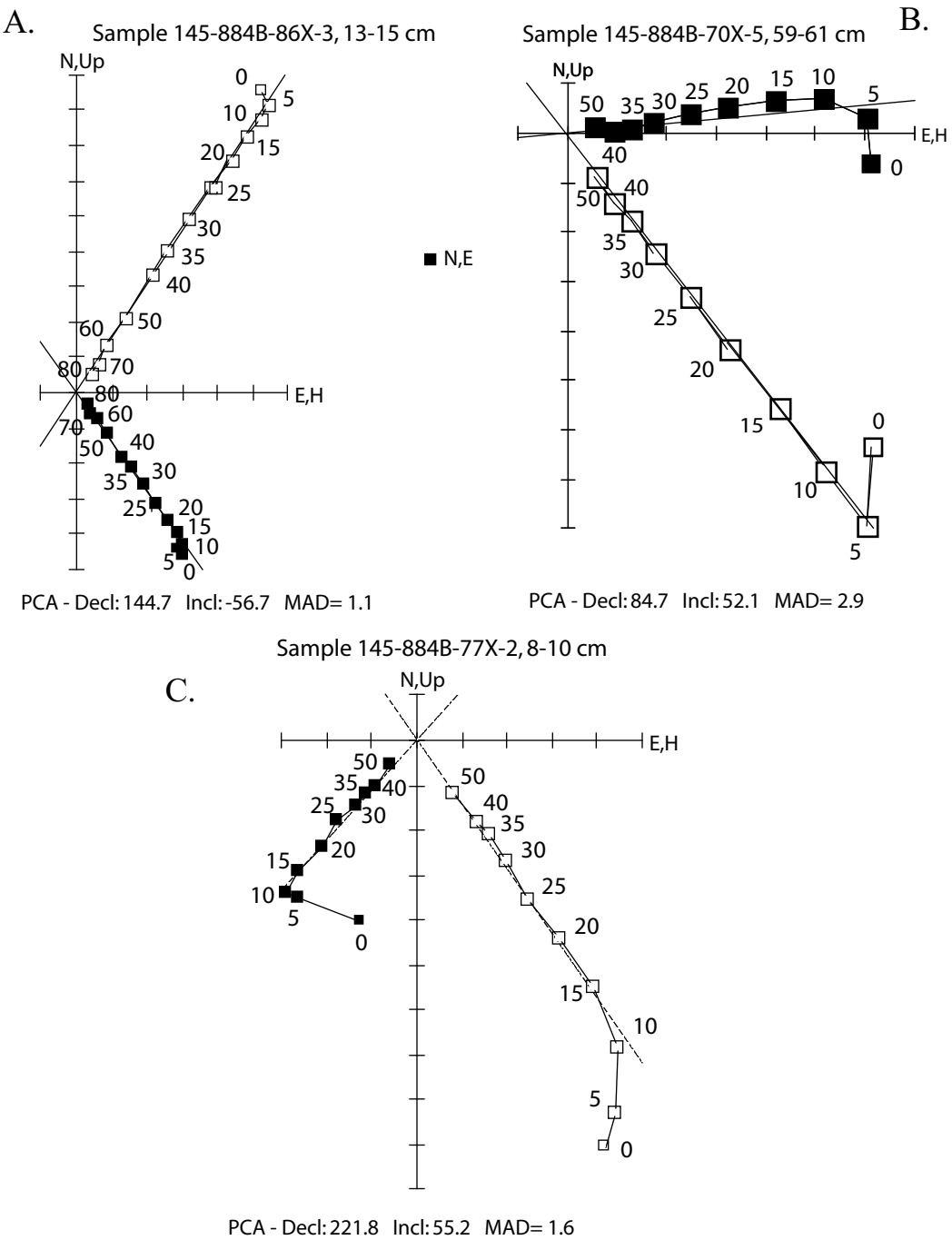

Figure A2. Zijderveld diagrams showing principal component analysis and stable inclinations of three Hole 884B samples (anchored); squares denote AF demagnetization steps in milliteslas (mT); open squares are vertical plane; solid squares are horizontal plane. A) Sample 145-884B-86X-3, 13-15 cm; B) Sample 145-884B-70X-5, 59-61 cm; C) Sample 145-884B-77X-2, 8-10 cm.

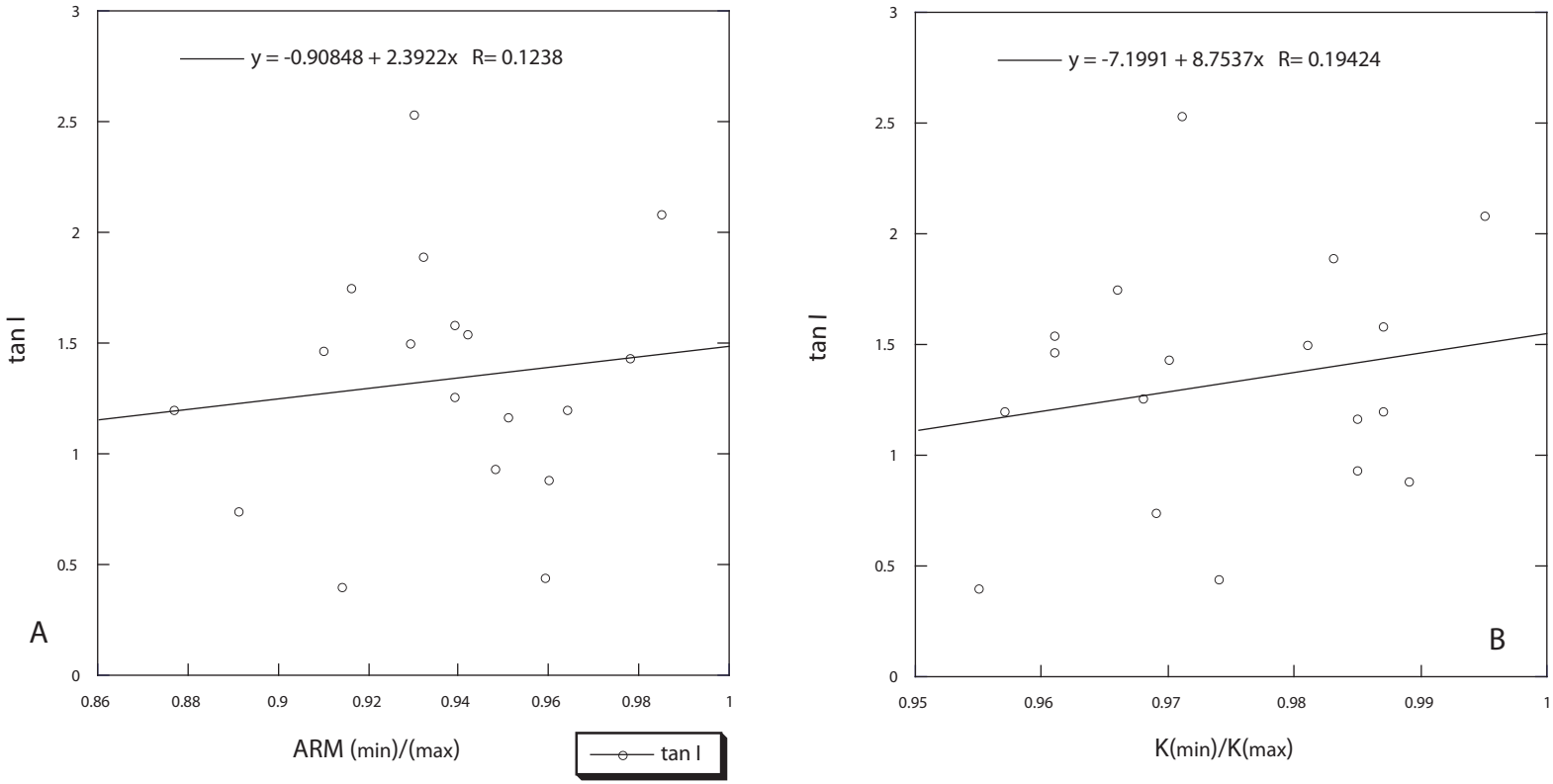

Figure A3. Estimation of pre-inclination shallowing tan I values from the remanence inclinations of Hole 884B sediments. Predicted tan I located at intersection of regression line and $ARM_{(min)}/ARM_{(max)} = 1$ or $K_{(min)}/K_{(max)} = 1$: (A) method using $ARM_{(min)}/ARM_{(max)}$ parameter from anhysteretic remanence and the tangents of the inclinations; (B) using susceptibilty value $K_{(min)}/K_{(max)}$ from anisotropy (AMS) measurements and tan I. Estimated tan I value used to calculate average inclination of sediments prior to inclination shallowing.

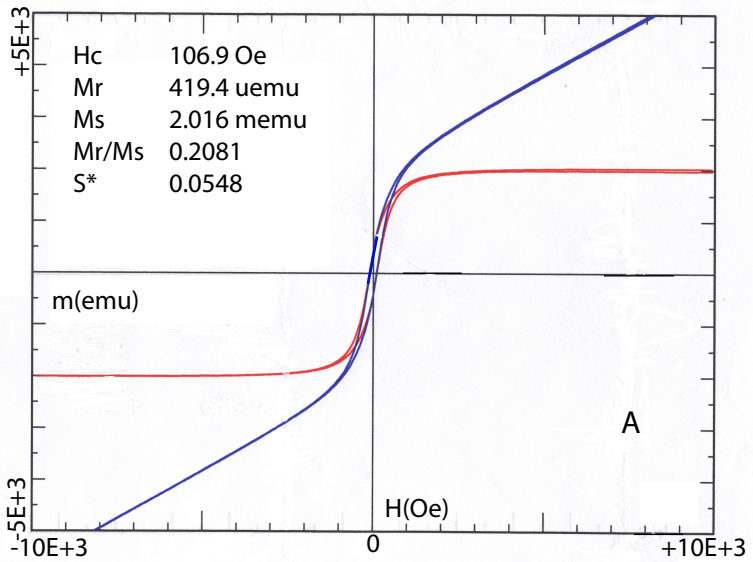

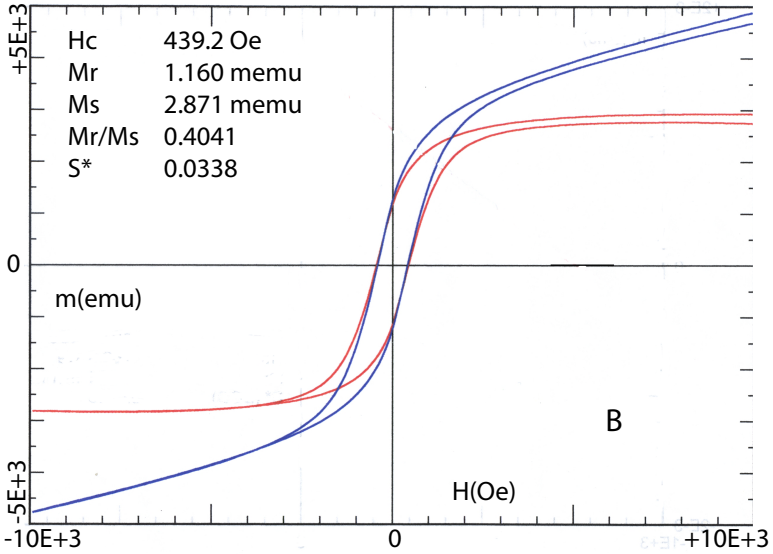

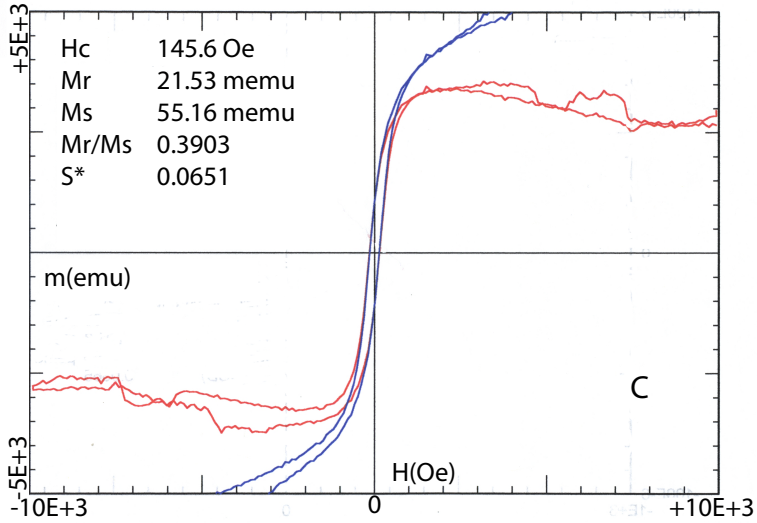

Figure A4. Selected examples of hysteresis analysis for Holes 884B and 869A. Hole 884B samples had higher magnetic intensities, producing results with less drift during analysis (A and B). Only a few Hole 869A samples were useable due to weak magnetic intensity and instrument noise. A) Sample 145-884B-70X-2, 40-42 cm; B) Sample 145-884B-83X-2, 15-17 cm; C) Sample 143-869A-5H-1, 27-29 cm. Narrow hysteresis loops (A and C) indicate presence of pseudo-single domain magnetite, (B) shows pseudo-single domain with single domain magnetite evidenced by wider curve. Blue curve is un-corrected data, red curve is de-trended.

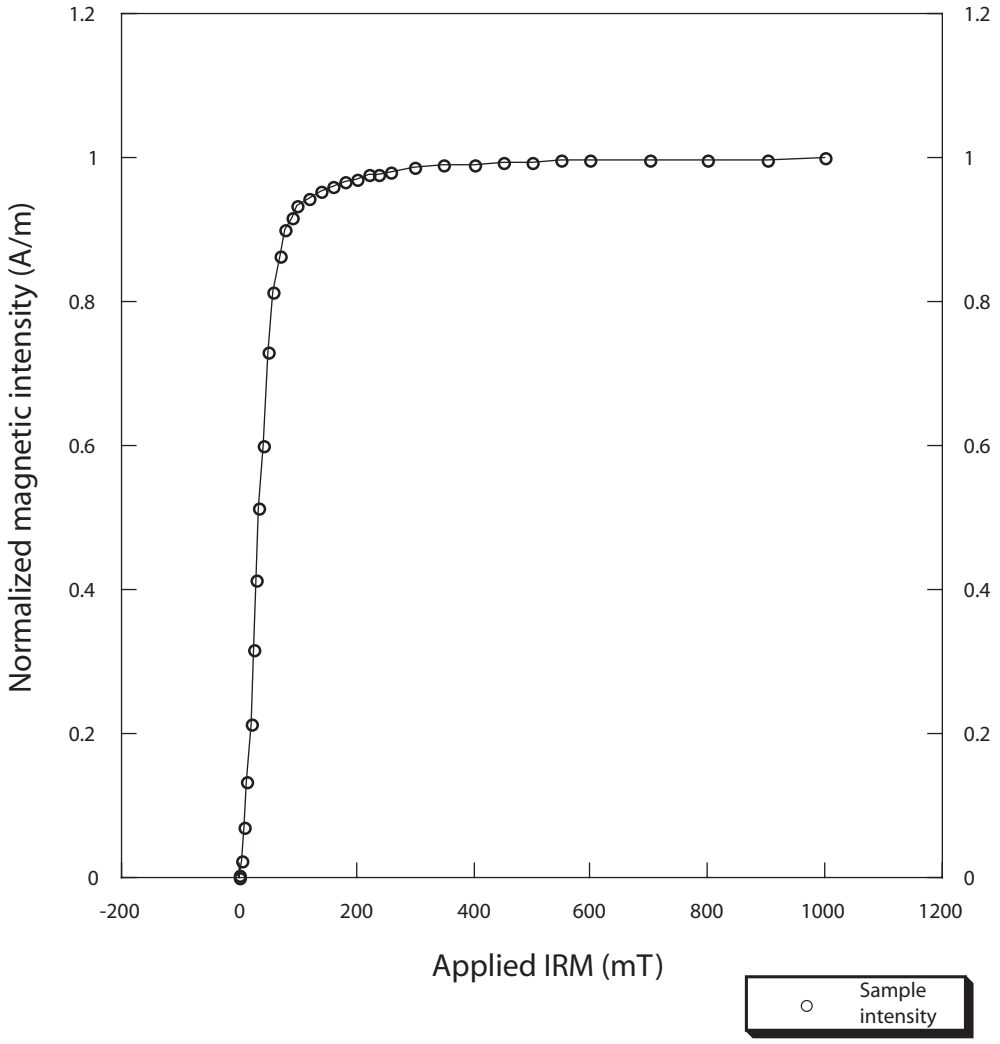

Figure A5. Average (N=35) normalized magnetic intensities of Hole 869A discrete samples when saturated by IRM pulse. Samples show samples are saturated by 200 mT of applied IRM. Samples show rapid magnetization saturation, which is characteristic of titanomagnetites.

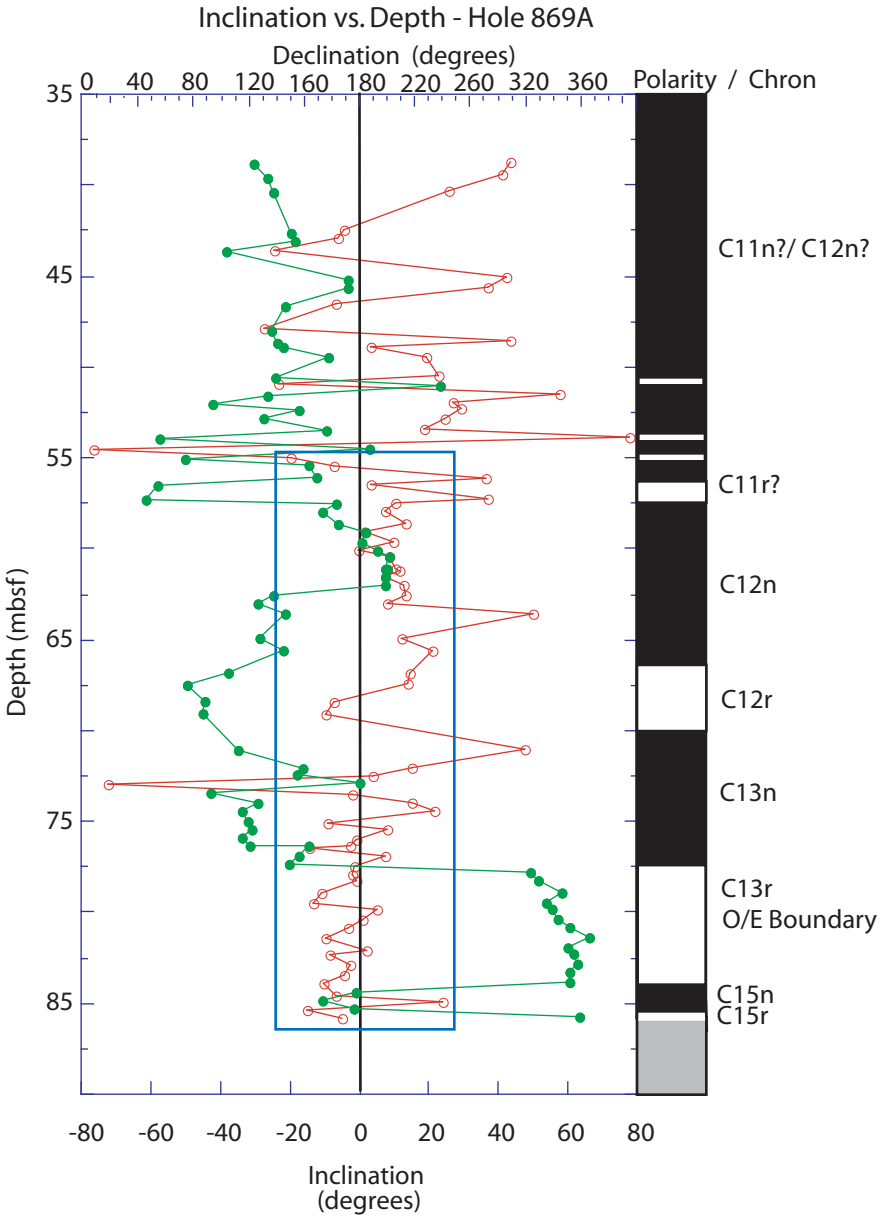

Figure A6. Magnetostratigraphy created for Leg 143 Hole 869A from discrete sediment samples of cores 143-896A-5H through 143-869A-9H. Polarity chron assignments based on biostratigraphy and ODP multishot tool corrected declinations [Firth, 1995; Shipboard Scientific Party, 1993; Gradstein et al., 2004]. Declination reversals used in place of inclinations to determine polarity due to proximity of site to equator. Open red circles denote inclination; filled green circles are corrected declination. Colatitude data shown in open blue box.

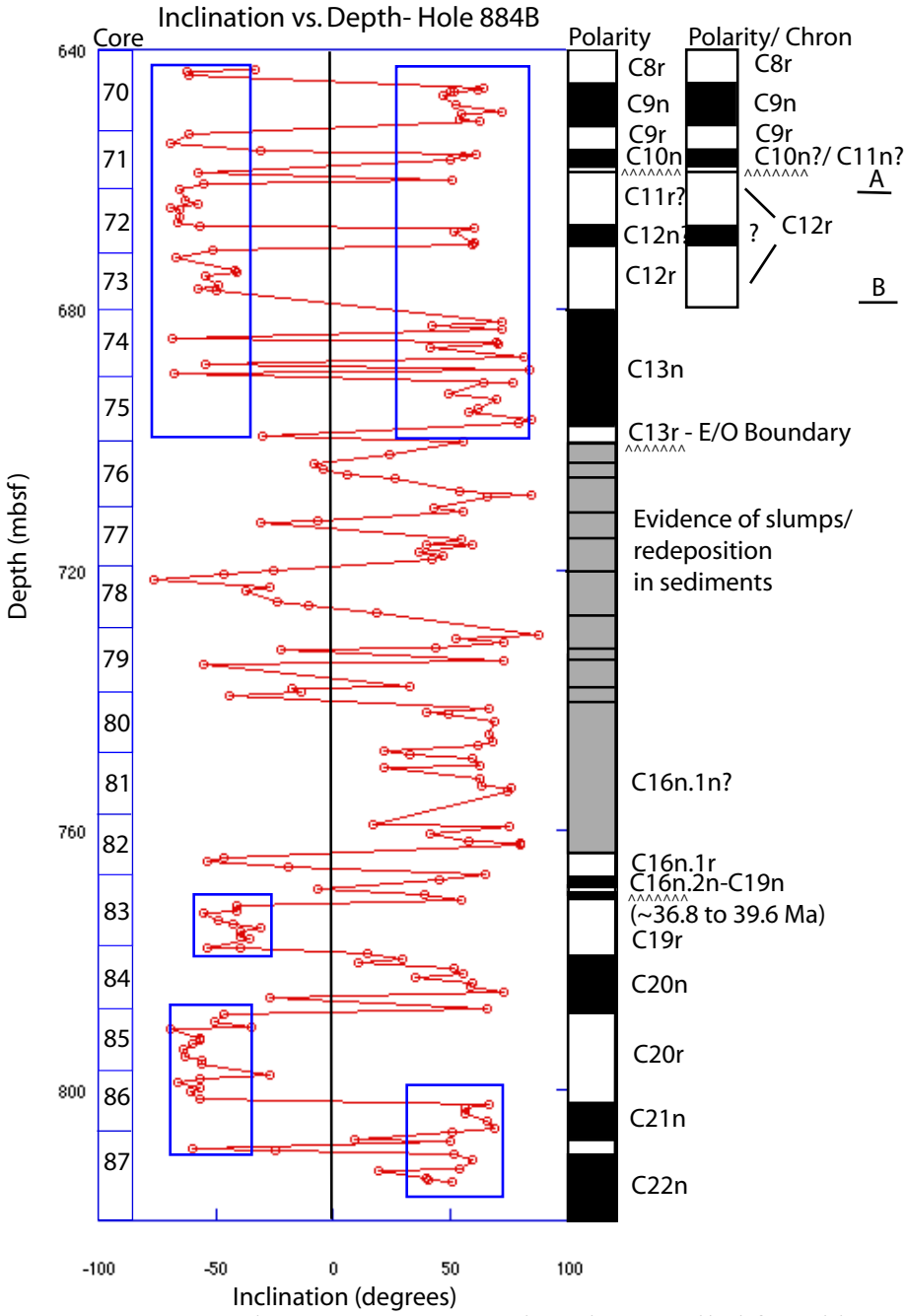

Figure A7. Leg 145 Hole 884B magnetostratigraphy compiled from biostratigraphy [Barron et al., 1995; Pak and Miller, 1995] and GPTS 2004 [Gradstein et al, 2004]. Upper section has two chron interpretations; interpretation on left based on biostratigraphy and chron lengths; interpretation on right based on biostratigraphy. (A) represents first occurrence of *Rocella vigilans* and last occurrence (LO) of *Reticulofenestra umbilica* ~32.4 Ma; (B) is LO of *Ericsonia formosa*, ~33.2 Ma. Carrat symbols represent unconformities. Middle section interpretation of Hole 884B is unclear due to sediment slumping/redeposition. Colatitude data shown in blue boxes.

VITA

Name: Melissa A. Beaman

Address: Department of Oceanography, Texas A&M University, Eller O&M Building MS 3146, College Station, Texas 77840

Email Address: oceanrocks@hotmail.com

Education: B.S., Geology, Arizona State University, 2003
M.S., Oceanography, Texas A&M University, 2006